# Peptide-guided Dental Tissue Regeneration for Oral Care

Deniz Tanil Yucesoy

A dissertation

submitted in partial fulfillment of the

requirements for the degree of

Doctor of Philosophy

University of Washington

2018

Reading Committee:

Mehmet Sarikaya, Chair

Sami Dogan

Candan Tamerler

Program Authorized to Offer Degree:

Department of Materials Science and Engineering

University of Washington

**Abstract**

Peptide-guided Dental Tissue Regeneration for Oral Care

Deniz Tanil Yucesoy

Chair of the Supervisory Committee:
Prof. Mehmet Sarikaya
Materials Science and Engineering

Oral diseases are one of the most prevalent health problems that affect quality of life and well-being. These diseases include: (1) Demineralization-related dental conditions such as hypersensitivity, caries, white spot lesions; (2) Aesthetic problems e.g., tooth staining; (3) Soft tissue-related ailments that can lead to periodontitis and gingival recession; and (4) Infections and inflammations e.g., mucositis and peri-implantitis leading to implant failure. Current therapies mostly rely on replacement of the defective hard tissues with synthetic restorative materials. The implant treatment is also a common viable option in the contemporary dentistry when synthetic restorations fail and tooth extraction is indicated. The long-term success of these synthetic material-based restorations, however, is still low and questionable; indeed, they often cause post-therapeutic problems such as inflammation of gingiva or formation of secondary caries. Moreover, the failure of implants due to inflammation of the peri-implant mucosa and peri-implantitis as well as bacterial infections are major concerns. The primary reasons for the failure of current dental restoration therapies are four-fold: (i) Limited ability to reinstate the structure-function of the lost tissue, (ii) Lack of structural and functional integration (interface problem), (iii) Low thermal, mechanical, and chemical durability, and (iv) Tissue toxicity and

low biocompatibility. The common denominator to overcome current limitations is to enable natural biomineralization *in situ* either on the defective hard tissues or at the tissue-material interface. The ideal approach would, therefore, be biomimetically developed repair and replacement materials, and regeneration therapies that follow the lessons from biology in dental tissue formation. Although numerous traditional biomimetic restoration approaches have been developed to reproduce biological minerals and tissues, these are still far from being feasible to use as a therapeutic and technological product due to the requirement of natural full-length proteins as the key enabling therapeutic agents. As an alternative route towards eliminating the inherent disadvantage of protein-based therapies, solid binding peptides have emerged as an effective molecular tool. These peptides are isolated through combinatorial mutagenesis and further engineered using bioinformatics and computational tools to epitomize the key functions of the natural proteins. Building upon molecular biomimetic principles, the hypothesis of this research is that "*Using solid binding peptides, it could be possible to remineralize and repair the dental hard tissues; e.g., dentin, enamel and cementum, and restore the structure and function of the tooth with a well-integrated and durable mineral layer that could be administered via variety of formulations such as aqueous solution, gel and lozenges."*

To demonstrate the validity of the hypothesis, it is planned to focus on four task areas including; ***Task-I:*** *In vitro Peptide-guided Biomimetic Repair of Dental Hard Tissues (enamel and dentin);* ***Task-II:*** *In vivo Peptide-guided Remineralization to Restore Dental Caries (animal model);* ***Task-III:*** *Development of Mineralizing Peptide-based Restorative/Therapeutic Dental Care Products (dental lozenges);* ***Task-IV:*** *Improving the functionality (preventing risks associated with failure) of dental implants*. The successful completion of these tasks will establish the basis of the peptide-guided remineralization therapy for developing a universal solution for oral care.

**Table of Contents**

**List of Figures**

**List of Tables**

**Acknowledgements**

I would like to offer my sincerest gratitude to my advisor, Professor Mehmet Sarikaya, for giving me close guidance in multiple regards and countless opportunities, throughout the years. He has taught me more than I could give credit for on these pages. Many thanks for genuinely caring about me and believing that I can succeed! You have set an example of excellence as a scientist, mentor and instructor.

I would like to also thank to Professor Candan Tamerler, whom I started my academic journey, for the constant guidance, insights and encouragement. I will not forget the time I spent at her laboratory and experiences that I learned. Much gratitude is extended to Professor Sami Dogan, our close collaborator, for his invaluable guidance during the course of my graduate research. His clinical and scientific input throughout my research was very significant to complete this thesis.

Special thanks to Dr. Hanson Fong for sharing his scientific and technical knowledge, starting from the first day of my PhD. Much of the work in my thesis would not have been possible without his help. It was also a great privilege to work together with Drs. Marketa Hnilova, Mustafa Gungormus, Carolyn Gresswell and Sefa Dag who helped me to learn new techniques in the field and without their help, the research would not have been completed.

Much gratitude to my Ph.D. supervisory committee, in particular Professors Susan Herring and Bruce Hinds for their efforts in making the process work smoothly. I would like to thank to the other members of GEMSEC for invaluable discussions and the undergraduate students who provided significant contribution in many parts of this thesis. Lastly, I thank to my wife, Duygu, for believing in me to pursue a PhD and giving me constant support and encouragement.

Chapter 1: Introduction – Statement of the Problem and Thesis Approach

*Current State of Oral Health Care and Scope of this Dissertation:* Oral health diseases are one of the most prevalent complications that affect society and in most cases, cause considerable discomfort and pain which often leads people to change even their eating habits, speech and quality of their life and well-being.[1-3] According to a World Health Organization (WHO) report, oral health problems are the fourth-most expensive diseases to treat causing a huge economic burden to society.[4] These diseases include: (1) Demineralization-related dental conditions such as hypersensitivity, white spot lesions, caries;[5, 6] (2) Aesthetic conditions e.g., tooth staining;[7] (3) Soft tissue-related ailments that can lead to periodontitis and gingival recession;[8] (4) Infections and inflammations e.g., mucositis and peri-implantitis, leading to implant failure[9] (**Figure 1**).

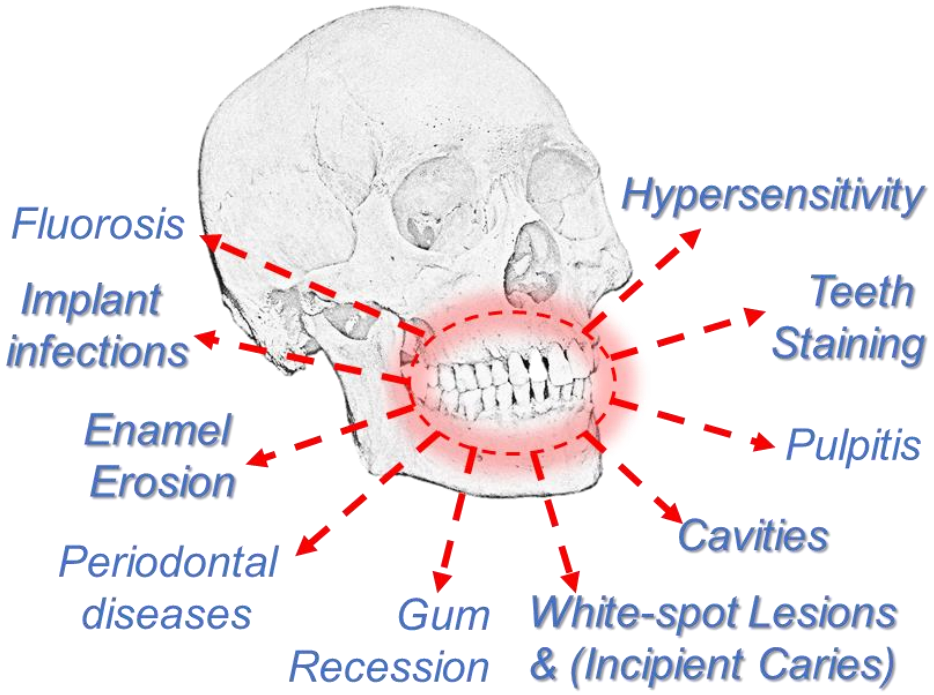


**Figure 1:** Common oral health problems.

Saliva is the natural defense mechanism against demineralization-related mineral loss from the tooth. Besides neutralizing the acid produced by the oral bacteria, causing dissolution of natural minerals, it is also the primary agent that enables restoration of the lost mineral (remineralization) of the tooth.[10-12]

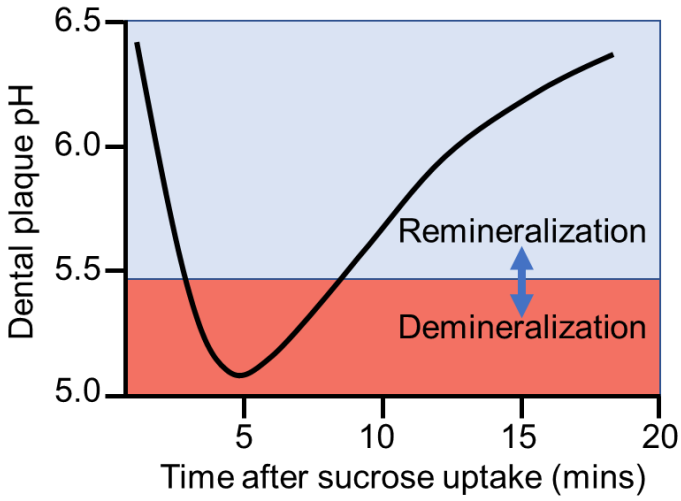


**Figure 2:** Schematic representation of equilibrium between demineralization and remineralization processes within the dental plaque in response to sugar uptake and subsequent clearance with saliva.

As depicted in **Figure 2**, in healthy patients, there is an equilibrium between demineralization and remineralization processes within the dental plaque whereby pH of the plaque decreases via metabolic activity of the bacteria and then returns to resting level with the buffering action of saliva.[10, 11, 13] However, when saliva secretion is limited or the buffering capacity is low, the equilibrium shifts towards demineralization (acidic pH) which leads to dissolution of tooth minerals and eventually formation of caries.[14-18] The critical pH for the enamel and dentin below which demineralization onset has been reported to be in the range of 5.2–5.8 and 6.0–6.9, respectively.[19-25]

*Statement of the Problem:* Current dental restoration therapies generally rely on replacement of the affected dental hard tissues with synthetic materials partially (e.g., fillers) or completely (e.g., implants).[26-30] However, the long-term success of these synthetic material-based restorations is still clinically questionable.[31-33] These treatments, in fact, often cause post-therapeutic problems such as formation of secondary caries.[34, 35] While the success rate of dental implants is

considerably high in contemporary dentistry, infection related failure of implants still poses a significant treat to patients.

The primary reasons for the failure of the general synthetic restorations are four-fold in addressing the following specifics:

i. Reinstating the structure and function of the lost tissue;

ii. Structural and functional integration (interface problem);

iii. Thermal, mechanical and chemical durability;

iv. Tissue toxicity and low biocompatibility.

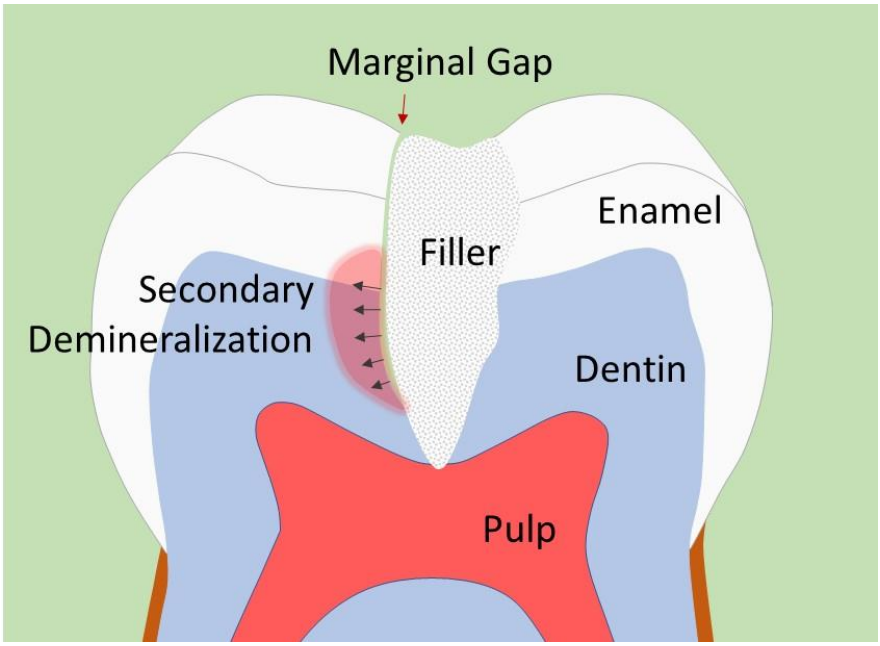


**Figure 3:** Schematic representation of marginal gap formed at the tissue-material interface causing secondary caries due to prolonged bacterial subsurface activity.

*The lack of structural integration* stems from the interface mismatch between dental tissues and restorative materials. Existing synthetic restorative materials, e.g., ceramics (zirconia), metals (titanium alloys), glass ionomers, resins, and polymers, have highly distinct physical (crystallography and morphology) and chemical (elemental compositions and compound phases) properties compared to the underlying tooth structure. Complete integration of these materials with

the natural hard tissues, therefore, cannot be established at the interfaces of these restorative materials and the existing tooth structure for simple reasons based on the thermodynamic and kinetics incompatibilities (such as mismatch of phase compatibilities, atomic and molecular structures, and elemental compositions).[36-39] These synthetic restorative materials eventually decouple from the teeth (**Figure 3**), which often leads to leakage of toxic ingredients to the surrounding tissues and causes more serious health problems..[40, 41]

*The lack of functional integration,* on the other hand, is related to the differences between the material properties of dental tissues and restorative materials such as thermal expansion coefficient, hardness, elastic modulus and toughness (**Figure 3**). In order to effectively integrate two different materials, there has to be a functional interface which can transfer the mechanical stress e.g., load during mastication or relieve the stress that may develop due to thermal expansion, from one material to another in a non-destructive and durable manner.[42, 43] One biological example that exemplifies a structurally and functionally integrated interface is the dentino-enamel junction (DEJ). The DEJ increases the contact area between the two hard tissues; dentin (tough) and enamel (hard) by forming a transition region across to 2-20 μm between these two phases.[44] This results in dissipation of the interfacial stresses and deflecting possible microcrack paths that may develop. Effective load transfer from the brittle enamel to soft dentin is, thereby, promoted during mastication.[45]

*The lack of thermal and chemical durability* is also another common problem which often prevents the application of resin-based dental restorations in dentin.[46, 47] Disintegration of these materials may evoke an inflammatory response and cause acute tissue toxicity.[48]

*Biomimetic Approach:* So far, there is still no universal therapy/material that can be used to restore the structure and function of the dental hard tissues. It is, therefore, desirable to generate novel

approaches that overcome current limitations of synthetic restorative materials. An ideal approach would be biomimetically developed replacement materials and regeneration therapies for dental hard tissues including enamel, dentin, cementum and bone, that mimic biological remineralization processes of saliva leading to self-driven tissue repair where the materials involved are biogenic and the structures developed are biomimetic. The common denominator in the proposed approach is to enable and guide natural biomineralization processes *in situ* on dental defects by forming an integrated interface with the underlying tissue while providing long-term durability.[1, 49] The proposed thesis research provides materials and methods to address the four-pronged questions highlighted above while providing potent formulations and procedures.

*Traditional Biomimetic Approaches and Their Limitation:* Within the last decade, numerous approaches have been developed in an attempt to reproduce biological minerals and tissues for biomimetic replacement therapies.[50-55] Among these, traditional biomimetic approaches aim to control mineral formation by using isolated proteins which are known to have regulatory roles in natural mineralization.[56, 57] These studies involve use of tissue-specific extracellular matrix (ECM) e.g., full-length amelogenin, dentin matrix protein 1, matrix metalloproteinase 20 (MMP-20), leucine-rich amelogenin protein (LRAP), and a variety of scaffolds e.g., agarose, polyacrylamide, chitosan.[50, 51, 58-60] However, the major drawback of this traditional approach is the limited ability to control mineral directing proteins under *in vitro* conditions. Being very sensitive to environmental changes e.g., pH, solvent, and ionic content and concentrations, these isolated proteins are prone to catalytic inactivation due to rapid degradation. In addition, the extraction and purification of these proteins requires highly optimized and strictly controlled labor-intensive procedures which often cause them to be far from feasible to utilize as a therapeutic and technological product.[54, 55, 61, 62]

*The Scientific Basis of the Thesis Approach:* As an alternative route towards eliminating such inherent disadvantages, solid binding peptides (also called GEPIs, Genetically Engineered Peptides for Inorganics) have emerged as a molecular tool to control biomimetic synthesis of minerals as well as to develop novel engineering materials.[63-65] These peptides are isolated through a process called combinatorial mutagenesis, first adapted in Sarikaya Lab, here at the University of Washington, and have been shown to exert material specific affinities to a variety of inorganic materials including metals, semiconductors, minerals and more recently two-dimensional atomically thin materials.[65-67] In this approach, randomly generated peptide sequences (usually 7- or 12-AA in length) are displayed on the surface of individual viral- or bacterial hosts. After exposing the complete peptide library to an inorganic target, peptide sequences with specific affinity to the targeted inorganic material are isolated through a process called biopanning which involves repeated rounds of washing, elution and amplification steps. The isolated host organisms are then subjected to DNA sequencing and the corresponding peptide sequences displayed on the host surfaces are identified. The number of peptide sequences identified through a complete round of combinatorial mutagenesis selection ranges from 40+ to 90+ sequences.[67, 68] The specific inorganic material binding affinities of individual peptides are determined via a series of characterization methods including spectrophotometric and fluorescent microscopy-based assays, surface plasmon resonance spectroscopy, quartz crystal microbalance, scanning probe microscopy. The ability of these sequences to control and enable mineralization is also characterized through targeted mineralization assays, which involve variety of characterization tools e.g., spectroscopy, electron microscopy and XRD. So far, our group and others have identified solid binding peptides specific to different inorganic materials and

demonstrated their utility for a variety of medical, nanotechnological, therapeutic and catalytic/synthesis applications.[69-71]

Besides their utility to engineer bio-solid interfaces to create novel hierarchically assembled biological devices, a considerable number of these peptides also presented remarkable catalytic capability during the biological synthesis of metals and minerals such as gold, silver, calcite, aragonite as well as hydroxyapatite. [54, 72, 73]

In particular, there are more than 150 different hydroxyapatite binding peptides (HABP's) (also called 1st generation peptides) isolated using phage-display libraries. Among these 150+ peptides, two peptides, namely HABP1 (high affinity) and HABP2 (low affinity), were further characterized in detail in terms of their influences on the formation of hydroxyapatite *in vitro*. These peptides demonstrated ability to control the rate of calcium-phosphate mineralization and the morphology and phase of the end mineral, hydroxyapatite. The molecular conformation analysis was also provided using molecular dynamic tools and circular dichroism.[54, 74]

In addition to mineralization in aqueous solution, the HABP's were also utilized for other biotechnological and medicine applications. For instance, the specificity of HABP1 peptide to hydroxyapatite mineral was exploited by chimerizing it with green-fluorescent protein (GFPuv) to create a hetero-functional fluorescent probe to target *in situ* mineralization and demineralized areas in the hard tissues.[75, 76] In another case study, a biogenic peptide based hydrogel was designed as a therapeutic agent especially for rapid healing of vertebral disc injuries and chimerized with HABP1 to enable *in situ* self-mineralization and healing.[74]

Following, the first-generation combinatorially selected peptides were used to design second-generation peptides through knowledge-based design. With this aim, two scoring matrices were designed for each set of first-generation peptides, HAp12I (for 12-AA long peptides) and

HApC7CI (for 7-AA long peptides). A new scoring matrix was designed by modifying the Point Accepted Mutation 250 (PAM 250) matrix to compensate for the relative abundance of amino acids within the phage-library and the codon usage of the host organism that is used to amplify the phages during the biopanning process. The second-generation peptides were identified based on the similarities between the strong, moderate and weak HABP's using these matrices. [66, 77]

Another important step towards creating highly effective biomineralizing peptides was achieved by designing the third-generation peptides beyond the combinatorically selected first generation and computationally designed second generation peptides for HA biomineralization. A novel algorithm has been developed to create protein-derived peptides by identifying the similarities between natural proteins and 1st- and 2nd-generation peptides. The recombinant mouse 180 amino acid long amelogenin (rM180) was selected as a first case study. Using this algorithm, 32 specific amino acid domains (each containing 15-40 amino acids) within the amelogenin protein (180 amino acid-long) were identified based on the similarities with a set (155 sequences) of HAp-binding peptides (HABPs) selected and designed previously. Briefly, the amelogenin was divided into short segments (7- and 12-AA in length) and each segment was compared and scored with each peptide (155 in total) through an iterative process. The regions that exhibited high similarity and low similarity scores against peptides were overlapped and identified as a single domain. Following, identified regions were further refined by protein structure prediction, calcium ion-binding domain predictions and meta-functional signature analyses. As a result, 8 different peptide domains were identified and named as Amelogenin-derived Peptides (ADP's).[55]

*The Specifics of the Proposed Approach and Focused Task Areas:* Within the set of these ADPs, one particular 22-amino acid long domain, called ADP5 was shown to facilitate cell-free and fast formation of a mineral layer on demineralized human root dentin. By containing the essence of

amelogenin, the key protein in enamel development, this peptide was shown to have catalytic functions on capturing the constituent ions, synthesizing the mineral and controlling its morphology on the surface of the tooth. The mineralized layer that is formed by the control of ADP5 was shown to be structurally and mechanically integrated into the underlying dentin, functionally resembling cementum, and to be mechanically and chemically durable.[55, 77]

Building upon molecular biomimetic principles, the hypothesis of this research is that "*Using solid binding peptides, it can be possible to remineralize/repair the dental hard tissues; e.g., dentin, enamel and cementum, and restore the structure and function of the tooth with a well-integrated and durable mineral layer mineral layer which could be administered via variety of formulations such as aqueous, gel and lozenge."*

To demonstrate the validity of this hypothesis, it is anticipated to focus on four main task areas that include;

***Task-I:*** *In vitro Peptide-guided Biomimetic Repair of Hard Tissues (Enamel and Dentin);*

***Task-II:*** *In vivo Peptide-guided Remineralization to Restore Dental Caries (Rat Model);*

***Task-III:*** *Development of Mineralizing Peptide-based Restorative/Therapeutic Dental Care Products (Dental Lozenges);*

***Task-IV:*** *Improving the functionality (preventing risks associated with failure) of implants*.

Briefly, in **Task I** the aim was to demonstrate that small peptide domains derived from amelogenin (ADP's) can be utilized to restore lost mineral on damaged human enamel and dentin *in vitro*. Findings of Task-I were expected to provide a fundamental information that is critical in designing the Task-II studies.

Following successful completion of *in vitro* proof-of-principle demonstration of peptide-guided remineralization, in **Task-II** the aim was to develop an *in vivo* rat caries model to test the efficacy

of peptide-guided remineralization for treating caries *in vivo*. The sub-tasks herein include: (i) development of a gel formulation to facilitate delivery and maximize the retention time of mineralization ingredients on defective tooth surfaces; (ii) development of an animal caries model; and (iii) treatment of the induced carious lesion using the peptide-gel formulation through remineralization.

Building upon these, in **Task-III**, the goal was to translate the remineralization technology (based on earlier findings in Tasks I-II) and develop a therapeutic product, oral lozenge, that can be utilized for daily and clinical remineralization purposes targeting demineralization related dental diseases (WSL, hypersensitivity) and aesthetic conditions (Tooth Staining).

The final task of this dissertation (**Task-IV)** thesis focuses on preventing the infection related failure of dental implants so that lifetime of the implants can be improved by following molecular biomimetic principles through solid-binding peptide based chimeric antimicrobial coatings.

As noted before, when the tooth decay is extended beyond repair or tooth extraction clinically required, implant treatment is one of the common remedies to restore function of the tooth. Although the clinical success implants are considerably high, the post-surgical failure of dental implants due to bacterial infections is still a significant concern. Herein, a series of hetero-functional peptides (solid-binding peptides chimerized with antimicrobial peptides) were developed and used as self-assembling antimicrobial coatings to develop infection-resistant dental implants. The successful completion of these task areas will establish the basis of the peptide-guided remineralization therapy towards developing a universal biomimetic solution for oral care (**Figure 4**).

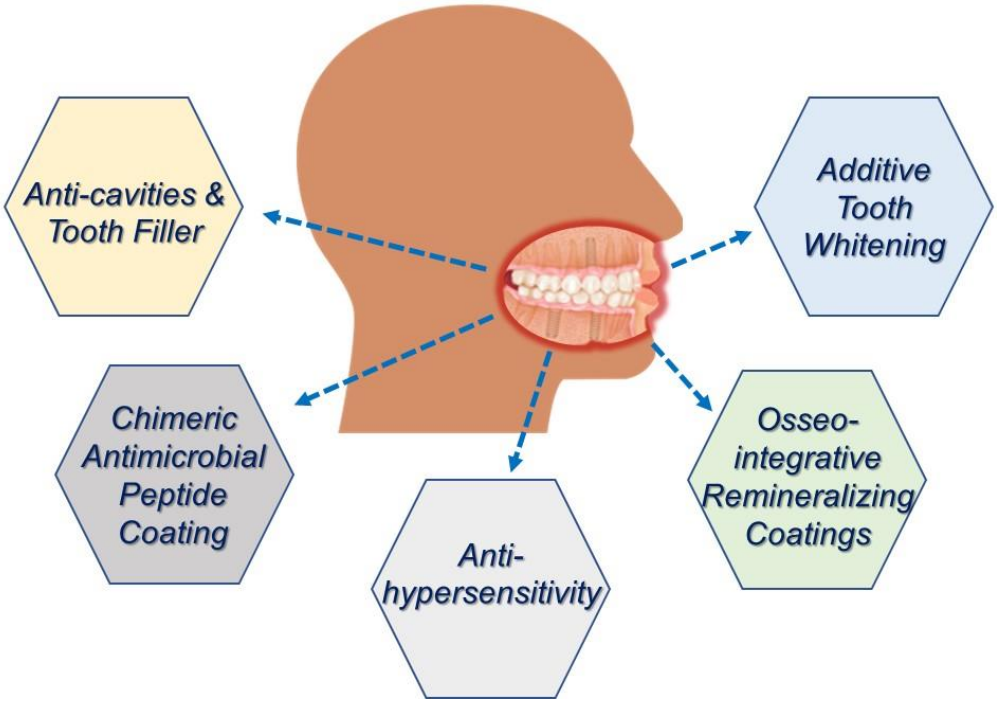


**Figure 4:** Schematics of peptide-guided biomimetic therapies for whole dental care.

Chapter 2: Design Principles and Mechanism-of-Action of Amelogenin-Derived Peptides

*Preamble: Design Principles of Biomineralization Directing Peptides:* Building upon previous studies that involved identification and characterization of 1st and 2nd generation peptides, in this study ADP5 peptide (22-amino acid long) was further engineered to have higher water-solubility by systematic removal of hydrophobic amino residues on each end while preserving the zwitterionic regions. The resulting 15-amino acid long is called shADP5 where "s" and "h" stand for "short" and "human", respectively.[78]

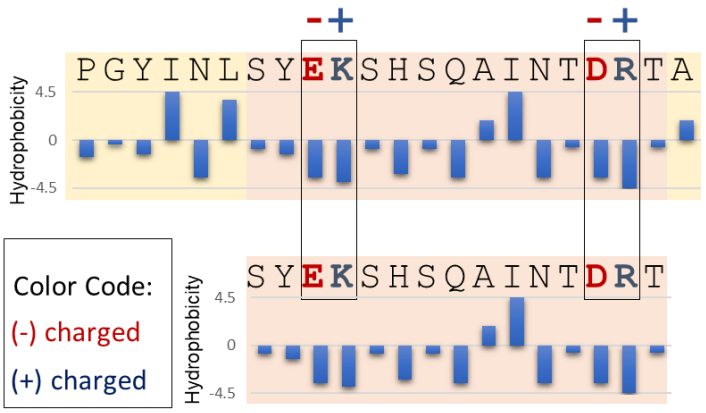


**Figure 5:** Schematic representation of hydropathicity distribution of ADP5 and shADP5.

As described, earlier, amelogenin-derived peptides were identified using a design algorithm that includes experimental selection of HAp-binding peptides (HABP's) isolated from a combinatorial phage display peptide library, which was followed by bioinformatics procedures that involve *de novo* design of peptides based on the similarities between the full-length amelogenin protein (rm180) and experimentally selected peptides (**Figure 6**).[54, 55]

Briefly, 7-AA and 12-AA long hydroxyapatite binding peptides (HABPs) were experimentally selected using the c7c- and 12-phage libraries (New England BioLabs Inc., Ipswich, MA, USA), respectively. Next, the 180 amino acid-long human amelogenin protein (rM180) was divided into 7-AA and 12-AA long segments and each segment was compared with all of the 155 experimentally selected HABPs. The regions with high similarity scores from 7-AA and 12-AA long segments were overlapped, and those coinciding high similarity regions were chosen as the

putative strong binding regions. These computationally determined high similarity regions were then refined to design the ADPs by protein structure prediction, $Ca^{2+}$ ion-binding domain predictions, and meta-functional signature analyses.

As a result, high and low similarity regions in relation to the amelogenin were identified (named as Amelogenin-derived Peptides; ADP's) and synthesized as individual peptides. Two separate assays were developed to characterize the ADPs'; i) Binding affinity to HAp and ii) Catalytic activity over calcium-phosphate mineralization in aqueous solution. Binding analysis demonstrated that the peptides derived from high similarity regions of amelogenin have high binding affinity to hydroxyapatite, whereas those derived from low similarity regions have lower binding affinity.

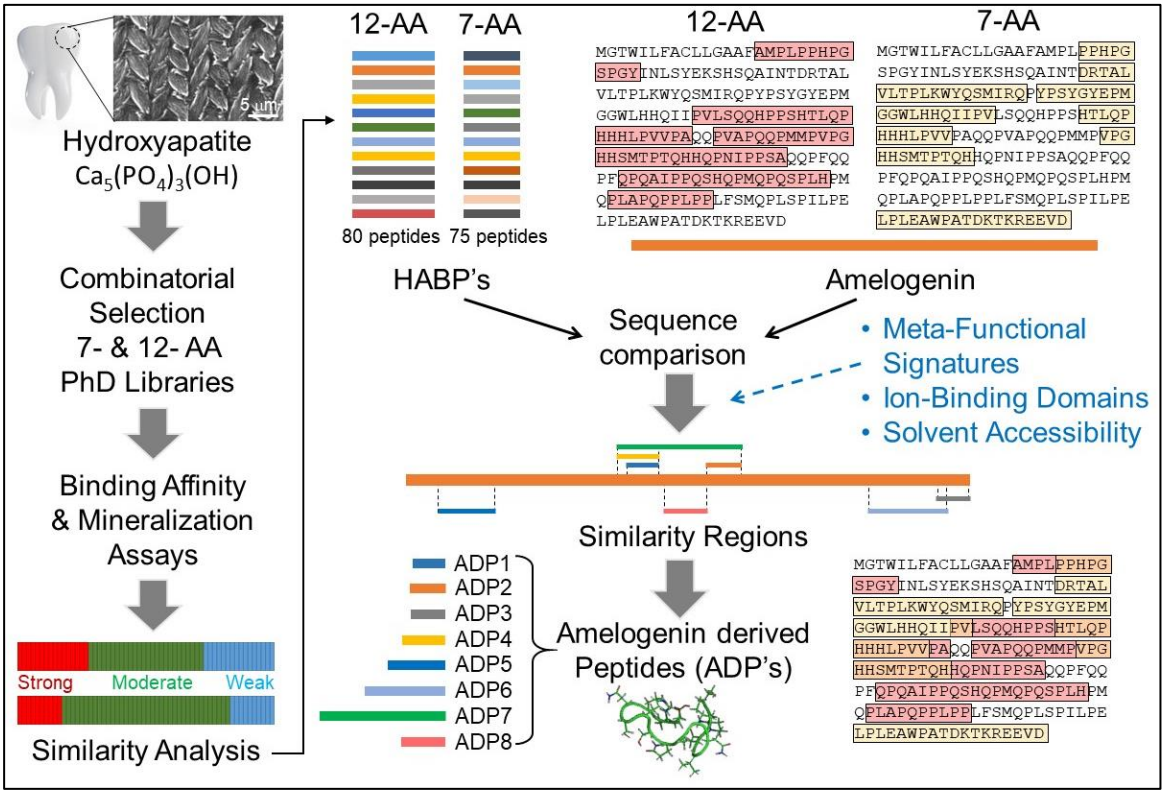


**Figure 6:** Schematic representation of the design-process for developing amelogenin-derived peptide using experimental selection and bioinformatics tools.

*The Mechanism-of-Action of shADP5:* The catalytic activity of the ADPs on calcium phosphate mineralization was studied by monitoring the depletion of soluble $Ca^{+2}$ ions in the mineralization solution, in the absence and presence of peptides. Amelogenin and ADP5 exhibited kinetic patterns of fast mineralization compared to no peptide, where more than half of the free $Ca^{+2}$ was consumed in 90 minutes.[54, 55] As a result, it is demonstrated that although ADP5 has a weaker binding affinity, it exerts the fastest mineralization kinetics that is very close to that of full-length amelogenin. The utility of ADP5 on directing the mineralization on the tooth surface was investigated in a case study that aims to remineralize human root dentin. The extracted dentin surface was coated with the peptide for 10 minutes and then placed into artificial saliva supplemented with 4.8 mM calcium and 2.88 mM phosphate precursor ions for 1 hour. As a result, a new mineral layer is formed which is well-integrated into the underlying sound dentin.[55]

Taken together, the ability of peptide to control calcium phosphate mineralization on the tooth surface suggests that peptide may have multiple functions; i) Binding function that enables recruiting the precursor ions onto the tooth surface and ii) Catalytic function that directs the formation of new mineral layer on the tooth surface.

**Figure 7** below depicts the possible mechanism-of-action of the peptide on tooth surface where 1) peptide binds to tooth minerals, and then self-organizes and covers the surface, 2) recruits the precursor ions, Ca and $PO_4$, towards the surface and 3) catalyzes the mineral formation resulting in a uniform mineral layer that grows as a continuum of the existing surface by establishing a coherent, well integrated interface (also called primary mineralization).

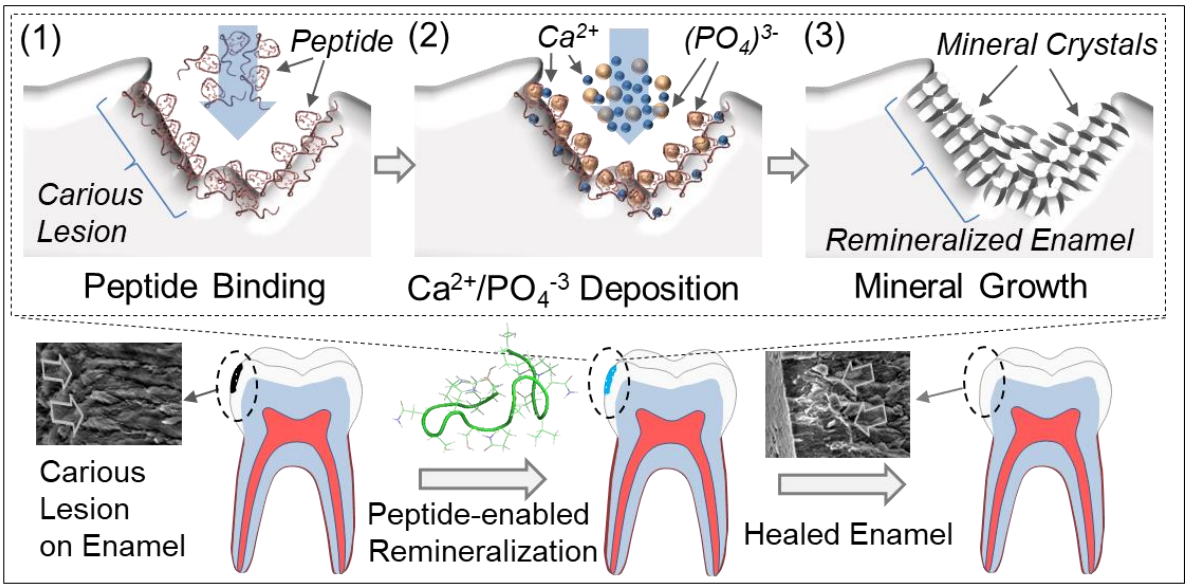


**Figure 7:** Schematic representation of the mechanism of action of shADP5.
(Reprinted from reference 72. Copyright (2018) of American Chemical Society)

A possible explanation for this catalytic behavior of the peptide could be that peptide can attract the free calcium and phosphate ions and thereby create a local supersaturation (i.e., binding affinity). Next, the subsequent interaction may involve conformational changes on the peptide resulting in a structural configuration that could stabilize the calcium phosphate clusters and thus lower the activation energy for nucleation and onset of the mineral growth.

The classical nucleation theory (CNT) can be used to understand the mineralization behavior of the peptide. Based on the classical nucleation theory, the activation energy for nucleation can be calculated as shown in Equation 1;

$$\Delta G = (\frac{4}{3}\pi r^3 \Delta G_v) + (4\pi r^2 \gamma) \quad (1)$$

where the bulk energy ($\Delta G_v$) of a nascent nucleus drives nucleation, whereas the generation of a phase interface and therefore the interfacial tension ($\gamma$) hampers nucleus growth (shown in **Figure 8**). It is noted that in this expression, the free energy (has a negative value) decreases with the third

power of radius. Therefore, the bulk energy begins to balance the energetic costs due to the generation of a phase interface. The activation energy at critical radius ($r_c$) can be expressed as;

$$\Delta G^* = \frac{16\pi\gamma^3}{3(\Delta G_v)^2} = \frac{16\pi\gamma^3 v^2}{3(kTlnS)^2} \quad (2)$$

Herein, the activation energy that is required for clusters to reach critical size to form stable nuclei, can be lowered by either decreasing the interfacial tension ($\gamma$) and/or increasing the saturation (S) in the solution.

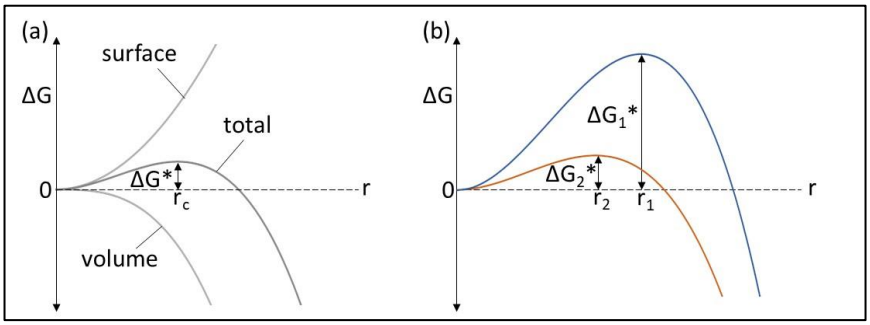


**Figure 8:** Free energy versus radius of nuclei in CNT. (a) Summing up the bulk (volume) energy and the surface energy, nuclei that are larger than the critical size ($r_c$) can grow. (b) Free energy versus radius of nuclei in the presence (orange line) and absence (blue line) of peptide.

As indicated by the Molecular Dynamics simulations (Schrödinger™, Desmond package) shown in **Figure 5 and 9a**, the zwitterionic residues located on the both ends of shADP5 (EK and DR) initially attract the calcium and phosphate ions (Figure 9b-d) and thereby create a local supersaturation within a proximity of the peptide. Next, peptide undergoes a conformational change and folds over the calcium phosphate pre-cluster (Figure 9e). This new structural configuration stabilizes the calcium phosphate seed crystal (Figure 9f) and maintains its own conformation until morphogenesis (Figure 9g). Taken together, the initial electrostatic interactions and conformational changes adapt the nuclei to lower the activation energy for nucleation and drive the mineral growth.

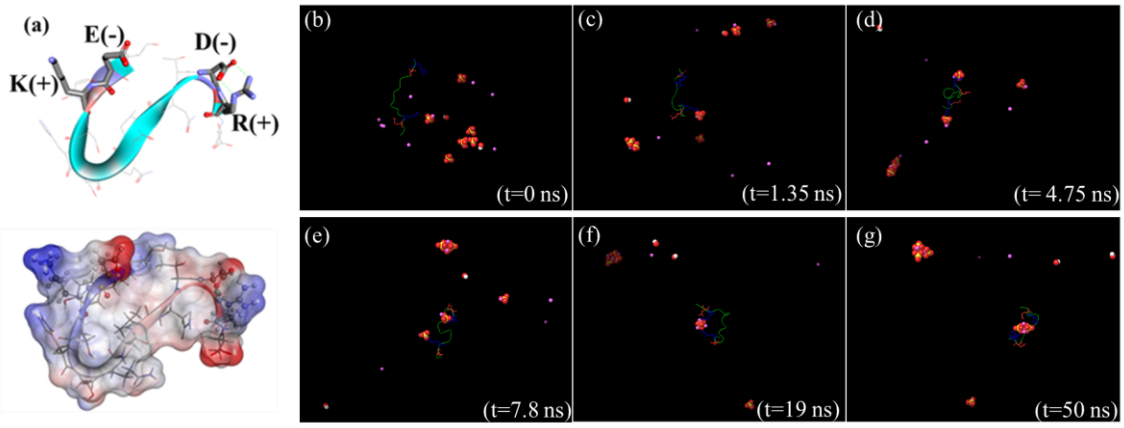


**Figure 9:** (a) Molecular structure of shADP5 obtained from molecular dynamics (MD) simulations. The MD simulations of the shADP5 in the presence of precursor calcium and phosphate ions. Frames captured at (b) t=0 ns, (c) t=1.35 ns, (d) t=4.75 ns, (e) t= 7.8 ns, (f) t=19 ns, and (g) t=50 ns. Simulation was performed with OPLS3e force field (Schrodinger Desmond package) under TIP3P water model and NVT microcanonical ensemble at 300K for 50 ns. Minimization was performed with the steepest descent algorithm and initial structures were obtained from Monte Carlo-based torsional sampling.

In the presence of a tooth surface, heterogenous nucleation is the dominant mechanism for the mineralization as the activation energy for nucleation is lowered due to the reduction of surface free energy ($\gamma$). Herein, the surface defects are the favorable regions for mineralization due to the reduced free energy.

**Figure 10** shows scanning electron microscopy images of an extracted human dentin specimen treated with 4.8 mM calcium and 2.88 mM phosphate (in Tris Buffer) for one hour, in the presence (Figure 10a) and absence of shADP5 (Figure 10b). As shown in Figure 10a, when the specimen is preincubated with the peptide to cover the surface, mineralization takes place uniformly and establishes a continuous mineral layer over the tooth surface. However, in the absence of peptide, the mineralization takes places in discrete sites creating patches of mineralized regions (Figure 10b). A possible explanation for this behavior could be that when the tooth surface is covered with the peptide, peptide molecules collectively recruit the ionic calcium and phosphate from the

solution to the surface and drive the formation of nuclei over the entire tooth surface in a uniform fashion. However, in the absence of a peptide, surface cracks are the favorable site on the tooth surface for heterogenous nucleation and the nuclei preferentially form over these regions and thereby result in formation of non-mineralized and mineralized regions.

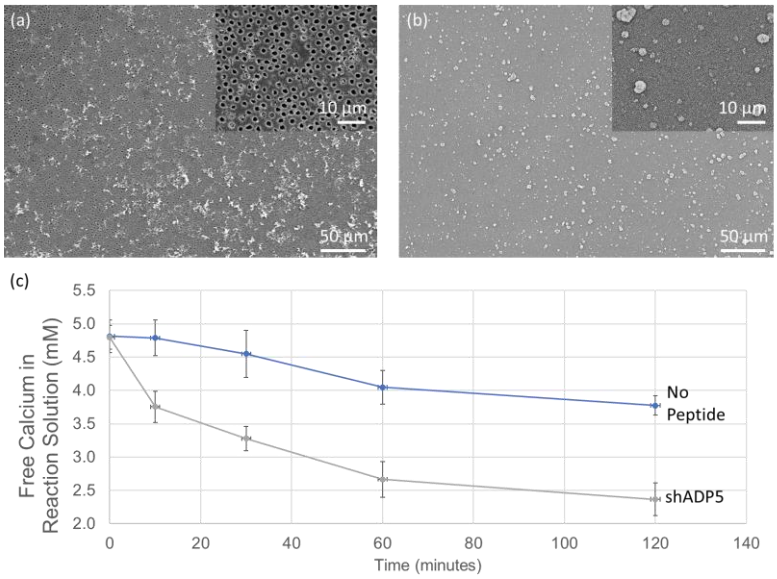


**Figure 10:** Scanning electron microscopy images of etched dentin surface treated with mineralization solution for 1 hour in the (a) presence and (b) absence of peptide. (c) Calcium consumption assay showing the depletion of free calcium ions in the biomineralization solution in the presence (gray) and absence of shADP5 (blue).

Chapter 3: *In vitro* Peptide-guided Biomimetic Dental Hard Tissue Remineralization

*Preamble: The Preliminary Demonstration of Biomineralization Action of shADP5 in Forming a Mineral Layer on Enamel and Dentin Tissues*

White spot lesions/incipient caries and dental hypersensitivity are the earliest clinical outcomes of demineralization and cavities. If left untreated, these lesions can progress and may cause complex restorative procedures or even tooth extraction which destroy soft and hard tissue architecture as a consequence of connective tissue and bone loss. Current clinical practices are still insufficient in treating these dental problems. A long-standing practical challenge associated with demineralization-related dental diseases is incorporating a functional mineral microlayer which is fully integrated into the molecular structure of the tooth.

In this chapter (Task I) the aim was to demonstrate that small peptide domains derived from amelogenin (ADP's) can be utilized to restore lost mineral in dental tissues, e.g., enamel and dentin, and reinstate the structure and function of the tooth. With this purpose, efforts were devoted to establish a method for biomimetic treatment of two common dental problems in two different case studies; (i) Incipient caries representing enamel lesions and (ii) Dental hypersensitivity representing demineralized dentin lesions (**Figure 11**). Findings of this study are expected to provide fundamental information that is critical in designing the Task-II study.

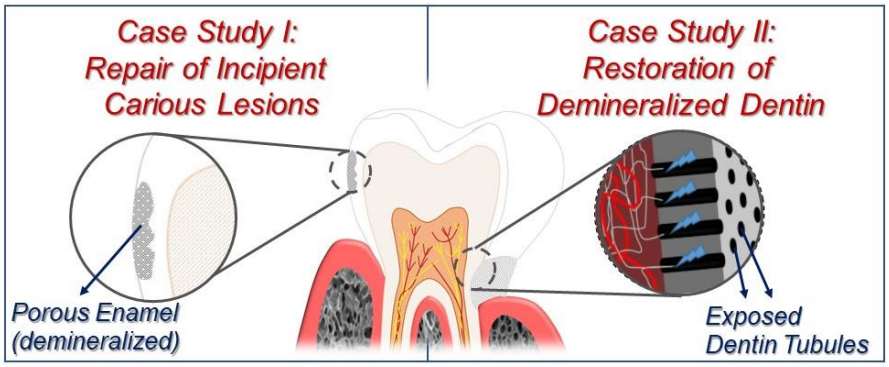


**Figure 11:** Schematic representation of incipient caries and dental hypersensitivity.

### 3.1. *In vitro* Biomimetic Repair of Incipient Caries in Human Enamel

#### 3.1.1. Introduction

*Statement of the Problem*:

Dental caries is one of the major public health problems and it is a highly prevalent disease among the global population.[1] Incipient caries and white spot lesions (WSL) as well as hypersensitivity, are the earliest clinical evidence of enamel demineralization and dental caries.[79] Caries forms when tooth enamel is exposed to acid produced by cariogenic bacteria. As a result, acid diffuses into surface enamel and dissolves hydroxyapatite (HAp) mineral. Due to its non-regenerative nature, enamel is unable to heal and repair itself post-demineralization.[49, 80]

*Current Approaches:*

Traditionally, fluoride (F) has been used as the key agent in prevention of caries. Fluoride functions primarily *via* topical mechanisms.[81-84] It is believed that fluoride forms a thin layer of new but harder mineral, namely fluorapatite (FAp) which is incorporated into the existing HAp mineral on the tooth surface.[84] There is a trend of enhancing the remineralization effect of fluoride with calcium and phosphate supplementation in high risk individuals.[85-90] Although controversial, the use of fluoride products remains the primary treatment modality for caries prevention and remineralization, with major limitations regarding the efficacy of these products for the reversal or prevention of dental caries. Fluoride delivery systems, therefore, are not sufficient to overcome the high caries risk, especially in younger and elderly populations.[91]

Despite dental caries being a preventable infectious disease,[92] oral health promotion and prevention can fail due to many factors.[93] The advanced cavitation of the carious lesion necessitates restoring the tooth with materials such as metals, composite resins and ceramics to replace the lost enamel or, even, dentin. However modern dental materials to repair cavitated

carious lesions are not compatible with biological tissues at the lesion/restorative material interface mainly because of their physical (crystallography and morphology) and chemical differences (elemental compositions and phases) compared to the natural tooth structure.[38] Even though treatment of early caries lesions by the application of various types of nano-sized HAp or $CaPO_4$ with or without F has received considerable attention, their clinical validation is still lacking.[94-97] Low solubility of the calcium phosphates, particularly in the presence of fluoride ions, is the main difficulty with the clinical application of remineralization. Using biomimetic pathways, a considerable number of attempts have been made to form a remineralized layer on the surface of enamel or dentin, or even cementum, to repair or reconstruct the lost mineral and hence, restore the original structure and the resulting function.[51, 55, 58, 77, 98-103] These studies included the use of full-length amelogenin,[51, 58, 99-101] LRAP,[102] peptides,[100, 101] dendrimers,[103] and physical chemistry approaches.[51, 99-103] These studies contributed to the general knowledge of tooth surface remineralization; so far, however, no clinical remineralization system has emerged to promote biomimetic enamel remineralization *in vivo*.

*The Proposed Approach:*

A novel protocol was developed recently to identify peptide sequences from native proteins with the potential to repair damaged dental tissues by biomimicking HAp biomineralization.[55] Using a newly developed bioinformatics scoring matrix,[77] specific amino acid domains (each containing 15-40 amino acids) within the amelogenin protein (rM180, 180 amino acid-long) were identified based on the similarity with a set (155 sequences) of HAp-binding peptides (HABPs) which were originally selected by 7-AA and 12-AA phage display peptide libraries.[54] Among these amino acid domains, referred to as amelogenin-derived peptides (ADPs), a 22-amino acid long peptide, ADP5, was shown to facilitate cell-free and fast formation of a mineral layer on demineralized

human root dentin. Dubbed as cementomimetic layer, the newly formed mineralized coating was found to be structurally and mechanically integrated into the underlying dentin, resembling cementum and is mechanically and chemically durable as well as biogenic, allowing PDL cells to attach, grow and proliferate.[55] The ADPs in general, and ADP5, in particular, epitomize the unique features of the natural protein amelogenin, the key protein in enamel formation[104-106] especially in the enzymatic function of capturing the constituent ions, synthesizing the mineral and controlling its morphology on the surface and the root of the tooth.

Incorporating a functional and biomimetic mineral layer to the molecular structure of the tooth to repair damaged enamel tissue has been a long-standing challenge. A better understanding of peptide-guided remineralization on human tooth and, therefore, the ability to control the mineral layer properties, with no, low or high-F content, has enormous clinical implications to restore enamel and other dental hard tissues. As a major step towards this overarching goal, the objective of this study has been to develop an *in vitro,* cell-free, natural remineralization model on artificially induced enamel lesions. Because of its unique biomineralization characteristic and its short and simple sequence, shortened ADP5 (shADP5) has been used in this research as the active ingredient in solution for the formation of mineralized layer. The work presented herein could eventually form the foundation of developing clinical treatments for the restoration of early stage cavities, e.g., incipient caries, white spot lesions, and hypersensitivity.

### 3.1.2. Materials and Methods

*Sample Preparation and Test Groups:*

Extracted human molar teeth with no visible white spot lesions, caries, or any other kind of restorations were collected from dental clinics around the King County area (WA, United States) and disinfected in 10% aqueous bleach solutions. [Human Subject Division (University of

Washington) approved the application for nonidentifiable specimen use on 04/19/2016. It should be noted that for the extracted teeth, the identification of the patients was not made and, therefore, approval from the ethical committee was not needed.] Prior to the experiments, the teeth were cleaned to remove visible blood, gross debris, and soft connective tissue using a dental scaler under a light microscope.

**Table 1:** Experimental Test Groups and Mineralization Treatments.

| Test Groups | Treatment | # of Samples |
|---|---|---|
| Group-1 (Negative Control) | No Treatment | 5 |
| Group-2 ($Ca^{+2}$ / $PO_4^{-3}$ only) | 4.8 mM $Ca^{+2}$ / 2.88 mM $PO_4^{-3}$, 1 hour | 5 |
| Group-3 (Fluoride - Low Conc.) | 1100 ppm F (common fluoridated toothpaste concentration), 4.8 mM $Ca^{+2}$ / 2.88 mM $PO_4^{-3}$, 1 hour | 5 |
| Group-4 (Fluoride - High Conc.) | 20000 ppm F (Clinical F-Varnish concentration), 4.8 mM $Ca^{+2}$ / 2.88 mM $PO_4^{-3}$, 1 hour | 5 |
| Group-5 (shADP5 & $Ca^{+2}$ / $PO_4^{-3}$ & Fluoride - Low Conc.) | 1. 0.8 mM Peptide, 10 minutes<br>2. 1100 ppm F + 4.8 mM $Ca^{+2}$ / 2.88 mM $PO_4^{-3}$, 1 hour | 5 |
| Group-6 (shADP5 & $Ca^{+2}$ / $PO_4^{-3}$) | 1. 0.8 mM Peptide, 10 minutes<br>2. 4.8 mM $Ca^{+2}$ / 2.88 mM $PO_4^{-3}$, 1 hour | 5 |

*Formation of Artificial Lesions:*

Enamel was demineralized to create artificial lesions to mimic white spot lesions and/or incipient caries using a protocol as outlined in **Figure 12**. The teeth were covered by lacquer leaving a 4-mm wide square window in the enamel close to cemento-enamel junction. The exposed areas of 4x4 mm enamel were treated with a cocktail of acetic acid/$CaCl_2$/$KH_2PO_4$ for 2 weeks to establish up to 200 µm deep artificially created non-cavitated white spot lesions (WSL).[107-109] Specifically, lesions were produced by daily cycling at 37ºC between demineralization and neutral solutions for 6 hours and 17.5 hours, respectively. Demineralization solution was made of 1.2 mM $KH_2PO_4$

(USB Corporation, Cleveland, OH, USA), 2.0 mM $CaCl_2$ (Johnson Matthey Inc., Seabrook, NH, USA) and 75 mM acetic acid (EMD Chemicals, Savannah, GA, USA) in deionized water at pH 4.2. Neutral solution was made of 0.9 mM $KH_2PO_4$ (USB Corporation, Cleveland, OH, USA), 1.5 mM $CaCl_2$, 150mM KCl (Johnson Matthey Inc., Seabrook, NH, USA) in 20 mM Tris (EMD Chemicals, Savannah, GA, USA) buffered at pH 7.0. The demineralization solution was replaced daily. Samples were then divided into control and test groups. Test groups were treated either with peptide, fluoride, or combination of both (**Table 1**).

*Peptide Design and Synthesis:*

The peptide shADP5, shortened ADP5, was generated using a procedure that was developed for designing protein-derived peptides, as described. (**Table 2**) Peptide was synthesized by using an automated solid-phase synthesizer (CS336X; CS-Bio, Menlo Park, CA, USA) through *Fmoc*-chemistry. In this procedure, in the reaction vessel, the Wang resin (Novabiochem, West Chester, PA, USA), was treated with 20% piperidine in dimethylformamide (DMF, Sigma-Aldrich, St. Louis, MO, USA) to remove the preloaded *Fmoc* group. Next, the incoming side chain

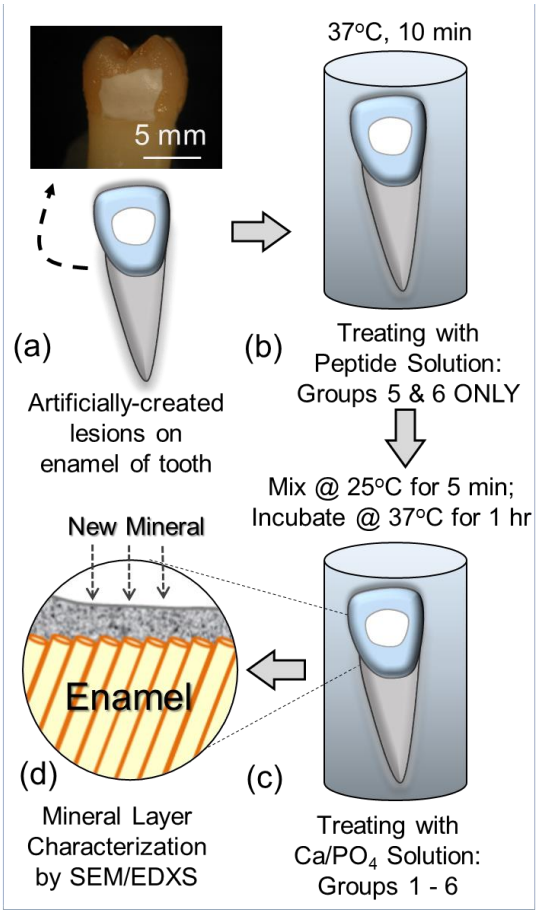


**Figure 12**. (a) White spot lesion was artificially created by exposing a window on tooth surface for demineralization; (b) Group 5 & 6 samples were exposed to shADP5 solution for 10 minutes at 37°C; (c) Samples were then incubated in $F/Ca^{2+}/PO_4^{3-}$ or $Ca^{2+}/PO_4^{3-}$ solutions for 1 hour at 37°C; (d) New mineral layer was characterized structurally and mechanically.

protected amino acid was activated with N,N,N′,N′-Tetramethyl-O-(1H-benzotriazol-1-yl)uronium hexafluorophosphate (HBTU; Sigma-Aldrich, St Louis, MO, USA) in DMF, and then transferred into the vessel where it was incubated with the resin for 45 min. After washing the resin with DMF, this protocol was applied for the addition of each of the next amino acids and the synthesis reaction was monitored by UV-absorbance at 301 nm. Following synthesis, the resulting resin-bound peptides were cleaved and the side-chain de-protected using reagent-K [TFA/thioanisole/$H_2O$/phenol/ ethanedithiol (87.5:5:5:2.5), Sigma-Aldrich, St Louis, MO, USA] and precipitated by cold ether. Crude peptides were purified by RP-HPLC with up to >98% purity (Gemini 10u C18 110A column). The sequence of the peptides was confirmed by MALDI-TOF mass spectrometry with reflectron (RETOF-MS) on an Autoflex II (Bruker Daltonics, Billerica, MA, USA).

**Table 2:** Molecular characteristics of the peptide shADP5.

| shADP5 (AA sequence) | MW | pI | G.R.A.V.Y. | Charge |
|---|---|---|---|---|
| SYEKSHSQAINTDRT | 1736.8 | 6.47 | -1.627 | 0 |

*Remineralization Protocol:*

Prior to remineralization, samples requiring peptide treatments (Groups 5 & 6) were incubated in 50 μL of 0.8mM peptide dissolved in 50 mM Tris Buffer Solution (TBS) (pH:7.4) for 10 minutes at 37°C. Next, treatment samples were placed into 50 mM TBS containing $Ca^{2+}$ / $PO_4^{3-}$ (Groups 2, 5) or $Ca^{2+}$ / $PO_4^{3-}$ / $F^-$ (Groups 3, 4, 6) at concentrations as listed in Table 1 for 1 hour at 37°C, then rinsed with de-ionized (DI) water, dried by forced air and stored at room temperature until characterization.

*Sample Characterization by SEM and EDXS Analyses – Imaging and Elemental Composition*:

After remineralization experiments were completed, secondary electron imaging (SEI) in the scanning electron microscope (SEM) was used to characterize the surface morphology and to show the thickness of the newly formed mineral layer in cross-sections where applicable. Specimen preparation for SEM involved cutting a notch on the back side using a low speed saw (IsoMet$^{TM}$, Buehler, Lake Bluff, IL, USA) before they were subjected to WSL formation and remineralization as described above. After the remineralization step was completed, specimens were rinsed with DI water, air dried gently (<5 PSI), then carefully fractured into 2 pieces along the notch. One of the fractured pieces was mounted on a SEM stub with the mineralizing surface facing up for imaging the surface morphology and second piece was mounted with the cross-section facing up to show the thickness of the mineral layer. Mounted specimens were then stored in vacuum for at least 2 hours to remove residual moisture and were then sputter coated with 5-nm thick platinum (SPI-Sputter Module Coater, SPI Supplies, West Chester, PA, USA). SEM characterization was performed using a FEI Sirion microscope (Sirion, FEI, Hillboro, OR, USA) operating at 10kV acceleration voltage. The chemical composition was measured by an onboard energy dispersive X-ray spectroscopy (EDXS) system (X-Max$^{N}$ Si drift detector with AZtecEnergy software package, Oxford Instruments, Abingdon, Oxfordshire, UK). The measurements for each group were pooled from 5 specimens per group. The average values and standard deviations were calculated and expressed as the mean ± standard error. Possible mineral phases were deduced from these EDXS measurements. It should be noted that given the energy resolution of the instrument and topographical variations, precision of the EDXS measurements was > 2%.

*Structural Characterization by Transmission Microscopy (TEM):*

After remineralization steps were completed, TEM samples were collected by carefully shaving off the top most surface of the remineralized layer from the artificially created white spot lesion using a clean razor blade. The shaved particles were suspended in 100% ethanol, and the suspension was drop-casted onto a carbon coated TEM grid, which was then vacuum dried before TEM characterization. TEM bright field imaging (BF) imaging and diffraction were carried out using a FEI Tecnai TEM (FEI, Hillboro, OR, USA) operating at 200keV.

*Mechanical Properties Characterization:*

Similar to SEM specimen preparation, tooth samples were notched from the back of the tooth before remineralization, then fractured along the notch. The specimens were then mounted in a room temperature-cure epoxy, and the cross-section of the fracture was polished to 0.1 μm finish using diamond lapping films (Allied High-Tech Products Inc., Rancho Dominguez, CA, USA). Nanoindentation measurements were made using a Triboindentor nanoindentation system (Hysitron Inc., Minneapolis, MN, USA) in air. Hardness ($H$) and elastic modulus ($E_r$) were determined by the software accompanying the nanoindentation unit.[110-112] In order to obtain the values that were not indentation volume dependent, maximum indentation depth for all measurements was kept at 120 ± 10 nm. All reported $H$ and $E_r$ values were averaged over 20 measurements.

In addition to nanoindentation measurements, microhardness testing was also performed on the surface to quantitatively assess the mechanical properties of the mineral layers with larger areas and volumes including the underlying enamel as a composite. The microhardness measurement was performed at room temperature using Vickers indenter on a Wilson Hardness Tukon 1202

microhardness tester at 10kg applied load (Illinois Tool Works, Lake Bluff, IL). At least 20 measurements per group were recorded for obtaining an average and statistical analysis.

3.1.3. Results

*Structural Characterization and Elemental Composition Analysis:*

The incubation of samples in demineralization cocktail exposed enamel rods on the surface of the samples before the remineralization treatment was undertaken, as shown in Group 1-Negative Control (**Figure 13a-b**). Elemental compositional analysis of the surface by EDXS gives a ratio of $Ca^{2+}/PO_4^{3-}$ 1.56 ±0.12 (Figure 13c). As seen in the cross-sectional view of (Figure 13d), well aligned enamel rods of ~3 µm diameter extend to the exposed surface where they display HAp crystallites constituting the rods. After 1-hour of exposure to $Ca^{2+}/PO_4^{3-}$ solution, no substantial remineralization was observed on the samples in Group 2. Considering that the imprints of enamel rods remained visible as shallow depressions on the enamel surface (Figure 13e-f, delineated with circles) any possible deposit of solid material, possibly the result of $Ca^{2+}$ and $PO_4^{3-}$ ions reacting to form an amorphous deposit, remained extremely thin. In fact, a very thin (<1 µm) layer

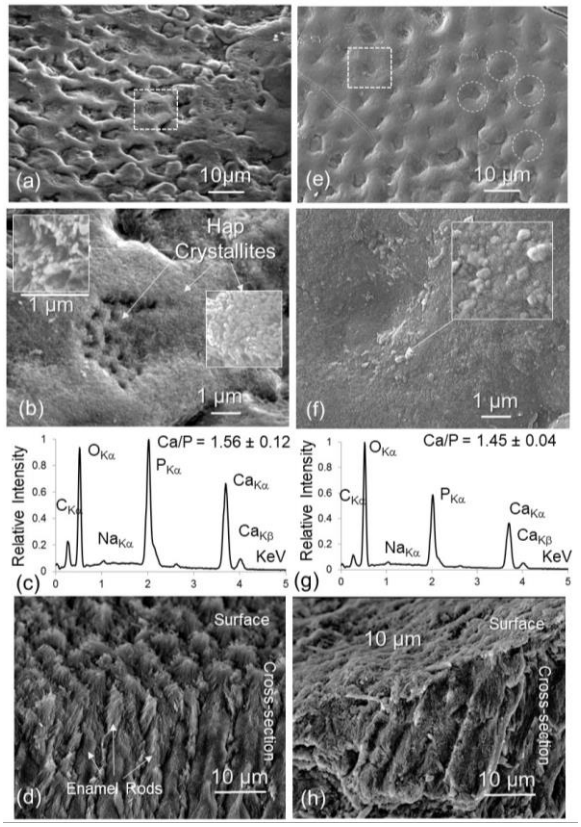


**Figure 13:** Face-on (a, b) and edge-on (d) SEM images and EDXS analyses (c) of Group 1: Negative Control. Face-on (e, f) and edge-on (h) SEM images and EDXS analysis (g) of Group 2: $Ca^{2+}$ and $PO_4^{3-}$ only. Insets in 2b and 2f show enamel rods and HAp plate-like crystallites exposed on the surface of damaged enamel as a result of demineralization. The inset panels are 1 µm x 1 µm.

is barely visible in the SEM image of the cross-sectioned sample shown in Figure 13h. Elemental analysis of the surface by EDXS gives a ratio of $Ca^{2+}/PO_4^{3-}$ 1.45 ±0.04, possibly indicating a mixed mineral composition (Figure 13g; also see **Table 3**).

In Group 3 (low concentration fluoride), 1100 ppm F was applied in the presence of $Ca^{2+}$ and $PO_4^{3-}$ ions. The concentration of 1100 ppm fluoride corresponds to the concentration of the most commonly used toothpaste available over the counter for daily home care.[5-7] The analysis of the SEM images suggests a non-uniformly deposited layer with a fine (<1 μm) roughness (**Figure 14a-b**). A detailed analysis of the surface structure, e.g., at higher magnification image in Figure 14b, reveals fine nanoparticles of diameter 20-50 nm. The cross-sectioned samples reveal a new layer with a thickness of about 1 μm covering the surface of enamel in the lesion (Figure 14d). The elemental composition analysis from the surface revealed prominent peaks of $O_{K\alpha}$, $P_{K\alpha}$, and $Ca_{L\alpha}$ as well as a small peak corresponding to $F_{K\alpha}$. Ca/F ratio gives a value of more than 30 while the Ca/P ratio is close to 1.70 (Figure 14c).

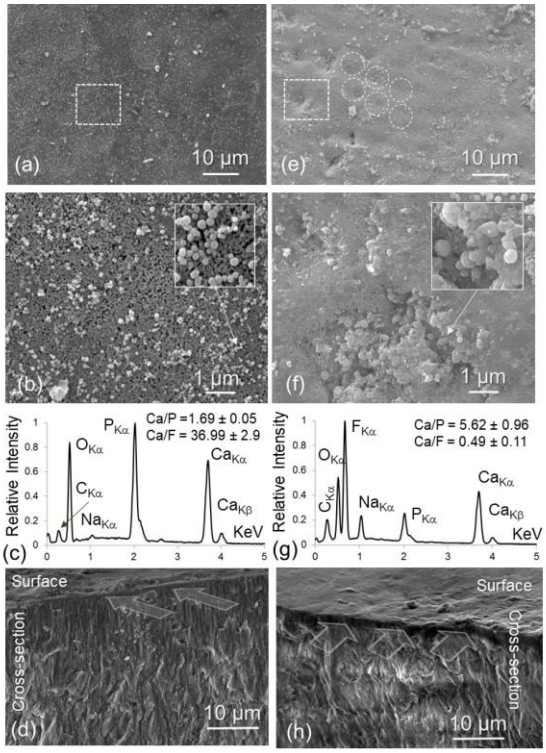


**Figure 14:** Face-on (a, b) and edge-on (d) SEM images and EDXS analysis (c) of Group 3: 1100ppm $F^-$ + $Ca^{2+}/PO_4^{3-}$. Face-on (e, f) and edge-on (h) SEM images and EDXS analysis (g) of Group 4: 20,000ppm $F^-$ + $Ca^{2+}/PO_4^{3-}$ . Insets in 3b and 3f show loosely packed nanospherical particles (of dia. ~20-30 nm) as a result of F deposition. The inset panels are 1 μm x 1 μm. Wide arrows in (d) and (h) indicate the boundary between the new layer and original tooth.

In Group 4 (high concentration fluoride), 20,000 ppm fluoride (concentrations of most commonly used dental varnishes) was applied with $Ca^{2+}$ and $PO_4^{3-}$ ions.[81-83] The analysis of the SEM images recorded from this treatment displayed significantly different surface topography, structures, and elemental composition as compared to the samples in the previous groups of non-fluoride or low concentration F treatment. Although at low magnifications (Figure 14e) the surface appears fairly smooth, higher magnification (Figure 14f) revealed small spherical particles of 100-200 nm diameter covering the overall surface (indicated by arrow in Figure 14f). The secondary electron images, recorded with the SEM, from the cross-sectioned samples reveal an about one micrometer-thick new layer on the surface of the teeth (Figure 14h). The EDXS spectra acquired from the surface gives a high concentration of $F_{K\alpha}$ peak, the most prominent among all the peaks in the spectra from this group of samples (Figure 14g). The quantitative analysis of the spectra from the samples prepared in this group exhibited the Ca/F ratio of 0.49 (Table 3).

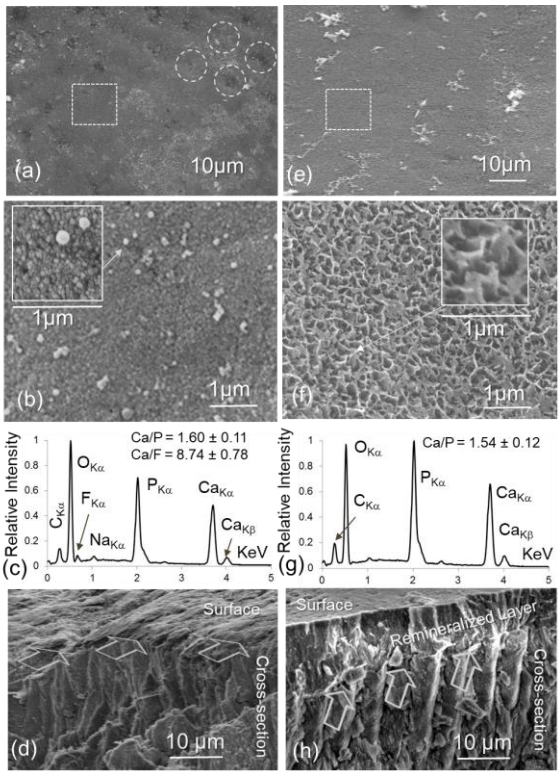


**Figure 15**: Face-on (a, b) and edge-on (d) SEM images and EDXS analyses (c) of Group 5: shADP5 + 1100ppm F- + $Ca^{2+}/PO_4^{3-}$. Insets in 4b show loosely crystallized regions of accumulated 100-nm dia. spherical nanoparticles on the surface. Face-on (e, f) and edge-on (h) SEM images and EDXS analysis (g) of Group 6: shADP5 + $Ca^{2+}/PO_4^{3-}$. Inset 4f displays a highly uniform, plate-like HAp crystallites within newly formed (h) mineral layer in shADP5 + $Ca^{2+}/PO_4^{3-}$ treatment. The inset panels are 1 µm x 1 µm. Wide arrows in (d) and (h) indicate the boundary between the new layer and original tooth.

In group 5 (the peptide with low concentration fluoride) shADP5 was applied with 1100 ppm fluoride along with $Ca^{2+}$ and $PO_4^{3-}$. The microstructure of the samples displays a fairly smooth surface with about 1-2 µm thickness (**Figure 15a-d**). Enamel rod imprints remained visible in the lower magnification image (Figure 15a). Higher magnification images of the sample surface, however, exhibit two different surface morphologies (see insets in Figure 15b); somewhat loosely deposited nanoparticles of 50-100 nm diameter and dense structure composed of rod-like nanoparticles of a few tens of nanometers in diameter with the diameter/length aspect ratio of 1/5. Elemental analysis of the samples from this group revealed a fairly noticeable $F_{K\alpha}$ peak in addition to highly prominent $Ca_{K\alpha}$ and $P_{K\alpha}$ peaks with the elemental ratio of Ca/F, 8.7 (Figure 15c).

**Table 3:** Elemental composition analyses of the remineralization test groups by EDXS.

| Test Group | Remineralized Layer Composition | | | Possible Mineral Formed |
|---|---|---|---|---|
| | Ca/P | Ca/F | Ca/O | |
| 1-Control | 1.56±0.12 | - | 0.51±0.11 | Only HAp |
| 2-Ions Only | 1.45±0.04 | - | 0.28±0.02 | Amphs Ca-P Trn Phs |
| 3-Low F | 1.69±0.05 | 36.99±2.9 | 0.74±0.15 | Ca-P-F Trn Phs + $CaF_2$ |
| 4-High F | 5.62±0.96 | 0.49±0.11 | 1.01±0.16 | Mainly $CaF_2$ |
| 5-Low F & Peptide | 1.60±0.11 | 8.74±0.78 | 0.34±0.08 | FAp + some $CaF_2$ |
| 6-Peptide Only | 1.56±0.12 | - | 0.56±0.13 | Only HAp |

In Group 6 (shADP5 + $Ca^{2+}/PO_4^{3-}$), the SEM images in Figure 15e-f give a continuous layer of plate-like crystals growing from the surface of the underlying enamel lesion when the surface is exposed to aqueous peptide plus $Ca^{2+}/PO_4^{3-}$. Compared to the negative control (Group-1) or low concentration fluoride treatment (Group-3), the enamel rod imprints in the face-on images are no

longer visible, indicating that the new mineral layer is thick enough to mask the exposed enamel rods (Figure 15e-f). The cross-sectional image in Figure 15h shows a 10 µm thick continuous remineralized layer with fairly smooth surface topography. Elemental analysis of the samples from this group revealed prominent $Ca_{K\alpha}$ and $P_{K\alpha}$ peaks with a ratio of 1.54 ±0.12; this is close to the ideal ionic ratio of 1.6 in HAp composition (Figure 15g; Table 3).

To further analyze the structural characteristics of the mineral layers, imaging and diffraction analyses were carried out on samples by using transmission electron microscopy. The TEM samples were prepared by gently shaving fragments off the surface of tooth specimens. In group 1, which received no remineralization treatment, enamel fragments were analyzed. As shown in **Figure 16 a – c**, textured elongated HAp crystals of 30 – 50 nm were encountered, typical of prismatic rods constituting the enamel rods in healthy enamel tissue. In the case of high concentration F treatment (group 4), generally round particles of $CaF_2$ in the range of 100 – 250 nm in diameter were observed (Figure 16 d – f). On the peptide treatment group (group 6), particles (in the shown projection) of HAp were found (Figure 16 g – i) possibly corresponding to plate-shaped mineral.

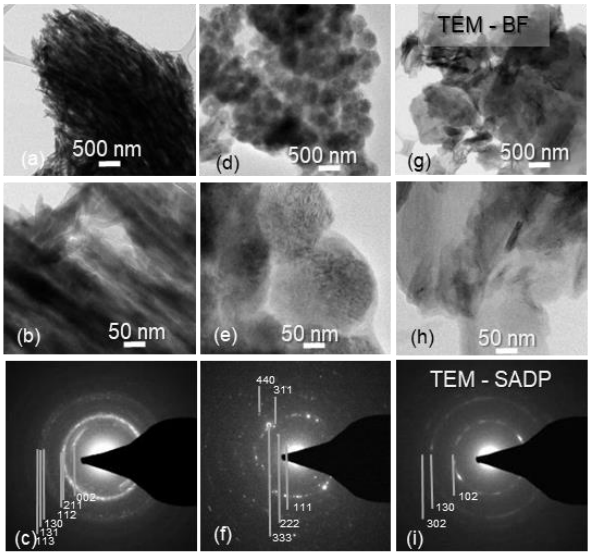


**Figure 16:** TEM bright field images and corresponding selected diffraction patterns for no-treatment negative control (group 1) (a–c), showing high-aspect ratio rod-like HAp crystallites; high concentration F-treatment (group 4) (d–f), exhibiting $CaF_2$ particles, and peptide-treatment (group 6) (g–i), showing plate-like HAp crystallite formation.

*Micro- and Nano-mechanical Characterization:*

Mechanical properties of the mineralized layers were determined using two different tests. The microhardness test was carried out using a Vickers indenter loading on the mineralized tooth surface. The hardness for the negative control group (Group 1 - no treatment) was 128.1 $\pm$ 8.0 HV10. This was used as the baseline figure representing microhardness of the surface of bare, artificially created WSL which other experimental groups were compared against. As further reference, the microhardness tests were also conducted on healthy enamel and dentin, away from the demineralized surface. As shown in **Table 4**, values for groups 2 to 5 ranged between 130.1 $\pm$ 11.7 HV10 to 133.5 $\pm$ 12.4 HV10. Unequal variance t-test between group 1 and each of other groups revealed no statistically significant difference ($p > 0.05$). Microhardness of group 6 had slightly higher average value of 141.1 $\pm$ 7.8 HV10. Unequal variance t-test against group 1 revealed significant difference with $p << 0.01$. The results indicate that the microhardness values of group 6 as well as the rest of experimental groups fell between that of enamel and dentin.

**Table 4**: Vicker's microhardness of all experimental groups, $n \geq 20$.

| Test Groups | Hardness (HV10, MPa) | Std Dev (MPa) |
|---|---|---|
| Group 1 (Negative Control) | 128.1 | 8.0 |
| Group 2 (Ca/PO4 Only) | 130.1 | 11.7 |
| Group 3 (Low Conc. F) | 130.6 | 12.6 |
| Group 4 (High Conc. F) | 131.8 | 12.9 |
| Group 5 (shADP5 + Low Conc. F) | 133.5 | 12.4 |
| Group 6 (shADP5) | 141.1 | 7.8 |

Nanomechanical tests were also conducted using nanoindentation that not only provided hardness ($H$) values but also elastic modulus ($E_r$). The tests were carried out on spatially selected regions as the test facilitates scanned surface images. The nanoindentation tests of all the experimental groups were conducted on samples in cross-sectioned geometry, i.e., indentor direction is parallel to the surface (as opposed to vertical in microhardness tests). The results revealed a trend similar to the those of the microhardness data, no significant differences were encountered among samples from the no treatment negative control and each of the groups 2 through 5, in both hardness and reduced elastic modulus, $p > 0.05$ in all cases. However, the average hardness and elastic modulus for group 6 were higher than those of the no treatment samples with hardness of $2.23 \pm 0.23$ GPa vs. $2.10 \pm 0.26$ GPa, $p = 0.02$ and elastic modulus of $58.6 \pm 4.7$ GPa vs. $55.1 \pm 4.3$ GPa, $p = 0.02$. Not surprisingly the healthy enamel and dentin had respectively higher and lower values of both hardness and elastic moduli compared to the experimental groups involving remineralization. In conclusion, the mechanical properties (H and E) are higher than those of dentin, but lower than the healthy enamel.

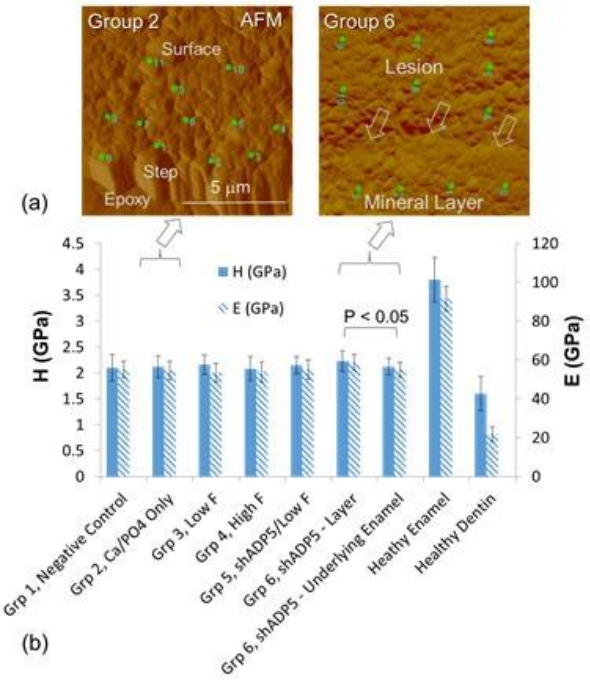


**Figure 17:** (a) Atomic force microscopy images of the surfaces of the mineralized layers in samples from Group 2 (left), where there is no apparent mineral layer on the lesion and Group 6 (right) showing a clear boundary between the lesion and newly formed mineral layer (arrows). (b) Hardness (left) and elastic modulus (right) of the experimental groups used here were measured by nanoindentation, $n > 20$.

3.1.4. Discussion

A natural, cell-free, biomimetic model was developed to remineralize artificially induced lesions on human enamel using a 15-amino acid long amelogenin-derived peptide, shADP5, along with properly tuned ionic concentrations of $Ca^{2+}$/$PO_4^{3-}$ *in vitro* in the presence and absence of low and high fluoride content that were chosen based on the values in frequently used dental treatments. Significant differences were encountered among the surface characteristics of the 6 samples from six different groups. The surface of the artificially demineralized enamel displayed enamel rods, which appeared as up to 3-μm diameter depressions exposed on the surface with a roughness of approximately 1-μm (Figure 13a-b). Another prominent feature was the fine structure of the individual rod-shaped HAp crystallites of a few tens of nm thickness that constitute the enamel rods. When ionic precursors are used alone (Group 2), the treatment resulted in a thin (<1 μm) layer with a highly porous morphology on the surface. The composition was off stoichiometric for that of HAp with Ca/P ratio of <1.5 which might be due to the formation of calcium-phosphate transition phases (Table 3). The effect of F on mineral formation was examined under two different fluoride ion conditions, 1100 ppm in Group 3 and 20,000 ppm in Group 4, which were specifically chosen to mimic the F concentrations of everyday tooth paste and fluoride varnish used in the clinic, respectively. The surface structures of the teeth in these two treatments revealed different morphologies. Firstly, fluoride treatments resulted in aggregates of nanoparticles in Group 3 and a thin mineralized layer about 1 μm in Group 4. The layers were composed of nanoparticles which were about an order of magnitude smaller in Group 3 than in Group 4 samples, 20 nm versus 200 nm, respectively. The application of F in dental care products primarily focuses on remineralization aided by F or incorporation of F into the existing HAp structure, desirably forming fluorapatite (FAp). In this respect, the results of the elemental analyses obtained from the

fluoride-treated surfaces are quite intriguing. The Group 3 samples, with low-F, presented hardly any F peaks in the EDXS spectra, giving a Ca/F ratio of almost 40. The elemental composition analysis of the sample surface displayed relatively high relative peaks of $O_{K\alpha}$, $P_{K\alpha}$, and $Ca_{L\alpha}$ as well as a minor peak corresponding to $F_{K\alpha}$ ($Na_{K\alpha}$ and $Cl_{L\alpha}$ peaks are from the treatment solutions). Possible sources of the low F concentration might be explained either as being due to the formation of a very thin newly deposited layer in the signals originating from the underlying healthy enamel as measured by EDXS or due to the very low amount of F incorporated into the newly formed surface layer. The F concentration in the newly formed layer may imply that majority of F was not delivered to the desired mineralization site on the enamel surface in the peptide-free samples. The presence of nanoparticles deposited on the surface, therefore, may be due to F reacting with the excess Na in the buffer solution forming NaF.

In Group 4, the new layer is predominantly composed of aggregated spherical nanoparticles. Considering the ideal Ca/F ratio of 0.5 in $CaF_2$ the spherical particles are likely to be $CaF_2$. Another major difference in this group was the value of $Ca_{K\alpha}$/ $P_{K\alpha}$ ratio being > 5.0. Even considering that some of the Ca ions might be confined to $CaF_2$, this ratio still indicates unusually high concentration of Ca trapped in the newly formed surface layer. Calcium fluoride is a highly stable compound, likely to form under the experimental conditions used in this study. The clinical products that contain high F concentration are designed for forming apatite in the demineralized product. However, as shown here, the mineral formed is most likely calcium fluoride. In summary, neither of the F-samples exhibited the ideal ratio of Ca/P of 1.6 for HAp (Table 3), meaning that F alone was not incorporated into the enamel or remineralized layer. These findings are consistent with previous studies that reported $CaF_2$ formation under home-use (low-F) and clinical (high-F)

products. It has been suggested that CaF2 may serve as a reservoir of fluoride, presumably, to be incorporated later into the structure of enamel.

In Group 5 and 6, the peptide was used as the precursor in the remineralization procedure. In Group 5, shADP5 was applied in the presence of 1100 ppm fluoride, resulting in the formation of the spherical particles as aggregates as opposed to being widely disseminated on the tooth surface compared to the same F concentration without peptide in Group 3. Enamel rod imprints remained visible in the lower magnification image (Figure 15a-b) although these were less prominent than those seen in the no-treatment samples (Figure 13a-b). The resulting mineralized structure presented two morphologies: clusters of 50-100 nm diameter spherical nanoparticles accreted non-uniformly on the surface; and a structure primarily composed of highly dense nanorods. There was considerably more prominent F peak compared to the no-peptide samples, with an overall Ca/F ratio of 8.74 ± 0.78. This explains that there was considerably more F in the mineral formed with the peptide containing low-fluoride treatment compared to the samples with low-fluoride only (Ca/F = 36.99 ±2.9). If the presence of FAp is considered, i.e., corresponding to the dense nanorods, the ideal ratio of Ca/F turns out to be 5.0 (Table 3), then the rest of the fluoride in the mineral layer could account for the formation of NaF nanoparticles. Considering that the observed Ca/P ratio reflects either HAp or FAp stoichiometry (Table 3), the new mineral was formed on the tooth surface by partially incorporating F in the presence of peptide. The presence of F could be explained in, at least, two ways; either the fluoride was incorporated into the newly forming HAp mineral replacing OH partially or both HAp and FAp were formed on the surface. In both cases, the effect of peptide appears to be necessary to incorporate fluoride into the structure since in the absence of shADP5, very little or no F was found in the remineralized layer. The significance here is that dental formulations used in the current treatments, e.g., pastes, gels, varnish, and solutions,

could contain peptide as a means to effectively carry F to the surface and help incorporate it into the remineralized HAp on the tooth surface.

In Group-6, shADP5 peptide in addition to calcium and phosphate precursors were used which remineralized a thick (>10 μm) layer composed of crystal morphology specific to HAp among the calcium phosphate polymorphs. Considering that he observed Ca/P ratio is 1.54, close to that of ideal HAp composition, it is concluded that the peptide was capable to catalyze a newly mineralized layer composed of HAp crystallites (Figure 16g-i). As evident from SEM images (Figure 15e-f), the roughness of remineralized surface was reduced (<300 nm) compared to the demineralized surface in Group 1 (Figure 13a-b, d).

The loading in the microhardness tests was carried out in the direction relevant to functional dental loading while using the lowest possible Vickers indentation load to maximize the contribution from the mineralization layer. Even with the lowest load, however, the indentor likely penetrated through the thin mineralized layers in the samples from groups 2 – 5 as no discernable measurements were determined among these groups compared to the no-treatment negative control group. The SEM observations supported these findings as the mineral layers in groups 2 through 5 were significantly thinner (~1-2 μm or less) and discontinuous. The remineralized layer, however, was thicker in the peptide-guided remineralized group, reflected in higher microhardness values, although slight, compared to the negative control group.

3.1.5. Conclusions

The present *in vitro* study demonstrated that crystalline mineral layer is formed on an artificially created lesions on human enamel in the presence of $Ca^{2+}$ and $PO_4^{3-}$ ions under physiologically viable conditions by using shADP5, a 15-AA long amelogenin-derived peptide (**Figure 18**). This

study also showed that the presence of the biomineralizing peptide also facilitated the delivery to tooth surface and incorporation of fluoride ions into the remineralized layer even at low F concentrations, providing an opportunity for dental health products to incorporate both elements in potential clinical and everyday dental product formulations.

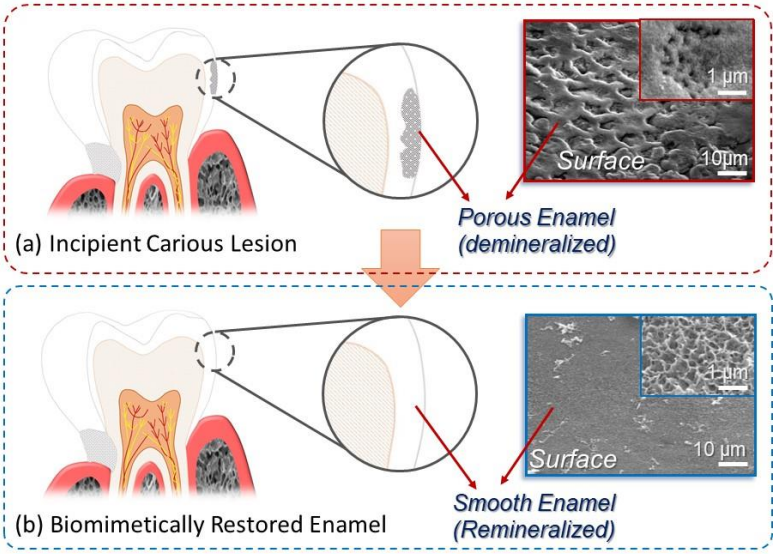


**Figure 18:** Schematic representation and scanning electron microscopy images of incipient carious lesions (a) before and (b) after remineralization treatment.

Establishing the scientific foundations for remineralization has a high potential to empower practicing dentists to address caries-related dental problems due to enamel demineralization, the origin of most dental ailments. Although remineralization of human teeth *in vitro* using peptides on artificially damaged enamel discussed herein provides guidance towards addressing this challenge, the procedures developed need to be further optimized towards clinical applications. Further research concerning the repair of enamel defects is necessary to achieve an easy-to-apply, fast-growing enamel-like biomineralized tissue for biomimetic tooth repair. Future studies include implementing this advanced remineralization technology under *in vivo* conditions by utilizing clinically applicable peptide delivery systems (e.g., gels or pastes with or without F) and applying tests to the mineralized layer to ensure its mechanical and chemical durability and adherence to the underlying tooth structure.

This section (Chapter 3.1) was reprinted with permission from *Dogan S., Fong H., Yucesoy D.T., Cousin T., Gresswell C., Dag S., Huang G., Sarikaya M. (2018) Biomimetic Tooth Repair: Amelogenin-derived peptide enables in vitro remineralization of human enamel. ACS Biomaterials Science & Engineering 4 (5), 1788-96.* Copyright (2018) American Chemical Society.[78]

## 3.2. *In vitro* Biomimetic Repair of Hypersensitivity in Human Dentin

### 3.2.1. Introduction

*Statement of the Problem:* Demineralization, loss of natural mineral from tooth, is the leading cause of many dental diseases and conditions.[113-116] Dentin hypersensitivity (DH) is a prevalent dental condition affecting majority of the population.[117-119] DH is defined as a short, yet sharp pain arising from exposed dentin tissue in response to an external stimulus, typically thermal, evaporative, tactile, osmotic or chemical, which cannot be ascribed to any other dental defect or disease.[120, 121]

As a living tissue encompassing the nerve ends inside its microtubules, dentin is naturally covered and protected from the oral cavity by highly mineralized dental tissues, e.g., enamel at the crown and cementum on the root of the tooth. When these protective tissues are worn off and lost through demineralization, mainly due to poor oral hygiene, aging, acidic diet or use of abrasive whitening agents, dentin tubules underneath become exposed to the oral environment.[122, 123] As a result, nerves located within these tubules become susceptible to external stimuli and in turn trigger pain. Among the explanations about the underlying mechanism of DH is the "hydrodynamic theory" which ascribes the movement of the fluids through the dentinal tubules due to the pressure fluctuations across the dentin tubules which activate mechano-receptors.[124-127]

More than half of the US population currently experience discomfort from DH.[127-129] As the life expectancy is rising and more people are retaining viable teeth, the demineralization and wear-related problems, especially DH, are likely to be more frequent, affecting the well-being of the patients and their quality of life. [115, 128, 129] The leading causes of loss of these tissues are recession of the gingival margin due to mechanical stress, e.g., abrasive tooth brushing procedures and frequent use of toothpicks and other similar tools.[130] Besides mechanical wear, demineralization

due to acidic attack (as a result of acid-producing bacteria or acidic diet) may remove the thin cementum tissue and create DH.[131] Periodontal procedures such as gingival surgery, and orthodontic and prosthetic treatments, have been reported to increase the risk of DH.[125, 132, 133] Frequent use of tooth whitening products which remove tooth discoloration by dissolving natural mineral from tooth surface by the action of highly abrasive hydrogen peroxide agent, even worsens this serious dental health condition.[127, 134]

*Current Approaches:* Current anti-hypersensitivity products are generally designed to alleviate the dental pain by either: (i) Desensitizing the nerves using potassium nitrate[135, 136], or (ii) Physically blocking tubules via (a) Protein precipitating agents, e.g., glutaraldehyde[137], or (b) Solid precipitates, e.g., calcium phosphate, sodium fluoride, or bioglass.[138-143] Although these products can help to relieve the pain to an extent, their effects are usually transient. The key issue, therefore, is the lack of physical, chemical, and structural compatibility between the underlying dentin and deposited mineral which cannot form a natural integration into the existing dental tissue.[142, 143] This is due to the fact that non-specific and secondary mineral deposits are susceptible to mechanical wear and chemical dissolution.[78, 144, 145]

In healthy patients, saliva is highly effective in reducing DH by supplying calcium and phosphate ions into the open dentin tubules and gradually occluding them by forming a protective surface layer that also contains salivary glycoproteins.[146] The ideal DH treatment, therefore, should mimic natural desensitization/remineralization process leading to self-driven occlusion of dentin tubules.[147]

*Traditional Biomimetic Approaches:* Biomimetic restoration of dentin through a natural remineralization process that could grow the new mineral atop of demineralized dentin may provide an ideal solution to combat hypersensitivity. So far, using biomimetic pathways, a variety

of strategies has been developed to remineralize dentin tissue by using tissue-specific extracellular matrix (ECM) proteins, e.g., full-length amelogenin, dentin matrix protein 1, matrix metalloproteinase 20 (MMP-20), and leucine-rich amelogenin protein (LRAP) with various scaffolds, e.g., agarose, polyacrylamide, and chitosan.[51, 58, 102, 148] However, the major drawback of these approaches is that extraction and purification of these proteins requires highly optimized and strictly controlled labor-intensive procedures which often causes them to be far from feasible to use as a therapeutic and technological product.[54, 55, 74] Therefore, although these investigations have been adding to the general knowledge of remineralization, overall, however, they still face an ongoing challenge to be translated into a clinical product.

*The Proposed Approach:* A novel biomimetic remineralization procedure that enables remineralization of dental hard tissues through the guidance of peptides have been reported.[55] These peptides were identified using a biomimetic algorithm which involves the isolation of genetically engineered peptides through a combinatorial mutagenesis procedure. Following the identification of short peptide sequences which had ability to direct calcium-phosphate mineralization, the next generation of peptides were developed using a knowledge-based design approach which involves finding the similarity regions between the set of peptides and the natural mineralizing protein, amelogenin. After refining these high and low similarity regions within amelogenin, the identified domains were individually synthesized as a set of short peptide sequences and utilized as a catalytic molecule to direct and regulate mineralization. Using these peptides, biomimetic mineralization of human dental tissues has been demonstrated *in vitro.*[54, 55, 74, 78] In this study, the aim is to investigate the therapeutic potential of shADP5 peptide to create a mechanically and structurally stable mineral layer mimicking the function of cementum tissue on exposed human dentin *in vitro*. Herein, we report the use of shADP5 to promote functional

remineralization of human dentin and thereby occlusion of exposed tubules through a durable mineral layer. The principles laid out in this work have the potential to be developed into an anti-hypersensitivity product with long- term therapeutic effect under clinically relevant conditions.

3.2.2. Materials and Methods

*Sample Preparation and Test Groups:*

Extracted human molar teeth with no visible defects or restorations were collected from University of Washington School of Dentistry Clinics and disinfected in 10% (v/v) bleach solution for 72 hours. Prior to the experiments, the teeth were cleaned to remove soft tissues using a dental scaler under a light microscope.

*Preparation of Exposed Dentin Specimen:*

Dentin specimens with exposed tubules were prepared using a protocol as outlined in **Figure 19.** Dentin discs with an average thickness of 2 mm were cut using a low speed saw (IsoMet™, Buehler, Lake Bluff, IL, USA) with a diamond blade from mid-coronal dentin (Figure 19).

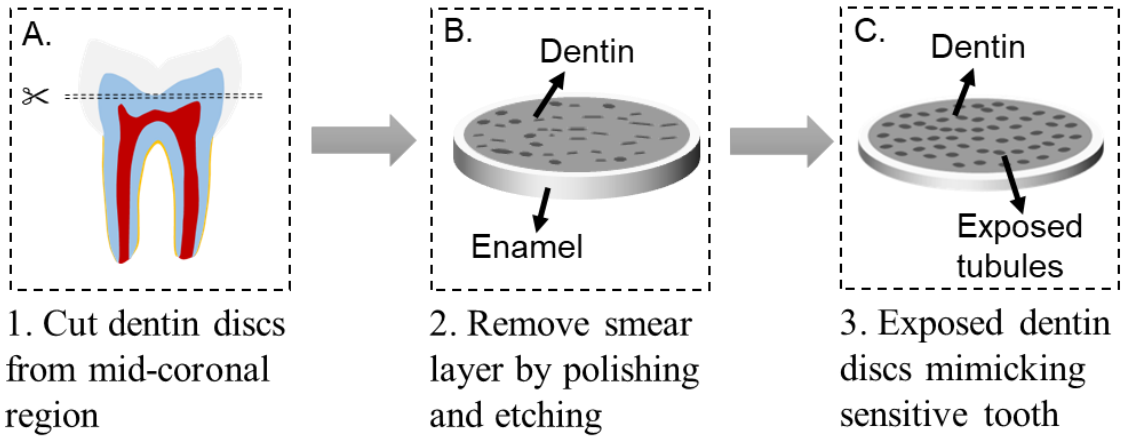


**Figure 19:** Schematics of dentin discs preparation procedure from mid-coronal region.

The surface was then polished to 0.1 µm finish using diamond lapping films. Specimens were ultrasonicated for two minutes in order to remove the smear layer and then etched for 30 seconds

with 10% citric acid solution. Excess acid was removed by rinsing the samples with deionized water. Samples were then divided into control and test groups (**Table 5**).

**Table 5**: Test groups and treatment procedures.

| Test Groups | Treatment Procedure | # of Samples |
|---|---|---|
| Group 1 (Negative Control) | No Treatment | 5 |
| Group 2 ($Ca^{+2}$ / $PO_4^{-3}$) | 3.2 mM $Ca^{+2}$ / 1.92 mM $PO_4^{-3}$ | 5 |
| Group 3 (shADP5 & $Ca^{+2}$ / $PO_4^{-3}$) | 1. 0.8 mM Peptide, 10 minutes<br>2. 3.2 mM $Ca^{+2}$ / 1.92 mM $PO_4^{-3}$ | 5 |

*Remineralization Protocol:*

Prior to remineralization treatment, specimens were pre-wetted with 20mM Tris Buffer Solution, pH:7.4 (TBS). Next, dentin discs were placed into 0.8 mM shADP5 peptide solution (See section 2.1.2 *Peptide Design and Synthesis*) and incubated for 10 minutes at 37C (Group-3). After removing the excess peptide by blotting, samples (Group 2&3) were transferred into 20 mM TBS containing 3.22 mM $Ca^{2+}$ / 1.92 mM $PO_4^{3-}$ for 1 hour at 37°C (**Figure 20A**). The specimens were rinsed with de-ionized water, dried by forced air and stored at room temperature until characterization. For repeated rounds of remineralization, samples were subjected to remineralization treatment immediately after water rinse.

*Sample Characterization by SEM and EDXS Analyses – Imaging and Elemental Composition*:

Prior to SEM imaging, samples were coated with 5 nm of gold. SEM characterization was carried out in a JSM 6100 SEM (JEOL) operating at 10kV accelerating voltage. For cross-sectional images, samples were fractured in half in the sagittal direction prior to coating. Recorded images were analyzed using ImageJ™ image processing software and thickness of the mineral layer and width of the tubules were averaged from 5 images per sample (5 samples per test group).

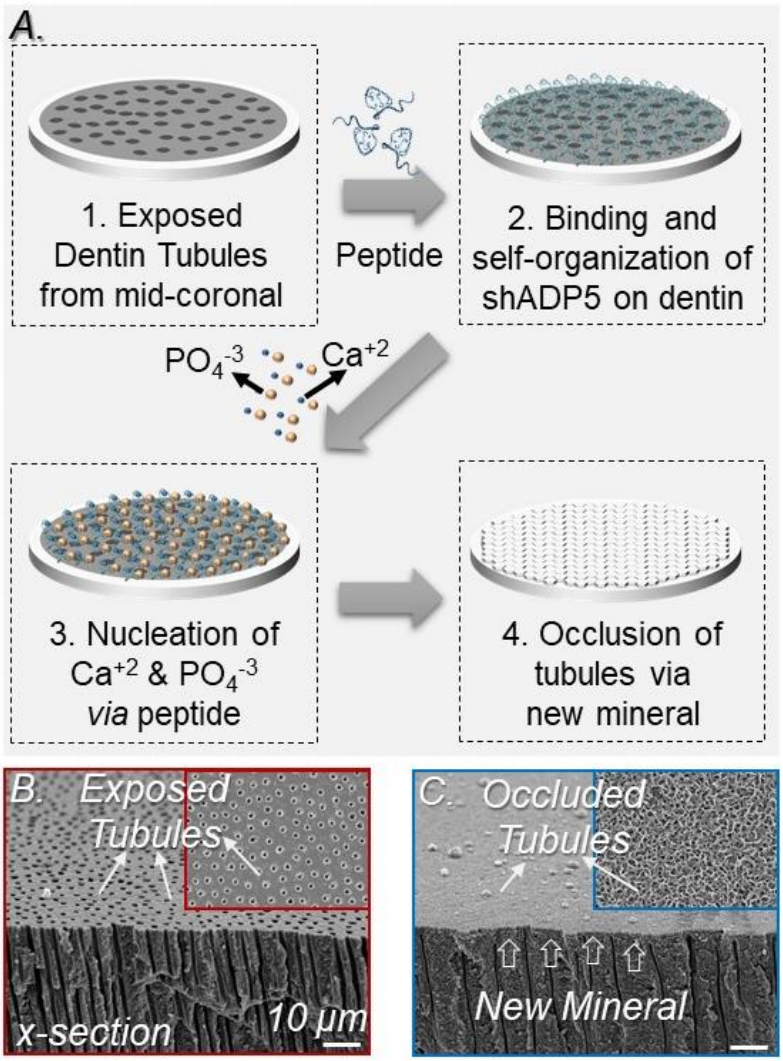


**Figure 20:** Schematics of peptide-guided remineralization procedure. Edge-on and surface (inset) SEM images of dentin discs (b) before and (c) after mineralization treatment.

*Stability Assays via Thermal Aging Assay:*

The durability of the remineralized layer that occludes the dentin tubules is tested by a thermal cycling assay adapted from the ISO/TR dental materials testing procedure (1994). Briefly, exposed dentin discs with four notches on the apical surface were subjected to remineralization treatment.

Next, the specimen was fractured into two pieces and one half was subjected to thermal cycling while the other half was kept in artificial saliva at 4ºC degrees. The assay procedure includes soaking the testing specimen into 10 ml of artificial saliva (containing 130 mM KCl, 20 mM HEPES, 1.5 mM $CaCl_2$, 0.9 mM $KH_2PO_4$ and 1 mM NaCl; pH:7.0) and solution temperature is cycled through two temperature extremes, 5ºC and 55ºC, for 30 seconds at each temperature. The procedure was repeated for 200 and 2500 cycles to mimic 7 and 90 days of aging, respectively. Following the thermal cycling, the specimen was rinsed with deionized water and dried by forced air. Prior to SEM characterization, the specimen was fractured in half from the notches opened on the untreated side.

3.2.3. Results

*Occlusion of Dentin Tubules through the Peptide-guided Remineralization Treatment:*

The formation of new mineral on top of exposed dentin in response to repeated rounds (0-3 rounds) of peptide-guided remineralization was studied through SEM characterization. The representative SEM images of parasagittally sectioned mid-coronal samples before the remineralization treatment (shown in Figure 20b and 11a) displayed exposed dentin structure with dentin tubules extending toward the surface plane.

The average dentin tubule diameter was measured as ~2 µm. Following a first round of peptide-guided remineralization, a continuous mineral layer was formed which covers the exposed dentin surface. The average thickness of the mineral layer was measured through microdensitometer trace analysis using ImageJ and found to be 0.80 ±0.28 µm. The mineral formation extended into the dentinal tubules and thereby the average size of dentin tubule decreased to 1.25 ±0.45 µm at 10 µm region from the surface.

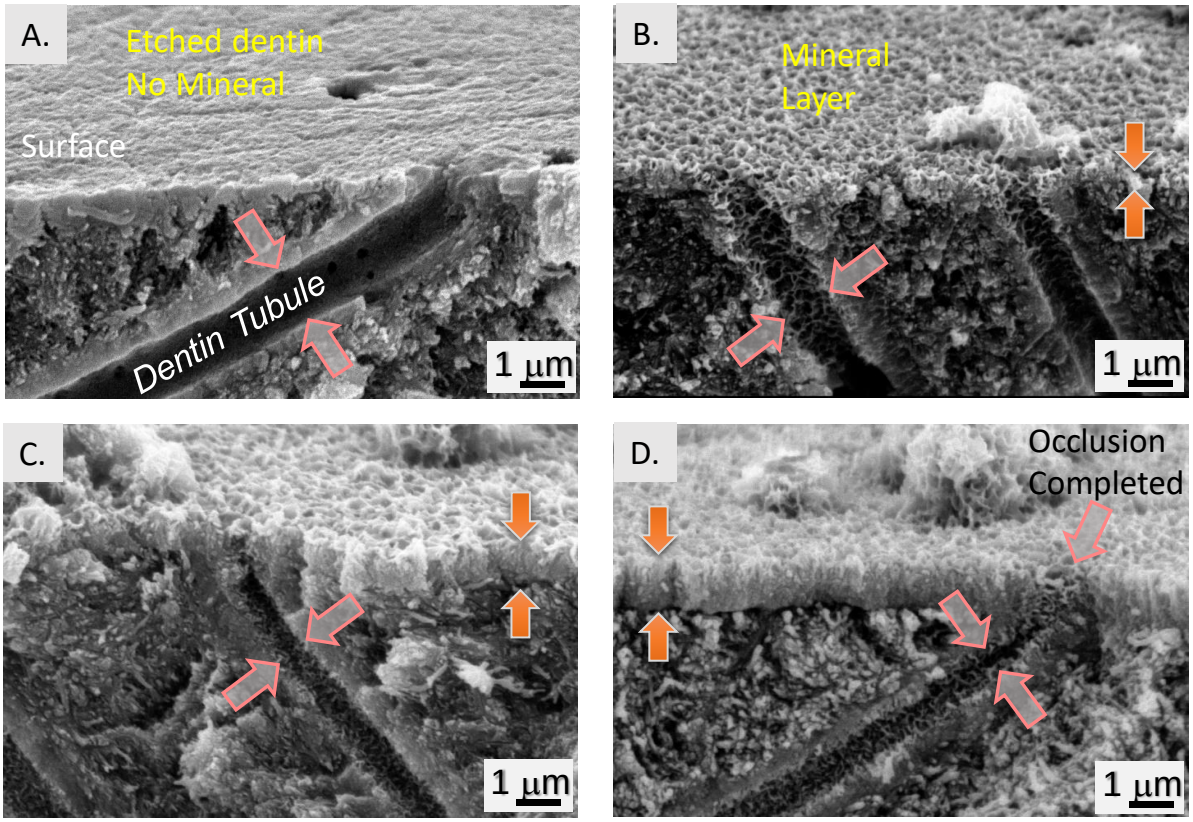


**Figure 21:** Edge-on SEM images of mid-coronal dentin discs (a) unmineralized- mimicking dentin hypersensitivity and after (b) single round of mineralization, (c) two rounds of mineralization, (d) three rounds of mineralization.

As shown in **Figure 21b**, although a continuous mineral layer was formed throughout the surface of exposed dentin, however, the occlusion of dentinal tubules has not completed. The second round of mineralization treatment added more mineral on top of the first layer. Through this layer-by-layer mineral formation, the final thickness of the mineral layer reached 1.05 ±0.36 µm while the average size of dentin tubule decreased to 0.80 ±0.27 µm. At this point, as seen in Figure 21c, tubule occlusion on the surface of dentin is nearly completed. After the third round of remineralization (Figure 21d), tubule size at 10 µm region from the surface was reduced to 0.66 ±0.33 µm while the top of the tubule is completely closed. The average thickness of mineral formed on the surface after the third round of remineralization was measured to be 1.3 ±0.19 µm.

*Durability of Biomimetic Mineral Layer:*

The thermal durability of the mineralized layer formed on top of exposed dentin was characterized through a thermal cycling assay. Etched dentin discs were subjected to three rounds of peptide-guided remineralization. Next, the samples were fractured in the parasagittal direction into three pieces. While the first two pieces were subjected to 200 and 2500 rounds of thermal cycling treatment, respectively, the third piece was kept in artificial saliva as a control. Following thermal cycling, samples were mounted next to each other and SEM characterization was performed. As shown in **Figure 22a**, the exposed dentin surface and tubules were covered with a continuous, 1.52 ±0.39 µm thick mineral (averaged over 300 µm, n=5) layer as result of three rounds of mineralization treatment. As shown in Figure 22b, no apparent change was observed on the overall thickness of mineral on dentin surface after 200 cycles of thermal cycling. The contrast difference between the newly formed mineral layer and underlying dentin (Figure 22a) disappeared following thermal cycling (Figure 22b). Similarly, as shown in **Figure 23**, 2500 rounds of thermal cycling (simulating 90 days of aging) did not cause any apparent alteration on the overall mineral thickness while the contrast difference between the newly formed mineral and dentin started to lesser.

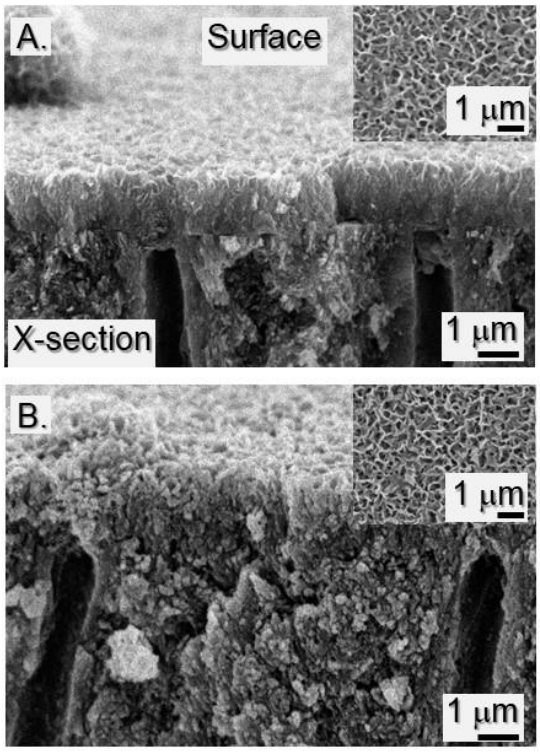


**Figure 22:** Edge-on (a, b) and face-on (insets) SEM images of dentin samples treated with three rounds of remineralization (a) before and (b) after 200 rounds of thermal cycling.

3.2.4. Discussion

A biomimetic, cell-free remineralization model was developed to treat artificially exposed human dentin using a 15-amino acid long amelogenin-derived peptide, shADP5, along with ionic calcium and phosphate molecule *in vitro*. Human dentin samples that were intended to mimic hypersensitive exposed dentin were prepared by mechanical removal of enamel (covering the tubules). The exposed dentin surface was then demineralized to the remove smear layer via acid treatment. Exposed dentin samples were subjected to repeated rounds of remineralization and the resulting mineral layer was characterized with scanning electron microscopy. As shown in Figure 21, peptide-guided remineralization treatment successfully created a continuous mineral layer penetrating into the dentin tubules. As indicated in Figure 21b-d, repeated rounds of remineralization enabled further growth of mineral on the dentin surface through a possible layer-by-layer mechanism. The occlusion of dentin tubules started with the first round where tubule width was significantly reduced through mineral penetration and formation on the tubule walls. Complete occlusion of dentin tubules was observed after the third round of treatment with a measured thickness of 1.3 ±0.19 μm. The conical shape of dentin tubules after three rounds of mineralization indicates that mineral growth at the dentin surface was bi-directional forming on

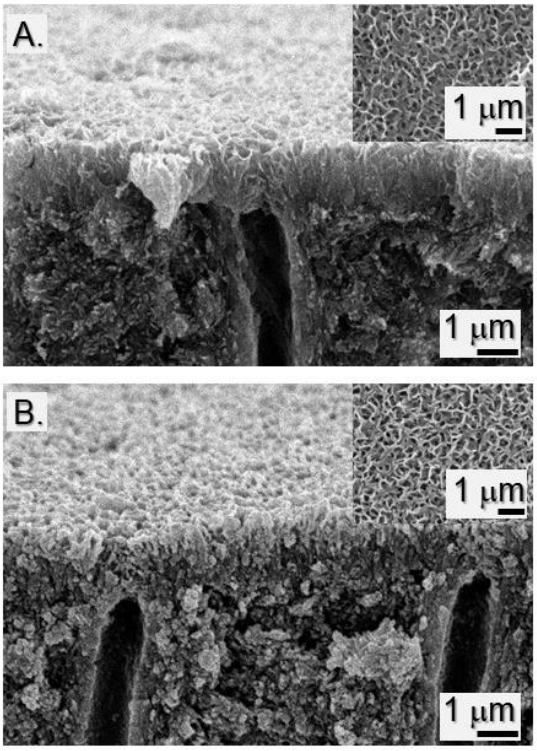


**Figure 23:** Edge-on (a, b) and face-on (insets) SEM images of dentin samples treated with three rounds of remineralization (a) before and (b) after 2500 rounds of thermal cycling.

the surface and inside the tubules. Following initial demonstration of the occlusion of dentin tubules, the durability of the newly formed mineral was characterized through a thermal cycling assay. As a result, neither after 200 cycles of thermal cycling nor 2500, (simulating 1 week and 3 months of aging, respectively) indicated an apparent change in mineral thickness on dentin surface.

3.2.5. Conclusions

Establishing the scientific basis for remineralization-based anti-hypersensitivity therapy has the potential to develop a long-term, permanent clinical solution for dental hypersensitivity. Herein, occlusion of dentin tubules through a thermally durable mineral layer that penetrates into dentin tubules using a biomimetically developed shADP5 peptide in the presence of calcium and phosphate ions under simulated oral conditions was demonstrated (**Figure 24**). Although initial steps of remineralization on exposed human dentin were established herein, these findings have to be validated further through other characterization methods and procedures. These future studies that are underway include chemical stability testing via pH cycling assay and mechanical sealing analysis through dye penetration tests.

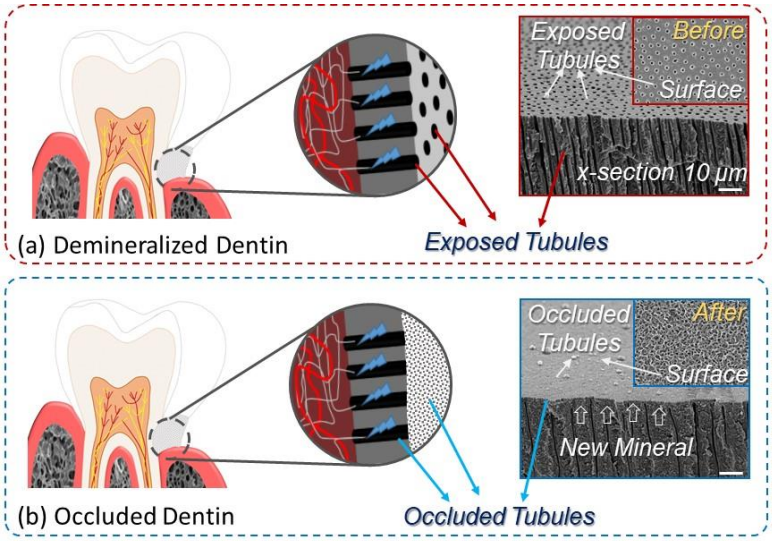


**Figure 24:** Schematic representation and scanning electron microscopy images of exposed dentin (a) before and (b) after remineralization treatment.

Chapter 4: *In vivo* Caries Formation and Remineralization-Rat Model

*Preamble: The Preparations Toward Biogenic Remineralization*

Dental caries is a complex multifactorial global disease of teeth. Demineralization of enamel is the earliest clinical sign of dental caries whereas remineralization is essential to maintain optimal tooth health. After successful completion of *in vitro* proof-of-principle demonstration of peptide-guided remineralization, in **Task-II** the aim was to test the efficacy of peptide-guided remineralization when incorporated into a gel formulation for treating caries in vivo using an animal caries model. The sub-tasks herein include: (i) development of a gel formulation to facilitate delivery and maximize the retention time of mineralization ingredients on defective tooth surfaces; (ii) development of an animal caries model; and (iii) treatment of the induced carious lesion using the peptide-gel formulation through remineralization (**Figure 25**).

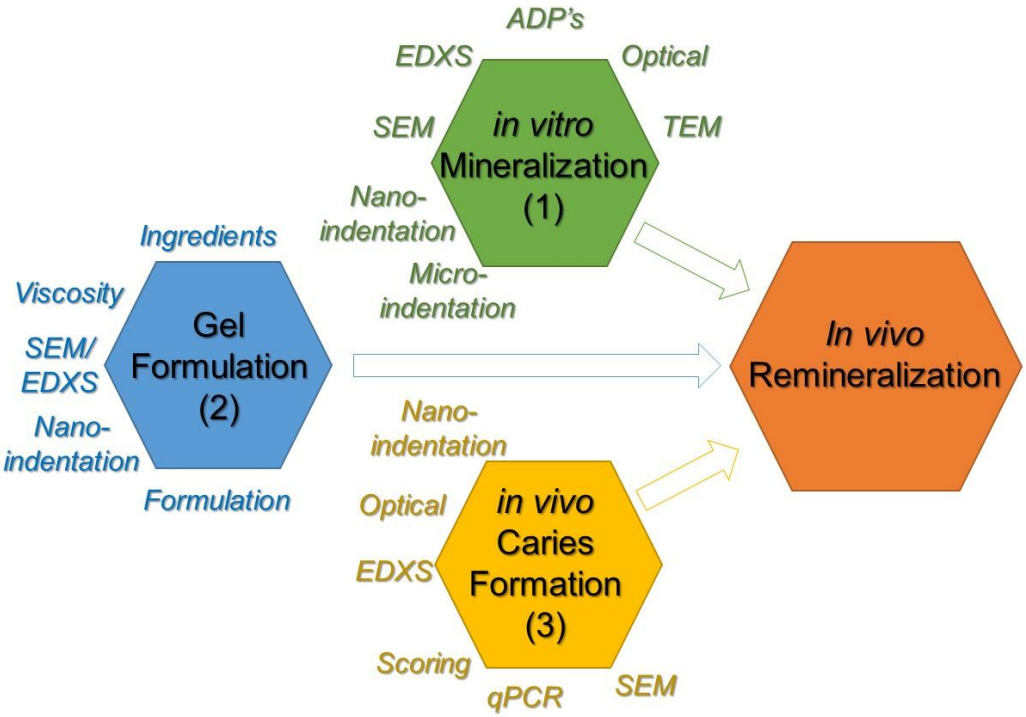


**Figure 25:** Schematic representation of experimental tasks planned to accomplish for testing peptide-guided remineralization treatment in rats.

## 4.1. A Revisit to the Formation and Characterization of Carious Lesions in an *in vivo* Rat Model

### 4.1.1. Introduction

*Limitations of Existing Animal Models for Caries Formation:* Animal models have made a substantial contribution in elucidating the etiology of caries and has led to the development of diagnostic and preventative products.[149, 150] A major issue of *in vivo* procedures, however, is the inconsistency of the parameters/factors that induce caries formation.[151] In particular, the lack of details about the cariogenic diet and feeding conditions[152-154], infectious organisms[155, 156], age of animals[157, 158], and housing conditions[159] often limit reproducibility of these procedures.[151]

*The Proposed Approach:* Colonization of cariogenic organisms is essential for caries formation. Although this can be achieved by direct inoculation of cariogenic bacteria[160], the removal of salivary glands and/or antibiotic treatment are still commonly utilized procedures.[150, 161, 162] Despite rapid colonization, these procedures often disrupt the balance of the oral microbiota and create a non-natural environment predominated by particular bacterial species.[163] Another common challenge is the limited detection of cariogenic bacteria levels in the oral cavity. Their presence in high levels in the oral flora is an indication of caries formation.[164, 165] An accurate detection and quantification of cariogenic organisms in animals is, therefore, crucial. The bacterial species in the current models are detected by agar plating. These methods, however, do not allow accurate quantification due to the biased growth of bacteria under *in vitro* conditions.[166] Quantitative real-time PCR (qPCR) assay is an alternative approach to conventional agar plating for early detection and real-time monitoring of cariogenic organisms in saliva.[167] Implementing qPCR to a rat model, therefore, could facilitate the quantification of the cariogenic bacteria during the progression of caries.

Another common challenge is the limited resolution of the conventional optical microscopy-based caries detection and scoring techniques.[160, 168-170] Due to this limitation, most animal models were developed to promote formation of relatively advanced carious lesions.[171, 172] Caries formation starts with initial demineralization and then progresses into the reversible early-stage lesion which, eventually, leads to an irreversible phase with cavitation.[173] Therefore, therapies that facilitate arresting and remineralizing early lesions need to be promoted to preserve the form and function of the tooth.[174, 175] The key to this vision is to modify current caries formation and scoring protocols so that new therapies targeting early-caries can be tested *in vivo*. At this point, presenting data only by conventional scoring may be incomplete or misleading. The caries scores should be supported by complementary methods that offer more explicit analyses.[176] Scanning electron microscopy (SEM) provides the resolution to detect and quantify subtle changes in the morphology and demineralization state of the hard tissues.[172, 177, 178] Furthermore, nanomechanical testing, e.g., nanoindentation, provides invaluable information about the local mechanical properties of hard tissues to correlate the function to the structure obtained from the SEM analysis.[47, 78]

In this study, the two-pronged aim was to develop a rat model that promotes slow progression of mild-caries with a strict monitoring of the colonization level of *S. mutans* by qPCR and to establish structure-function relationship by interrogating the local morphology, mineral content and mechanical properties of early fissure caries using light microscopy, SEM and nanoindentation. The principles laid out herein can be applied to other *in vivo* cariology models and developed into a standard protocol for future caries treatment and remineralization studies.

### 4.1.2. Materials and Methods

*Animals:*

13-day old, 14 female and 14 male SPF Sprague-Dawley (*Rattus norvegicus*, Crl:SD code 400; Charles-River, Wilmington, MA) rats were obtained with 7 dams and housed in plastic cages (Allentown Inc., Allentown, NJ) on corn-cob bedding with access to food and water *ad libitum*. Prior to shipping rats were screened by the vendor for the absence of specific pathogens. According to the health report provided (Kingston, K72 Rats report) rats tested negative for specific pathogens including common viruses e.g., SEND, PVM, SDAV, KRV, H1, RPV, RMV, REO, RTV, LCMV, HANT, MAV; bacterial species e.g., *B. bronchiseptica, CAR Bacillus, C. kutscheri, H. bilis, H. hepaticus, Helicobacter sp., K. oxytoca, K. pneumoniae, M. pulmonis, P. multocida, P. pneumotropica, Salmonella spp., S. moniliformis, Strep. pneumoniae, Beta Strep. sp. (Grp G), Beta Strep. sp., Pneumocystis spp.,* Tyzzer's disease; parasites e.g., *Ectoparasites, Helminths, Giardia sp., Spironucleus sp., E. cuniculi* and other protozoa. It is also reported that some of the animals were found to be *P. aeruginosa* (15 out of 56), *S. aureus* (35 out of 56), *S. agalactiae* (20 out of 72) positive in the breeding facility. None of these pathogens have primary cariogenic activity. Animals were handled in accordance to National Research Council Guide for the Care and Use of Laboratory Animals guidelines. All experimental procedures were approved by the Institutional Animal Care and Use Committee (IACUC) of University of Washington. The study is reported in accordance with the ARRIVE guidelines.[179]

*Bacteria Maintenance and Culturing:*

*Streptococcus mutans* UA159 American Type Culture Collection (ATCC) 700610 was utilized as a cariogenic bacterium and cultured according to ATCC instructions as described previously.[180] Briefly, The bacterial pellet obtained from ATCC was rehydrated in 0.5 mL of the brain heart infusion (BHI) broth media, and several drops of the suspension were immediately streaked on BHI agar plate. The BHI agar plate was then incubated at 37°C for 24 hours under anaerobic

conditions in an atmosphere supplemented with 5% $CO_2$. Next, a single-colony forming unit of *S. mutans* was aseptically transferred into 10 mL of BHI and incubated anaerobically at 37°C in the presence of 5% $CO_2$ for 16 h under static conditions. Finally, frozen *S. mutans* UA159 stock cultures were prepared in 25% (v/v) glycerol and stored at -80°C.

For animal inoculation, *S. mutans* was grown in BHI broth media anaerobically to a mid-log phase until an OD600 (optical density at 600nm wavelength) of 0.4 was reached. Cells were immediately harvested by centrifugation (2000 x g for 5 min) and resuspended again in fresh BHI broth media to a final concentration of ~$9x10^9$ cells/ml. Before inoculation, *S. mutans* was grown to a mid-log phase and were harvested at 2000 x g for 5 min and resuspended in fresh brain heart infusion broth.

*S. mutans Infection and Caries Formation:*

When pups were aged 14 days (Day-5), the dams were infected with *S. mutans* by pipetting 0.1 ml of a cell suspension containing ~$10^9$ CFU into their mouth. 4 pups were kept as negative controls. The infection procedure was repeated for five consecutive days (Day -5 to -1) to establish colonization of *S. mutans* in dams so that vertical transmission of infection to pups would occur.

The pups were weaned when aged 19 days (Day 0) and distributed by sex (4 animals per cage). Next, pups were infected directly with *S. mutans* for four consecutive days by pipetting 0.1 ml of a *S. mutans* suspension containing ~$10^9$ CFU into their cheek pouches. During the inoculation period (Day 0-3), access of pups to the bedding was restricted by placing a stainless-steel mesh on top of the bedding. All animals were fed with cariogenic MIT-200 powdered diet[181] (containing (w/w) 67% sucrose, 20% lactalbumin, 3% cottonseed oil, 6% cellulose, 1% vitamin mix #40060 and 3% mineral mix #70191; Harlan Labs, Indianapolis, IN) and filter-sterilized 10% sucrose water (w/v) *ad libitum*.

*Monitoring S. mutans Infection:*

*S. mutans* colonization in pups was monitored by colony counting and qPCR. On day -5, saliva samples were collected from 12 randomly selected rats. Animals were anesthetized with isoflurane and the saliva accumulated under their tongue and in cheek pouches was collected. Saliva samples were streaked on selective Mitis-Salivarius-Bacitracin (MSB) agar plates supplemented with 1% potassium tellurite and 0.2 U/mL bacitracin (selective for mutans group streptococci) and incubated at 37°C for 48 hours under anaerobic conditions.[182] Resulting colonies were enumerated.

For qPCR, oral swabbing did not generate enough sample for accurate analysis. Therefore, extracted teeth were used for sample collection. Animals (3 animals per each day) were randomly selected on days 0, 6, 12 and 25 and sacrificed by CO2 asphyxiation (n=3). Dissected jaws were placed in 5ml of sterile Dulbecco's phosphate buffered saline (DPBS; Gibco, Grand Island, NY) and sonicated for 15 seconds. Cells were harvested at 13000 x g for 2 min and genomic DNA was isolated using Wizard DNA purification kit (Promega, Madison, WI) and utilized as a template.

*Caries Assessment with Optical Microscopy:*

The rats were sacrificed by CO2 asphyxiation on day 50 and maxillas and mandibles were dissected. Surrounding soft tissues were defleshed by dermestid beetles. The cleaned jaws were then immersed in murexide solution (ammonium purpurate, 0.06% (w/v) in 70% ethanol) for 16 hours, and caries were scored using modified Keyes' method.[169, 170]

*SEM and EDXS Analysis:*

SEM and energy dispersive X-ray spectrometry (EDXS) characterization were carried out in a JSM 6100 (JEOL) at 15kV, as described previously.[78] Line profiles were obtained from different regions using ImageJ™ and mean profiles were calculated (n=5). Full-width-half-maximum

(FWHM) values of negative peaks appearing at dentino-enamel junction (DEJ) were determined after background correction using OriginPro 8 software.

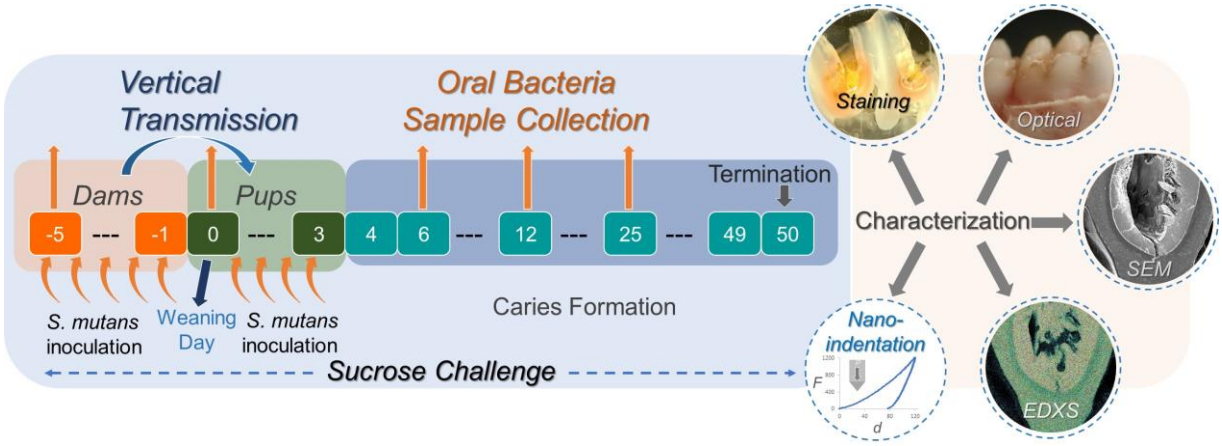


**Figure 26:** Schematics of experimental timeline of bacteria inoculation, sucrose challenge, infection monitoring during caries formation, and the characterization procedures used. Arrows pointing up indicate days of bacteria sampling. Inoculation days of dams and pups are depicted with curved arrows.

*Nanoindentation Tests of Carious Lesions:*

Nanoindentation measurements were carried out on hemi-sectioned teeth using an Ubi™ nanoindentation system (Hysitron, Minneapolis, MN) as described previously.[78, 112, 148] Maximum indentation depth for all measurements was kept at 120 ±10 nm. Results were averaged over 40 measurements.

*Statistics:*

Caries scores are expressed as the mean ±standard error. Statistical analysis was performed on relative abundance of *S. mutans* using Microsoft Excel Worksheet. Statistical significance of mean values was determined by Student's t-test, and a $P < 0.01$ was considered significant.

4.1.3. Results

Here, we report the development of a rat model that induce formation of mild carious lesions with a real-time monitoring of *S. mutans* infection. A detailed morphology, mineral content, and local

properties analyses of early fissure caries was done using optical microscopy, SEM and nanoindentation (**Figure 26**).

*Selection, Weight Gain and General Health of Animals:*

Both female and male rats were used to primarily eliminate any possible potential gender-bias in caries formation as discussed by the clinical studies.[183] All animals thrived throughout the experiment and no significant difference in their weight gain was observed.

*Monitoring S. mutans Infection:*

MSB agar plates that were inoculated with day -5 saliva samples (before bacteria inoculation) showed no evidence of *S. mutans* growth. The relative abundance of *S. mutans* in mouth flora at day 0 (weaning day) was 0.00112% (±0.00005), demonstrating that the vertical transmission from dams to pups was successful (**Figure 27A**). The relative amount of *S. mutans* increased gradually and reached 0.00671% (±0.00008) at day 6. The saturation point of *S. mutans* colonization was observed at day 12 with 0.01304% (±0.00012). Afterward, the relative abundance of *S. mutans* remained relatively stable at 0.01281% (±0.00015) without a significant change ($p=0.42$, *t*-test) in comparison with day 12 ($n=3$).

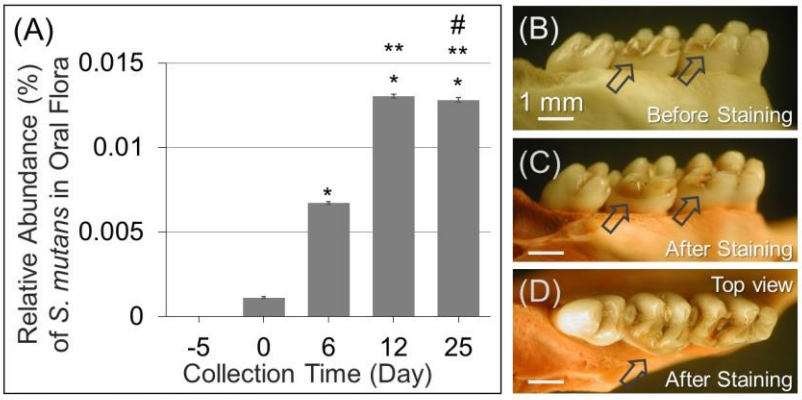


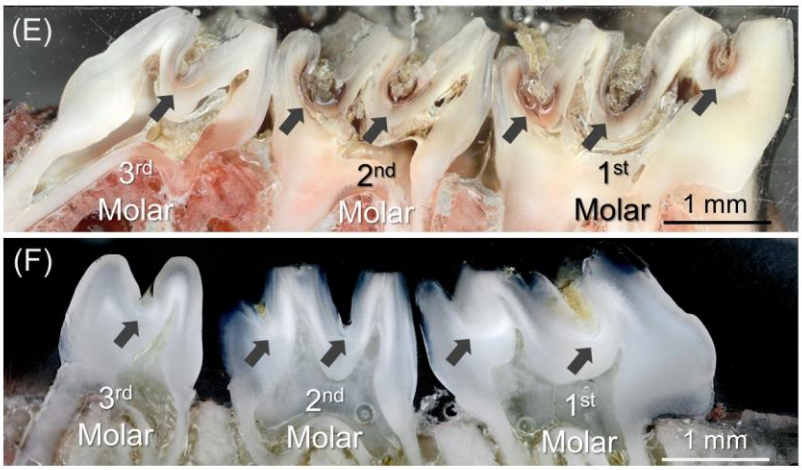


(G) Caries Scores (Mean ± SD)

| | E | $D_s$ | $D_m$ | $D_x$ |
|---|---|---|---|---|
| Buccal/Lingual | 11.8 ± 1.7 | - | - | - |
| Morsal | - | - | - | - |
| Sulcal | 2.6 ± 0.8 | 13.2 ± 2.4 | 8.2 ± 0.9 | 17.6 ± 4.20 |
| Proximal | 2.8 ± 1.1 | 1.5 ± 1.1 | - | - |
| Total | 17.2 ± 2.0 | 14.4 ± 3.3 | 8.2 ± 0.9 | 17.6 ± 4.20 |

**Figure 27:** Monitoring of *S. mutans* infection progression in rats and optical analysis of carious lesions with caries scores. (A) Relative abundance of *Streptococcus mutans* in oral flora (y-axis) on different days (x-axis) quantified by quantitative real-time polymerase chain reaction. *P < 0.01 vs. day 0. **P < 0.01 vs. day 6. #No significant difference vs. day 12. Representative carious lesions formed at day 50 (B) before and (C, D) after murexide staining. Representative hemisectioned teeth images from (E) infected and (F) noninfected (control) animals. Surface lesions are visible before and after staining, while fissure carious lesions dominate cross-sectioned images of teeth obtained from infected animal. (G) Mean caries scores per rat (12 animals, n = 12) categorized as enamel (E) and slight (Ds), moderate (Dm), or extensive (Dx) dentin-type lesions based on Keyes's scoring. Arrows indicate molar fissure regions where caries are present in infected rats (E) but not in the noninfected control group (F).

*Caries Assessment with Optical Microscopy:*

The carious lesions established on buccal/lingual (smooth), morsal, sulcal, and proximal sites were scored according to penetration depth of murexide as enamel or slight, moderate, or extensive dentin-type lesions. Representative images of average carious lesions obtained after 50 days of post-infection and resulting mean caries scores per animal (12 animals, n = 12) are shown in Figure 27B to 27E and 27G, respectively. Darker regions that are visible on buccal surfaces before (Figure 27B) and after (Figure 27C, D) staining were scored as enamel-type lesions.

On fissure/sulcal and proximal sites, dentin-type lesions were

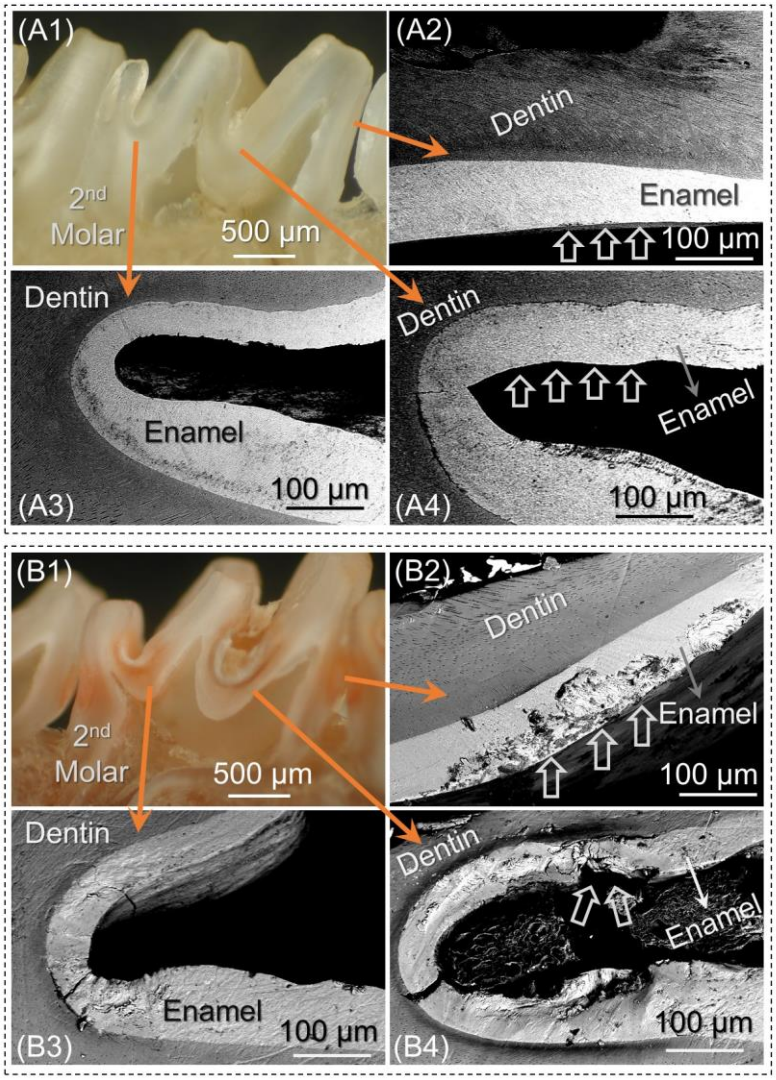


**Figure 28:** Hemi-sectioned molar teeth obtained from noninfected rats: (A1) optical and (A2–A4) backscattered electron images. The second molar showing a uniform contrast along enamel and dentin: (A2) proximal and (A3, A4) fissure surfaces. Hemi-sectioned molar teeth obtained from infected rats: (B1) optical and (B2–B4) backscattered electron images. (B2) An E-type lesion on proximal surface of the second molar. (B3, B4) Dx and Dm type of carious lesions in fissure sites. White arrows indicate comparable locations of the molars from the control (A2 and A4) and infected (B2 and B4) groups.

more prominent, possibly due to the more favorable microenvironment for colonization (Figure 27E). Especially in the distal fissures of first and second molars, lamination of dentin was visible, indicating the severity of lesions. Moreover, in the middle fissure of the first molar and mesial fissure of second molar teeth, enamel loss was very apparent. No carious lesion formation was observed in noninfected rats with murexide staining (Figure 27F). Overall, enamel-type caries with a slight dentinal involvement were more prevalent than moderate and extensive dentinal lesions (Figure 27G).

*SEM and EDXS Analyses of in vivo Caries:*

Backscattered electron (BSE) images of fissures after murexide staining are demonstrated in **Figure 28**. The murexide-negative fissures and proximal sites on the second molar (Figure 28A1) showed no cavitation on enamel. The uniform contrast of dentin underneath indicated no significant demineralization activity (Figure 28A2–A4). The murexide positive enamel-type lesion located on the proximal surface of the second molar (Figure 28B2), however, showed a cavitation about ~80 μm in depth. In contrast, 2 fissure lesions that were scored as extensive and moderate dentin lesions based on staining (Figure 28B3, B4) displayed superficial cavitation on enamel with an almost intact dentin underneath.

SEM classification of fissure caries is demonstrated in **Figure 29**, with 4 representative specimens—3 of which exhibited fissure caries with different degrees of severity and 1 with no caries. SEM images of the caries-free control sample (Figure 29A1), recorded in secondary electron imaging mode, showed no caries-like structural features. Moreover, the uniform contrast through the enamel and dentin in the BSE images and EDXS maps indicated that there was no demineralization. The narrow crack with smooth edges is more likely due to the drying process during sample preparation.

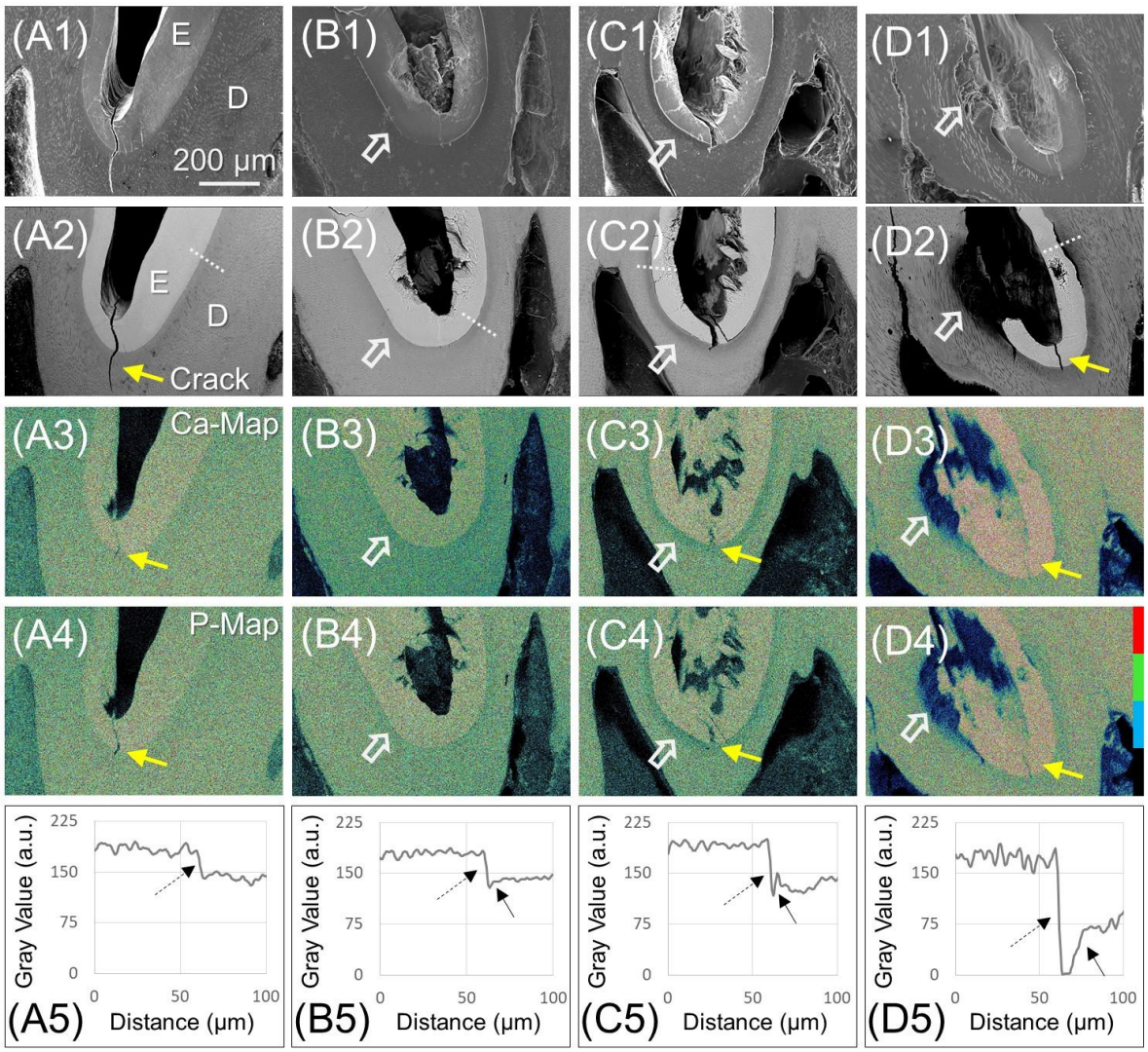


**Figure 29:** Hemisectioned rat molars: (A1–D1, first row) secondary electron imaging and (A2–D2, second row) backscattered electron images and associated (A3-D3, third row) calcium (Ca) and (A4–D4, fourth row) phosphorus (P) energy-dispersive X-ray spectrometry maps. (A5–D5, fifth row) Line profile analysis along the dotted line in A2 to D2 (row 5). Black arrows indicate crack positions on line graphs. Each sample was stained with murexide before cross-sectioning and scanning electron microscopy analysis. Murexide staining analysis demonstrated no caries on the first sample (column A), while others showed enamel (column B) and moderate (column C) and extensive (column D) dentin-type lesions. Elemental concentrations on energy-dispersive X-ray spectrometry maps were shown in an increasing order with black, blue, green, and red dots. Yellow arrows point out the crack positions on each image, while the white arrows highlight the demineralized regions adjacent to DEJ.

In the enamel-type lesion (Figure 29B1), the enamel layer at the lateral site of the fissure became thinner due to demineralization while the underlying dentin was still intact. The uniform contrast through the dentin in the BSE image of Figure 29B2 and EDXS calcium and phosphorus maps (Figure 29B3, B4) indicated that the mineral content was identical and that demineralization was restricted to enamel.

In the moderate dentin-type lesion (Figure 29C1), enamel cracks were more prominent lateral to the fissure. The long crack starting from the enamel and progressing into the dentin implies the presence of more severe demineralization as compared with the enamel lesion in Figure 29C. The dark gray area adjacent to the enamel (Figure 29C2) implies lesser mineral content versus the rest of dentin. The decreases in calcium and phosphorus contents in this particular demineralized area were confirmed with EDXS (Figure 29C3, C4). Here, dentin is still intact without any delamination, classifying it as moderate dentin-type lesion.

In the last set of images shown in Figure 29D, the enamel on one side of the fissure (highlighted with arrow) is lost completely, and the underlying dentin is delaminated. The loss of underlying dentin in this particular area was about 100 μm in depth, indicating extensive dentin lesion.

The dark gray regions adjacent to the DEJ were further analyzed by line profiling (Figure 29A2–D2, dotted line), and the change in the contrast by full-width half-maximum analysis provided the average width of the crack. The calculated values for caries-free, enamel, moderate, and extensive samples were 16.15 ± 1.25 μm, 2.50 ± 1.25 μm, 10.56 ± 1.27 μm, and 9.32 ± 1.25 μm, respectively (Figure 29A5–D5). The differences between the peak minimum and average background were 2.98, 9.47, 5.70, and 55.45 (gray values, arbitrary unit), respectively. The increase in the calculated peak minimum-average background values compared with the caries-free sample reflects the extent of the demineralized region due to cariogenic activity.

*Nanoindentation Tests:*

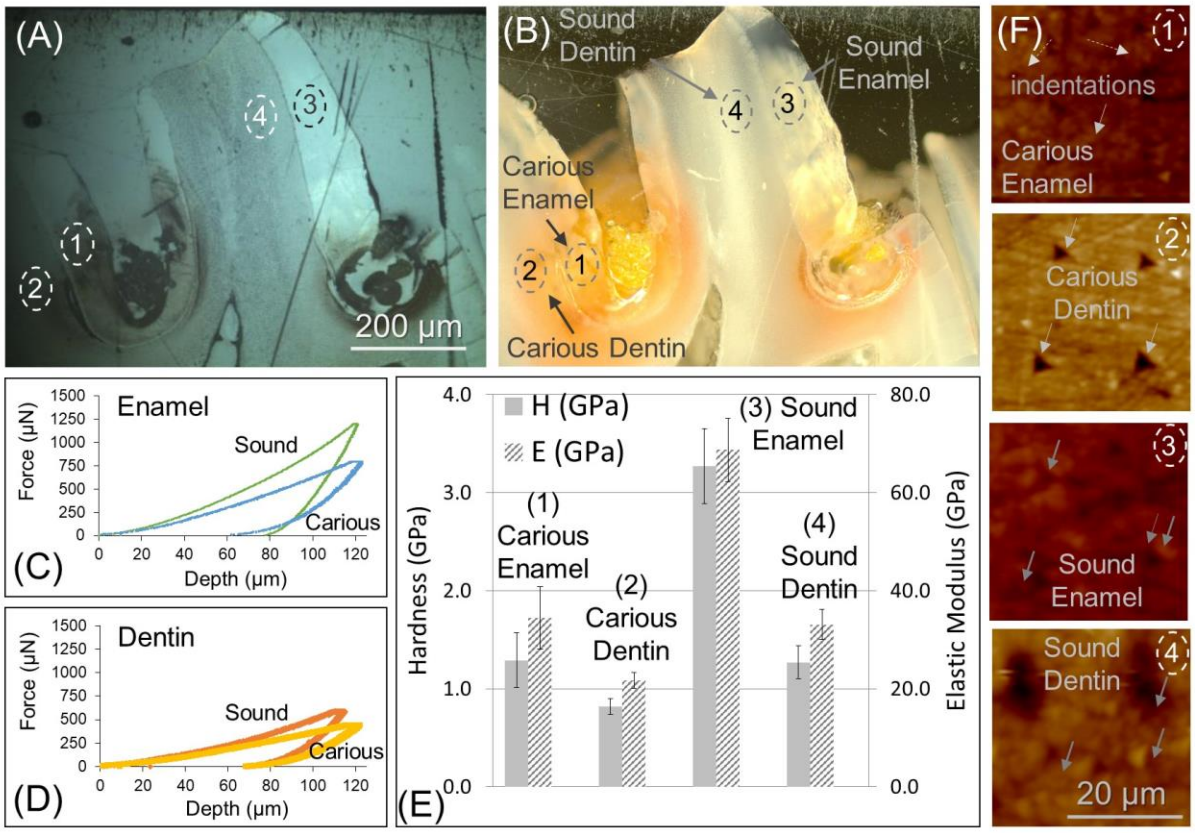


**Figure 30:** Nanomechanical characterization of carious and healthy dentin and enamel. (A, B) Light optical images of indentation sites. Average indentation curves (force-depth) of (C) enamel and (D) dentin. (E) Mean hardness (H) and elastic modulus (E) values of carious and sound dentin and enamel tissues. (F) Indentation footprints of indenter tip on carious and healthy dentin and enamel tissues.

Local nanomechanical properties of sound and carious tissues were determined with nanoindentation (**Figure 30A-F**). The measured hardness (H) and elastic modulus (Er) of the sound enamel were 3.27 ±0.38 GPa and 68.7 ±6.5 GPa, respectively. In carious enamel, about a 50% reduction in H (1.29 ±0.28 GPa) and Er (34.41 ±6.4 GPa) values was observed in comparison with the sound enamel. A similar decreasing trend in H and Er values was also observed in carious dentin (0.82 ±0.08 GPa and 21.7 ±1.6 GPa) in comparison with sound dentin (1.27 ±0.17 GPa and 33.1 ±3.1 GPa).

### 4.1.4. Discussion

An *in vivo* caries formation model promoting mild carious lesions in rats was developed in this study. The resulting carious lesions were then analyzed in detail via structural imaging and nanomechanical tests to develop an in-depth understanding of the nature of carious lesions. To ensure prominent caries formation, emphasis was placed on the age of animals, infection procedure, and diet. In contrast to the previously established models, *S. mutans* colonization was ensured by a prior inoculation of dams for vertical transmission of *S. mutans*, as well as direct inoculation of pups without the use of antibiotics. Moreover, during the inoculation process, pups' access to their bedding and any chewable objects were eliminated so that the possible tooth cleaning effect of chewing was prevented.[159, 184] Furthermore, the implementation of qPCR to the rat model facilitated monitoring of the colonization efficacy of *S. mutans* in oral flora and thereby, enabled assessment of the success of the inoculation procedure in real-time.

Following the Larson's scoring method[169], carious lesions were initially evaluated with murexide staining. While murexide staining was useful in locating the carious lesions (Figure 27), it was limited in revealing the details of the caries. This limitation, however, was alleviated by SEM imaging and nanoindentation testing. For example, in the light optical image in Figure 28B1, although all the regions (fissures and proximal) were murexide positive, it was unclear how advanced the carious lesions were in the 3 regions, shown by arrows. The SEM imaging revealed that the extent of enamel cavitation was the most severe in Figure 28B2 whereas the enamel was mostly intact in Figure 28B3. In all cases, SEM revealed a dark band at the DEJ indicating severe demineralization along the boundary between enamel and dentin tissues. However, the dark bands seen here are relatively narrow, within 20 μm, about an order of magnitude smaller than the width obtained by murexide staining (Figure 28B1). This suggests that the severity of dentin-type caries

might not have been as extensive as indicated with the staining visualized by optical microscopy. Since dentin is rich in organic content (i.e., collagen) and porous, the stain could have possibly penetrated the healthy dentin. It should also be pointed out that fissure cracks are occasionally created artificially on enamel during cleaning and staining steps, which involves drying of the tooth specimen. In such cases, the stain would penetrate through the artificially created fissure cracks and possibly cause false-positive caries scores. It is further noted that demineralization along the DEJ was prominent in Figures 29C2 and 29D2, a common observation of fissure caries by SEM analysis. The accompanying EDXS maps, indeed, confirmed a decrease in mineral content within the DEJ. Therefore, the demineralized region along the DEJ could be used as a specific feature in SEM and EDXS analyses to specify demineralized areas (Figure 29D1-4) and differentiate them from the drying artifacts (Figure 29A1-4).

The carious enamel and dentin along the DEJ were further quantified for mechanical properties by localized nanoindentations in discrete regions. As shown in Figure 30C-E, the carious enamel and dentin had elastic modulus and hardness values significantly lower than those corresponding to the sound tissues. Some carious regions, however, resulted in rougher surfaces after polishing, which prevented complete nanoindentation measurements on the entire surface. Nanoindentation in this work was nonetheless shown to be highly reliable tool in providing further insights into the nature of the carious versus sound tissues in examining the degree of demineralization quantitatively.

Taken together, the accuracy of overall caries score can be enhanced by SEM imaging with EDXS elemental analysis and nanoindentation. Incorporating these analytical techniques in caries scoring can help eliminate false-negatives or false positives that are prevalent in data relying solely on optical imaging.

### 4.1.5. Conclusions

In conclusion, an *in vivo* model promoting slow progression of mild caries in rats was developed. *S. mutans* colonization was facilitated via vertical transmission. Besides the conventional infection monitoring and caries scoring methods, more accurate modalities were implemented. First, unlike the conventional semi-quantitative agar plating procedures, qPCR was utilized to accurately quantify bacterial infection during caries formation. Second, in addition to murexide-based caries detection and scoring methods, SEM and EDXS analyses were carried out on carious and sound tissues that provided detailed structure, morphology, mineral content, and elemental compositional data. Third, nanoindentation tests quantitatively presented local mechanical property variations of carious lesions due to demineralization. The *in vivo* model reported in this work can be utilized in cariology research and may develop into a standard protocol for testing new caries prevention and treatment procedures.

This section (Chapter 4.1) was reprinted with permission from *Yucesoy D.T., Fong H., Gresswell C., Chung W.O., Dogan S., Sarikaya M. (2018). Early Caries in an In Vivo Model: Structural and Nanomechanical Characterization. Journal of Dental Research, 97 (13), 1452-59.* Copyright (2018) SAGE Publications.[185]

## 4.2. Amelogenin Derived Peptide-guided Biomimetic Tooth Repair *in vivo*

### 4.2.1. Introduction

*Statement of the Problem:* Demineralization is a leading cause of many common oral diseases which can be defined as the irreversible loss of minerals in dental hard tissues due to acidic attack.[186, 187] Acid-producing bacteria within the oral flora, acidic dietary products and gastroesophageal diseases are the most common sources of this subtractive process.[49, 93, 188, 189] This acidic attack primarily affects the enamel, the hardest tissue in human body constituting the outer layer of the tooth to provide physical protection.[190] Due to its non-regenerative nature, mature enamel is unable to heal and repair itself. Incipient caries and white spot lesions (WSL) as well as hypersensitivity, are the earliest clinical evidence of enamel demineralization, and if left untreated may easily progress into more serious oral health problems including dental caries, a prevalent oral disease among the global population. [1, 186, 191]

*Current Approaches:* In clinical dentistry, current treatments to restore dental tissues, in particular enamel, rely on synthetic restorative materials such as amalgam, ceramics, or polymer composites.[31, 32, 40, 192] However, these synthetic restorations may fail over time due to weak adhesion at the lesion/restorative material interface mainly due to their physical (crystallography and morphology) and chemical differences (elemental compositions and phases) with the underlying mineralized tissue.[36-38] In most cases, these decoupled interfaces provide a protected environment for bacteria to colonize and therefore shortly after synthetic restorations secondary caries arise.[193-195]

*Traditional Biomimetic Approaches:* Biomimetic restoration of dental hard tissues through a natural remineralization process may provide an ideal solution for the prevention of demineralization related dental diseases. So far, using biomimetic pathways, a considerable

number of attempts have been made to replace the lost mineral in dental tissues through remineralization which can restore the original structure and the resulting function.[50, 55, 58] These strategies include the use of full-length amelogenin, LRAP, peptides, dendrimers, ion containing hydrogels, and other physical chemistry approaches. [50, 51, 58, 59, 80, 101-103, 148] Although adding to the general knowledge of tooth surface remineralization, so far, no clinical remineralization system has emerged to promote biomimetic enamel subsurface remineralization *in vivo*. Although these investigations have been adding to the general knowledge of remineralization, overall, however, they still face an ongoing challenge in clinical dentistry.

*Proposed Approach:* We reported a novel protocol to identify functional domains within the natural proteins, amelogenin-derived peptides (ADP's), to guide cell-free remineralization of dental hard tissues.[54, 55] These peptides epitomize catalytic functions of the natural protein amelogenin, the key protein in enamel formation, which directs the recruitment of constituent ions, synthesizing the mineral as well as controlling mineral morphology on the surface of the tooth. Using these peptides, biomimetic reconstruction of a mineralized layer on demineralized human root dentin has been demonstrated *in vitro*.[55] The resulting mineral layer formed through this peptide-guided biomimetic process showed cementum like features by forming a strong structural and mechanical integration with the underlying dentin.

In this study, the aim is to investigate the therapeutic potential of shADP5 peptide to restore enamel tissue *in vivo*. We report the use of an shADP5-containing gel formulation to promote functional remineralization of artificial caries formed on enamel surfaces through bacterial attack in an *in vivo* rat model.

4.2.2. Materials and Methods

*Animals:*

13-day old, 12 female and 12 male SPF Sprague-Dawley (Charles-River, Wilmington, MA) rats were obtained with their dams and housed in plastic cages (Allentown Inc., Allentown, NJ) on corn-cob bedding with access to food and water *ad libitum*. Animals were handled in strict accordance to the guidelines of National Research Council Guide for the Care and Use of Laboratory Animals, and the experimental procedures for the care of animals were approved by the Institutional Animal Care and Use Committee (IACUC) of University of Washington.

*Caries Formation in Rats:*

Carious lesions in rats were induced to form using a procedure as described previously. (See Section 3.1) Briefly, animals (both dams and pups) were inoculated with cariogenic bacteria, *S. mutans* for 3 consecutive days before and after weaning and kept under sucrose challenge until the carious lesions formed. All animals were offered cariogenic MIT-200 powdered diet (Harlan Labs, Indianapolis, IN) and filter-sterilized 10% sucrose water (w/v) *ad libitum*.

*Formulating Toothpaste Ingredients:*

Three separate gel formulations were prepared, which contained aqueous solutions of shADP5 peptide, ionic calcium ($CaCl_2$), and ionic phosphate ($KH_2PO_4$). Each toothpaste shared the same inactive chemical constituents. shADP5 was synthesized in house to 99% purity (See Section 2.1.2). 1.6mM of shADP5, 960 mM of $CaCl_2$, and 575 mM of $K_2HPO_4$ were first prepared in 24 mM Tris buffer with final pH adjusted to 7.4. Separately the gel formulation was prepared by mixing potassium sorbate, propylene glycol, glycerol, 60% aqueous sorbitol, simethicone and cellulose gum using a low speed propeller at 50ºC. After the mixture cooled down to room

temperature, final formulations were made by 1:1 (v/v) mixing the solutions of 1.6mM of shADP5, 960 mM of $CaCl_2$, and 575 mM of $K_2HPO_4$ with the gel formulation using a low speed propeller.

*Test Groups:*

After formation of sufficient carious lesions in rats, animals were divided into six groups randomly. Treatment groups were:

1. Baseline #1 (No infection - euthanized at day 50)
2. Baseline #2 (*S. mutans* infection - euthanized after sucrose challenge)
3. Negative control (no treatment)
4. Positive control #1 (Ca/P only treatment)
5. Positive control #2 (1000ppm fluoride (toothpaste concentration) + Ca/P treatment)
6. Test group (Peptide + Ca/P treatment)

*Remineralization Procedure:*

Carious enamel lesions in rats were first cleaned by cotton swaps soaked in 1.5% hydrogen peroxide (HP) solution for 15 seconds. Excess HP solution was removed from the tooth surface by cotton swaps soaked in deionized water.

Peptide gel formulation was then applied by using a toothpick to an area covering the affected enamel surface and incubated for 10 mins. Then, an equal amount of the 960mM $CaCl_2$ or 575 mM $KH_2PO_4$ formulation was mixed together in a petri dish, and applied onto the affected tooth surface. During the remineralization treatment animals were kept sedated for 1 hour. Next, animals were transferred back into their cages and *fed ad libitum* with low calcium diet and deionized water. This procedure was repeated daily for 14 consecutive days.

*Sample Characterization by SEM and EDXS:*

The day after the completion of 14-day remineralization treatment, rats were sacrificed by $CO_2$ asphyxiation and their mandibles were dissected. Surrounding soft tissues were defleshed by dermestid beetles.

The parasagittally-sectioned samples were prepared by opening a notch on the underside of the dissected jaw using a low speed diamond saw (Isomet, Lake Bluff, IL) and then fractured in half in the sagittal direction to expose the interior of the teeth. Prior to SEM imaging, samples were coated with 5 nm of gold. SEM characterization was carried out in a JSM 6100 SEM (JEOL) operating at 15kV. Composition analysis was performed using the onboard energy dispersive X-ray Spectrometer (EDXS). Recorded images were analyzed using ImageJ™ image processing software and thickness of the mineral layer and width of the tubules were averaged from 5 images per sample (5 samples per test group). Results are expressed as the mean ± standard error.

*Nanomechanical Properties Characterization:*

Mandibles were prepared by cutting in half in the sagittal direction and embedded in room temperature cure epoxy to provide a continuous volume for indentation characterization. The cut interior surface was polished to 0.1 μm finish using diamond lapping films. Nanoindentation measurements were done using an Ubi™ nanoindentation system (Hysitron Inc., Minneapolis, MN, USA) in air. Hardness (H) and elastic modulus (Er) were calculated by the software accompanying the nanoindentation unit. In order to obtain indentation values that were not indentation volume dependent, maximum indentation depth for all measurements was kept at 120 ±10 nm. All reported H and Er values were averaged over 40 measurements.

4.2.3. Results

*Remineralizing Peptide Gel Formulation Preparation:*

A gel formulation containing 1.6mM of shADP5, 960 mM of $CaCl_2$, and 575 mM of $K_2HPO_4$ was developed using the basic inactive ingredients of common over-the-counter tooth gels. The viscosity of the gel formulation was adjusted to be comparable to toddler's tooth paste, which provides a retention time on the tooth surface that is needed for new mineral formation.

The peptide shADP5, shortened ADP5, was generated using a procedure that was developed for designing protein-derived peptides, as described previously (See Section 2.1.2). The peptide (**Table 6**) was synthesized by using an automated solid-phase synthesizer (CS336X; CS-Bio, Menlo Park, CA, USA) through Fmoc-chemistry and purified by RP-HPLC with up to >99% purity (Gemini 10u C18 110A column). The sequence of the peptides was confirmed by a MALDI-TOF mass spectrometry with reflectron (RETOF-MS) on an Autoflex II (Bruker Daltonics, Billerica, MA, USA).

**Table 6:** Molecular characteristics of the shADP5 peptide used in this work.

| shADP5 (AA sequence) | MW | pI | G.R.A.V.Y. | Charge |
|---|---|---|---|---|
| SYEKSHSQAINTDRT | 1736.8 | 6.47 | -1.627 | 0 |

*Caries Formation and Characterization:*

Carious lesions in rat molar teeth were developed using an *in vivo* rat model as described previously (See Chapter 3.1). Briefly, 13-day old, 12 female and 12 male specific-pathogen-free Sprague-Dawley (Charles-River, Wilmington, MA) rats were obtained with their dams and infected with cariogenic bacteria (*Streptococcus mutans* UA159 American Type Culture Collection (ATCC) 700610). During the infection period, rats' access to bedding was restricted by placing stainless steel mesh within the plastic cages (Allentown Inc., Allentown, NJ) on top of their bedding.

After the *S. mutans* colonization was ensured, the animals were transferred into new cages with corn-cob bedding with access to food and water *ad libitum.* During the caries formation period, the level of cariogenic infection was monitored using qPCR that is developed previously. At day 50, animals were distributed by sex (4 animals per cage). While the animals in Groups 1 and 2 (Baseline) were sacrificed and their teeth were extracted immediately to analyze resulting carious lesions, the rest were divided into 4 groups (See Materials and Methods, Section 3.1) to receive treatment for additional 14 days. All animals were sacrificed at the end of 14 days after the completion of treatment and their teeth were extracted and subjected to structural and mechanical characterization (**Figure 31**).

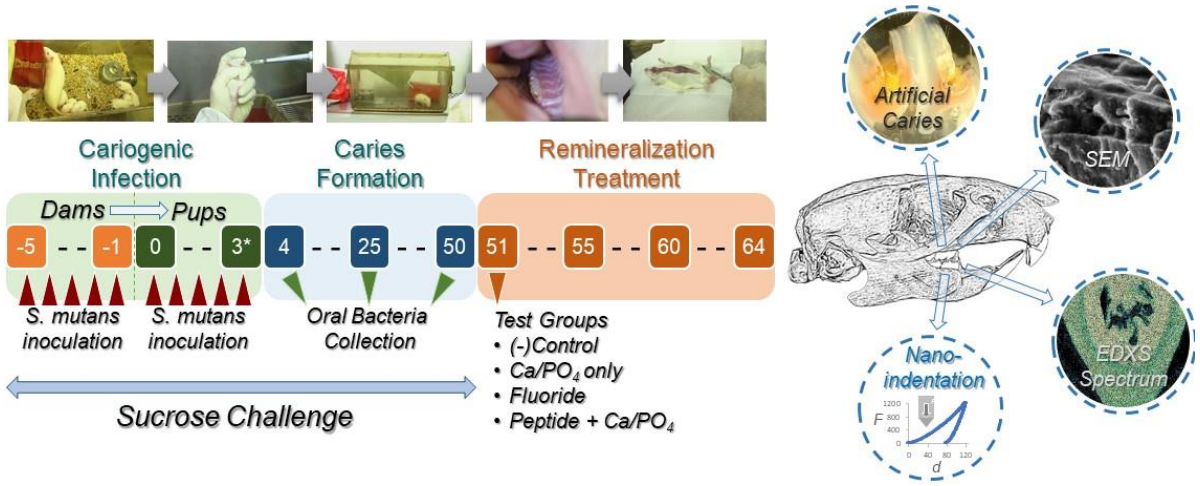


**Figure 31:** Schematics of caries formation and treatment procedure in rat model.

*SEM and EDXS analysis:*

Teeth fractured in parasagittal direction were subjected to structural and compositional analyses via SEM and EDXS, respectively. It is noted that due to the small size of the third molars, fracturing did not lead to clean cross-sectioned surfaces. Therefore, only the first and second molars generally were utilized for cross-sectional analysis. SEM images of carious enamel lesions in Groups 1 and 2 was shown previously (Section 4.1). Images taken from the teeth collected from

Group-3 animals that did not receive any treatment revealed highly rough enamel surface with exposed enamel rods (**Figure 32a**). On the other hand, highly smooth surface deposits (layer) with a thickness of 1.6 ±0.9 µm and 1.8 ±0.9 µm were observed in Positive Control #1 (no peptide, no fluoride) and Positive Control #2 (fluoride, no peptide), respectively. In contrast, in the treatment group (peptide), a 7.2 ±1.7 µm thick, continuous mineral layer was observed (Figure 32d).

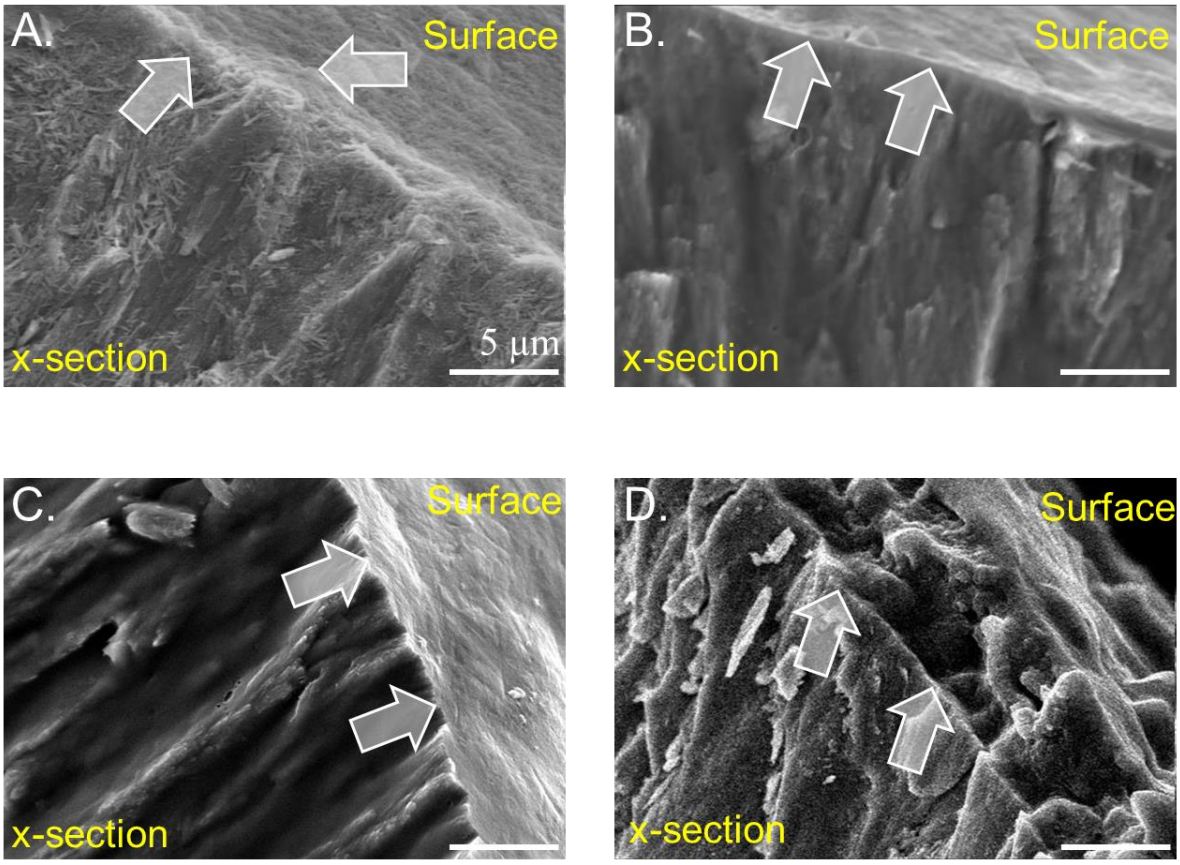


**Figure 32:** Representative SEM images of rat molar teeth, (buccal side of 1st molars) after 14 days of treatment: (a) no treatment (negative control), (b) Ca/PO4 gel only (positive control 1), (c) 1000 ppm F/ Ca/PO4 gel (positive control 2), and (d) peptide/ Ca/PO4 gel (test group). As shown in (a) through (c), the mineral layer on the enamel surface of negative control and the two positive control groups is almost non-existent. The peptide treated test group in (d) exhibited a mineral layer of 5 µm or more.

The SEM image shown in **Figure 33** reveals all three aspects of the remineralized structure: the side view of the enamel showing enamel rods; the surface of the carious lesion, displaying highly

rough topography, and the newly formed mineral with an integrated interface between the new layer and the existing carious structure. Furthermore, the elemental compositional analysis of these three distinct regions (the sound enamel, carious enamel and mineral layer) demonstrated that they all have similar calcium and phosphorus content ratios; 1.56 ±0.1, 1.51 ±1.0 and 1.55 ±0.9 respectively (**Table 7**). However, the carious region and the mineral layer showed significantly higher carbon content, 28.1 ±12.6 and 10.9 ±1.6, respectively, compared to the sound enamel which contains only 1.1 ±0.2% compared to overall elemental composition (Table 7).

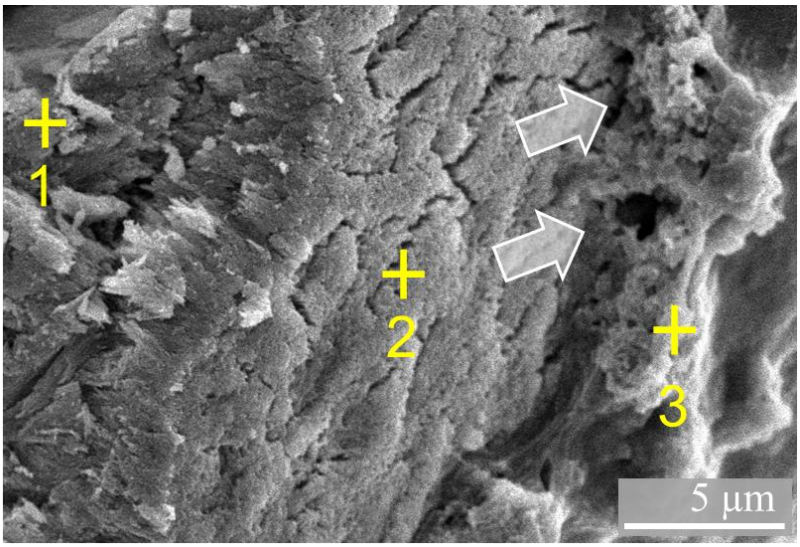


**Figure 33:** Representative image of i*n vivo* remineralized rat molar. The mineral layer is formed on the rough surface of the carious enamel lesion previously formed through cariogenic challenge. Numbers indicate the regions that EDXS analysis was performed.

**Table 7:** Elemental composition analysis of regions highlighted in Figure 33.

| EDS analysis site | Ca/P ratio | Carbon content (%) |
|---|---|---|
| Deep Enamel (#1) | 1.56 ±0.1 | 1.1 ±0.2 |
| Carious Enamel (#2) | 1.51 ±1.0 | 28.1 ±12.6 |
| Mineral Layer (#3) | 1.55 ±0.9 | 10.9 ±1.6 |

*Nanomechanical Characterization:*

The mechanical tests were conducted at the nanometer-scale by nanoindentation on the spatially selected regions. All measurements were conducted in cross-sectioned geometry by placing the indenter tip in a direction that is parallel to the surface.

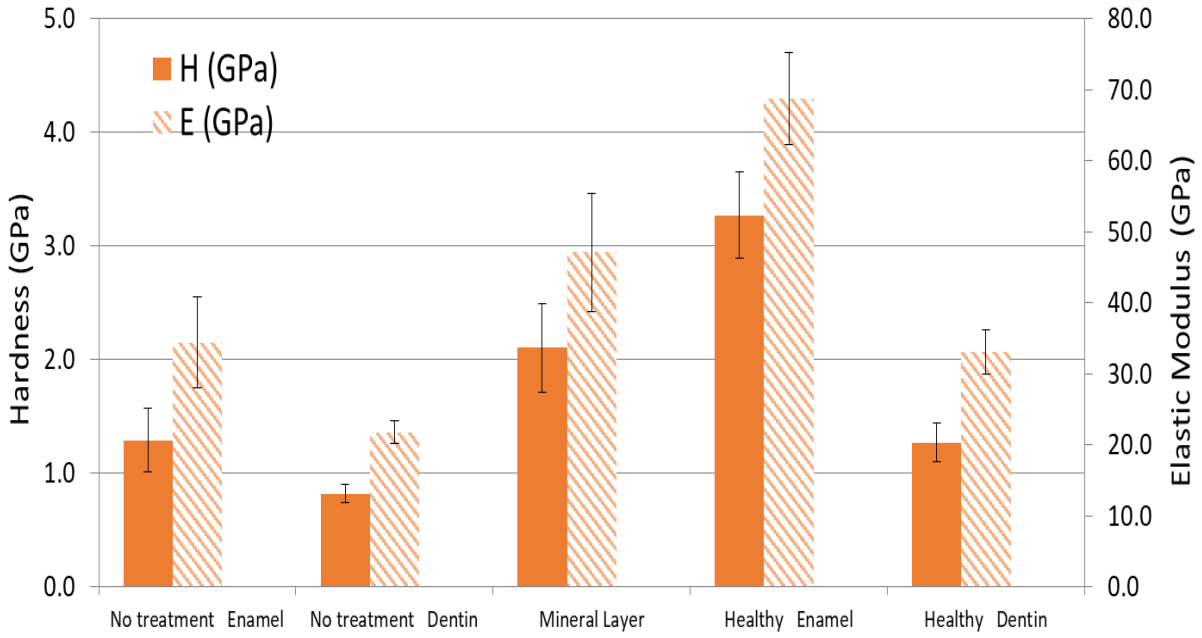


**Figure 34:** Hardness (left) and elastic modulus (right) of the selected experimental groups as measured by nanoindentation.

As shown in **Figure 34**, the average hardness and elastic modulus values for the enamel and dentin tissues obtained from Negative control (no treatment), were measured as 1.29 ±0.28, 34.41 ±6.40, 0.82 ±0.08, 21.70 ±1.60, respectively. On the other hand, in the treatment group two separate regions were targeted; the mineral layer itself and underlying carious enamel. While the hardness and elastic modulus of the mineral layer was measured as 2.10 ±0.39 and 47.07 ±8.37, the underlying enamel revealed hardness of 3.79 ±0.34 and elastic modulus of 90.71 ±7.97.

4.2.4. Discussion

A cell-free, biomimetic tooth gel was developed to remineralize artificially induced carious lesions on rat enamel *in vivo* using a 15-amino acid long amelogenin-derived peptide, shADP5, along with properly tuned ionic concentrations of $Ca^{2+}$/$PO_4^{3-}$ *in vitro* in the presence and absence of fluoride content which were chosen based on the values in the frequently used present dental treatments.

The carious lesions were developed using a procedure to form mild caries in rats.[185] After the sufficient progression of the cavities in rat molars, animals were distributed into different cages randomly and treatment was administered daily through topical application of anti-caries remineralization gel. To prevent the mechanical removal of tooth gel from the tooth surface through tongue movements, rats were kept sedated during the treatment.

The SEM images revealed that (Figure 32), a new mineral layer was formed on the teeth of peptide treated group with a thickness exceeding 7.2 ±1.7 μm. In contrast, in positive control groups, non-continuous deposits were observed with a significantly less mineral layer thickness. The presence of these mineral deposits in the two positive control groups were likely made possible by the repeated exposure to Ca/P treatment. The gel formulation itself might have acted as a mild adhesive. However, the peptide treated test group clearly showed a more favorable mineral layer deposition on the surface of the teeth. It was also noted that the carbon content in the new peptide directed mineral layer, as analyzed by the SEM's onboard energy dispersive X-ray spectroscopy (EDS), was higher than that of native enamel, which was likely contributed by the residual organics that were part of the gel formulation.

These results confirmed the efficacy of the amelogenin derived peptide (shADP5) to mineralize enamel surface when delivered in a gel formulation. As shown in Figure 33, the integration of the

newly formed mineral is significant from the point of mechanical durability of the mineralized layer and its function as part of the chewing surface of enamel.

The mechanical properties of treatment surfaces were acquired by nanoindentation (Figure 34). It is noted that specimens were tested dry in ambient air, which deviates from *in vivo* conditions. However, all measurements were done under the same conditions and therefore the differences between carious and sound areas are valid. The enamel tissues in both positive control and negative control groups revealed similar nanomechanical properties suggesting that mineral-like discontinuous deposits have no significant contribution to mechanical properties. On the other hand, the hardness and elastic modulus measured from the mineral layer itself (2.10 ±0.39 and 47.07 ±8.37) were significantly lower than underlying enamel but higher than sound dentin which has hardness and elastic modulus of 1.69 ±0.20 and 25.44 ±4.17, respectively.

4.2.5. Conclusions

In conclusion, a novel dental gel formulation was designed that contained a short, amelogenin-derived peptide, shADP5, and that provided the means to remineralize *in vivo* induced enamel lesions on the surface of rat teeth. Besides the active ingredient peptide in low concentrations, the dental gel formulation also contained relevant amounts of calcium and phosphate ions that supplemented the precursor materials on the surface of the lesions (**Figure 35**, steps 1-2). Next, formation of carious lesions on the rat molars through combination of bacterial and sucrose challenge over a period of 50 days Sprague-Dawley rats (Figure 35, step 3) was demonstrated. Furthermore, remineralization using the gel formulation applied over two weeks period. Structural and spectroscopic analyses demonstrated that the newly formed mineral is functionally integrated into the carious enamel and had a thickness of ~7 micrometer, covering the surface of the teeth (Figure 35, steps 4-6). The procedure outlined in this work has a high potential to establish the

scientific foundations for *in vivo* remineralization and to empower practicing dentists to address dental problems due to demineralization.

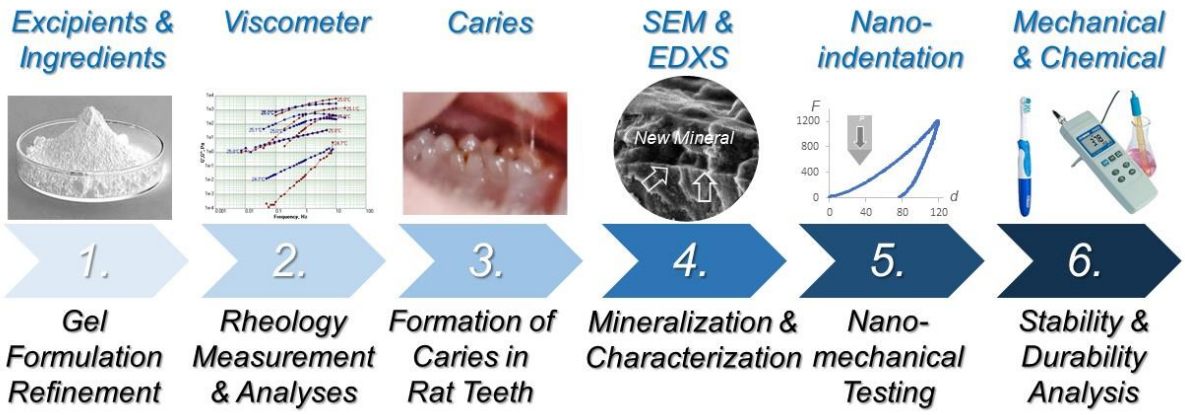


**Figure 35:** Schematic representation of tasks that are completed during the *in vivo* remineralization study.

# Chapter 5: Development of Mineralizing Peptide-based Restorative Dental Care Products

*Preamble: Translation of Peptide-guided Remineralization into Highly Potent Dental Products*

Building upon the findings of *in vitro* and *in vivo* studies, in **Task-III**, efforts were devoted to develop products that would be used as potential preventive, restorative, or therapeutic agents. One of these potential products (among the possible gels, pastes, chewing gum, mouth wash, etc.) is an oral lozenge, which was thought to possibly be utilized daily as well as clinical remineralization purposes targeting demineralization related dental diseases, e.g., WSL, hypersensitivity. The study (supported by Amazon-Catalyst program) led to the discovery that a lozenge pre-prototype was capable of not only producing a remineralized layer on the surface of human enamel under simulated saliva conditions, but also facilitating tooth whitening. This task, therefore was redesigned to systematically study both remineralization and also whitening of the teeth, and resulted in developing materials and methods for a whitening lozenge with a potential to be used for aesthetic implementation, an agent that reverses tooth staining.

## 5.1. Remineralizing Tooth Whitening Lozenges

### 5.1.1. Introduction

*Statement of the Problem:* Tooth discoloration is a common aesthetic concern for many individuals and in response the dental profession and public expend considerable amounts of time and money to improve the appearance of stained teeth.[196-198] Depending on the source and location of the stain deposits, tooth discoloration can be classified into different categories which may also be of merit to develop targeted therapies. These include, 1) Extrinsic discoloration where the chromogens deposit on the external surface of the tooth or within the pellicle layer such as tea, coffee, tobacco, metallic and salt components of dietary products (copper, sulphides);[199, 200] 2) Intrinsic staining where optical properties of the teeth are altered due to structural changes in the

inner tissues (dentin) as a result of metabolic diseases, e.g., alkaptonuria, congenital erythropoietic porphyria, congenital hyperbilirubinemia, amelogenesis imperfecta, dentinogenesis imperfecta, or presence of chromogens deposited during the dental development, e.g., tetracycline staining, fluorosis;[201-204] and 3) Stain internalization where extrinsic chromogen pigments are incorporated within the mineral tissue during the tooth development through enamel and dentin defects or leakage of dental restorative materials.[133, 205, 206]

*Current Approaches:* Current solutions for stained teeth range from standard oral hygiene processes such as tooth brushing and regular dental cleaning, to clinical and at-home use whitening agents and other restorative products such as veneers.[207-212] Over 100 million Americans use whitening products, including tooth whitening strips and pastes, veneers and crowns and according to the American Academy of Cosmetic Dentistry, total annual revenue in the whitening industry topped $11 billion at the start of 2015, with $1.4 billion spent on over-the-counter whitening products that year alone.[213] However, the existing clinical and at-home use whitening products are typically peroxide-based and remove discoloration by dissolving the stained mineral layer from the surface of teeth. Although this chemical-etching process reveals a fresh pristine surface, it is often at the expense of the enamel - the fully mineralized crown of a tooth which provides protection. While hydrogen peroxide content in at-home bleaching products ranges from 3 to 10%, in the clinical bleaching products it increases up to 35-40%.[205, 214] As a consequence, dentin, may become exposed—creating problems, such as hypersensitivity and increased susceptibility to cavities and tooth decay, that far outweigh any cosmetic benefits. The American Dental Association reports that enamel erosion caused by peroxide demineralization can lead to adverse effects: hypersensitivity (occurring in 64% of patients), gum recession, pulp inflammation and

cavities due to regular use of whitening products.[214, 215] To date, all whitening treatment options are limited to peroxide-based, mineral subtractive products.

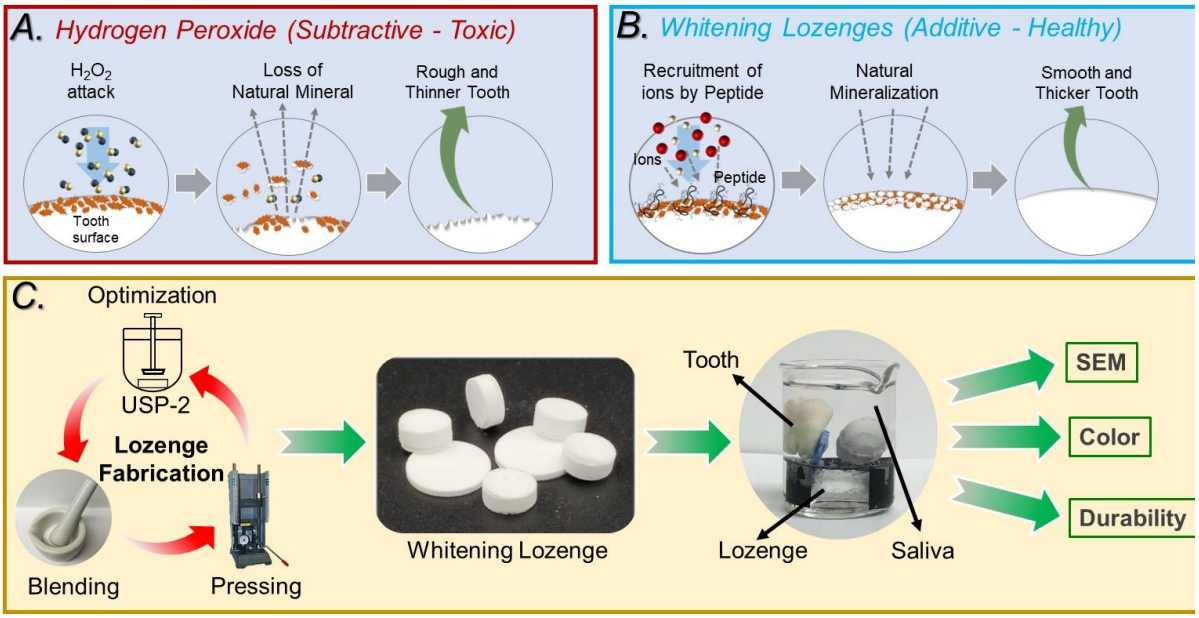


**Figure 36:** Mechanisms of action of (a) hydrogen peroxide and (b) peptide-guided remineralization-based tooth whitening. (c) A visual representation of the experimental approach.

*The Proposed Approach:* In order to provide a healthier solution to patients to improve the appearance of their teeth without permanently damaging the mineral tissues, it is, therefore, desirable to generate novel tooth whitening approaches.[216] Here, an ideal approach would be biomimetic restoration of tooth surface by adding new mineral layers atop discolored teeth and thereby giving a fresh, whiter appearance while masking the underlying discoloring stains. This could be achieved by using peptide-guided remineralization through the use of amelogenin-derived peptides.[55] In this study our aim is to develop a tooth whitening lozenge which could be used a vehicle to deliver mineralization ingredients, peptide and ionic calcium and phosphate, in a practical way and thereby provide tooth whitening through the additive, biomimetic process. The procedure and the lozenge developed in this study may provide a healthier, accessible solution to clinicians and the members of the public alike.

5.1.2. Materials and Methods

*Materials:*

99% $CaCl_2$ was purchased from Alfa Aesar (Ward Hill, MA). $KH_2PO_4$ was obtained from USB Corporation (Cleveland, OH). 99% D-Sorbitol was purchased from Sigma-Aldrich (Milwaukee, WI). All other chemicals and reagents were purchased from Sigma-Aldrich (Milwaukee, WI), and used as received unless otherwise noted. Tooth samples were donated from the UW School of Dentistry. A Minolta ChromaMeter CR-200 was obtained from Glen H. Johnson, DDS, MS, UW School of Dentistry. Ball mill, 13 mm and 9 mm metal dies, and Carver Model 3853 hydraulic press were used courtesy of the UW Department of Materials Science & Engineering.

**Table 8:** Ingredients of whitening lozenge

| | Lozenge Shell Formula | | Lozenge Core Formula | |
|---|---|---|---|---|
| **Ingredients** | **Amount (mg)** | **Weight %** | **Amount (mg)** | **Weight %** |
| Peptide | 3 | 3 | N/A | N/A |
| $CaCl_2.H_2O$ | N/A | N/A | ~93 | 54.65 |
| $KH_2PO_4$ | N/A | N/A | ~52 | 30.35 |
| Mg-Stearate | 5 | 5 | 8.5 | 5 |
| Sorbitol | 10 | 10 | 17 | 10 |
| Talc | 82 | 82 | N/A | N/A |
| Total | 100 | 100 | 170 | 100 |

*Formulating the Lozenge Ingredients and Tablet Fabrication:*

The remineralizing whitening lozenge was designed as core-shell structure where the shell contains the remineralizing peptide as an active ingredient while the core contains the ionic

calcium and phosphate. The design structure and basic composition of the lozenge layers (core-shell) is shown in **Figure 36** and in **Table 8**, respectively. To ensure homogenous disintegration of the lozenge, the powder mixture was blended according to weight percentages listed in Table 8 and ground in a ball mill at 87 rpm for 20 hours before being compressed via direct uniaxial compression (Figure 36).

*Lozenge Dissolution/Disintegration Time Analysis:*

To analyze disintegration time, a USP Dissolution 2 Apparatus was used. This apparatus is a simulated oral environment used in the literature where a paddle and shaft system stir artificial saliva at 37°C at 60 rpm. Testing was started with the addition of 9 ml of saliva into the system and then it was removed and replaced every one minute to mimic swallowing and salivation. Lozenges compressed at different forces and composed of varying ingredients were analyzed.

*Remineralization Characterization:*

To test the mineralization efficacy of lozenges, extracted human molar teeth (collected from UW clinics) were placed into the USP-2 apparatus during the disintegration testing and then rinsed with distilled water. Samples were dried with forced air and prepared SEM analysis using the procedure described previously (see section 3.1.2).

*Whitening Characterization and Color Quantification:*

Whitening quantification of lozenge treated human teeth was done using macro-photography imaging and Adobe Lightroom color analysis software. The specimen was mounted on metal strips and placed into Vita Shade Guide rock. Images were taken before and after lozenge treatment using a Canon Rebel T5i camera w/ Macro Lens 18-135mm within a custom-made photo-station equipped with white LED and diffuser. While semi-quantitative quantification was done based on visual shade comparison using vita shade guides, an absolute color analysis was performed by

analyzing the imaging using ImageJ and Adobe Lightroom color analysis software. Results were expressed with the CIE L*a*b* system.

*Head-to-head Comparison of Whitening Performance*

Whitening performance comparison was performed using extracted human teeth with similar shades that were collected from UW dental clinics and sectioned in sagittal direction. While the left half of each specimen was kept in artificial saliva as an internal control, the right halves were subjected to (1) No treatment (negative control), (2) Clinical whitening gel (containing 40% HP), (3) OTC whitening strips (containing 14% HP) and (4) Whitening-lozenge (Test sample) treatment for seven consecutive days. It is noted that the commercial products in group (2) and (3) were administered according to manufacturer's instructions while the lozenge treatment was performed under simulated oral conditions as described above. Following the treatment, specimens were mounted side-by-side and optical images were recorded with macro-photography under natural light. The change in the shades of the specimens were quantified by analyzing the images via Adobe Lightroom software and expressed in terms of both total gray value and CIE L*a*b units

5.1.3. Results

*Optimization of the Dissolution Rate*

The complete dissolution time of the lozenge was designed to be 15 minutes within artificial saliva. The core and shell parts of the lozenge were crafted using the common inactive ingredients of the existent lozenges and manufactured under different compression forces. Then, using the UPS-2 apparatus, disintegration profiles of both core and shell parts were obtained. The schematic representation of the testing procedure of lozenge disintegration time is given in **Figure 37a**.

The lozenge core was crafted to have a final 5:3 calcium to phosphate ratio, the stoichiometric ratio of calcium and phosphate in hydroxyapatite mineral. As shown in Table 8, sorbitol (sweetener) and magnesium stearate (lubricant) were used as inactive excipient. For the disintegration testing, core lozenges were fabricated using the stainless-steel die (9mm in diameter) and compressed under 9.1, 7.7 and 6.3 tonf/$m^2$ force for 2 minutes. It is noted that for initial dissolution testing, core and shell of the lozenge were fabricated separately in 300 mg. As shown

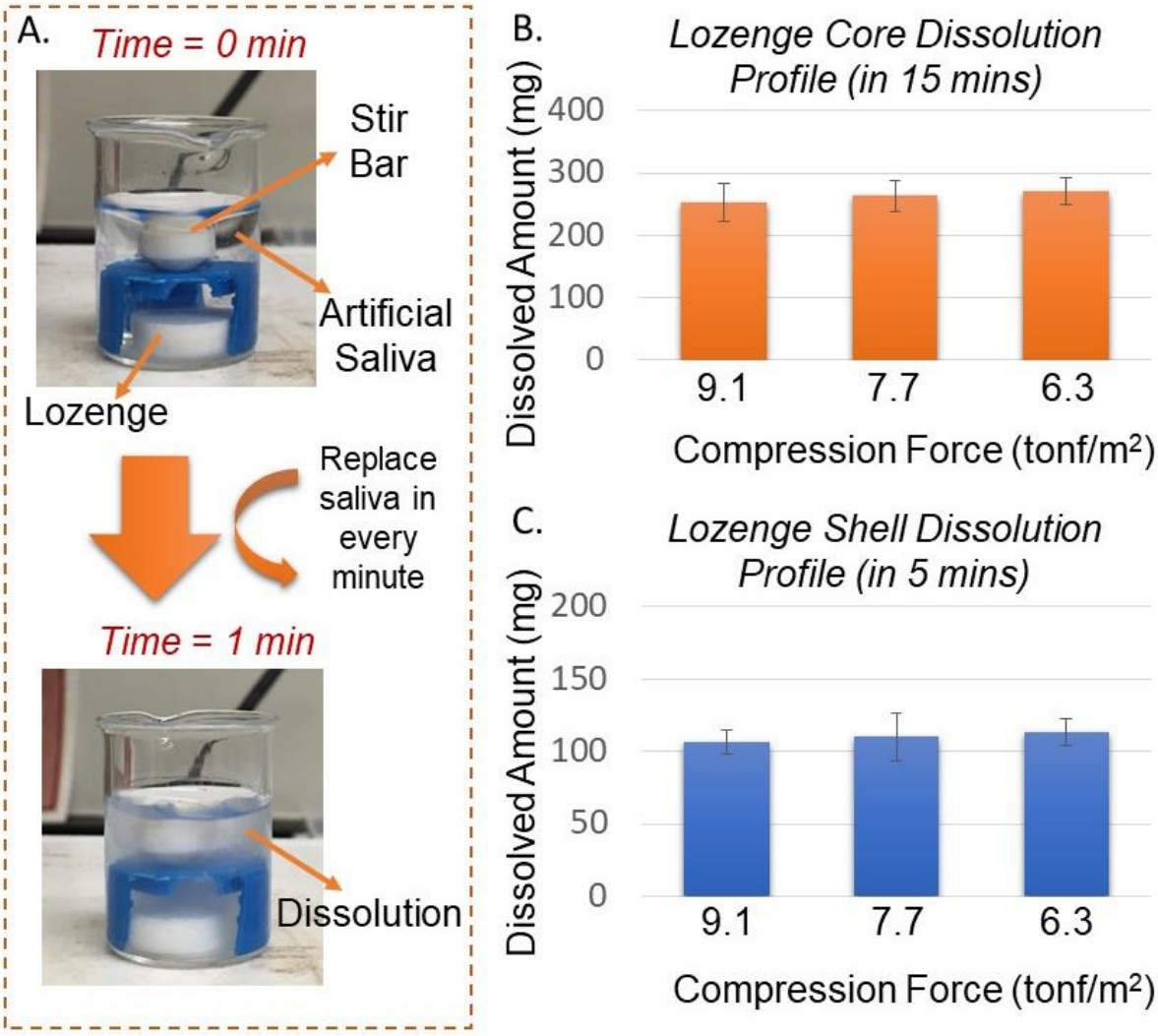


**Figure 37:** (a) Schematic representation of lozenge dissolution testing procedure; Effect of compression force and excipient content on dissolution rate of the lozenge (b) core and (c) shell; in artificial saliva at 37ºC.

in Figure 37b, the disintegrated (dissolved) amount in 15 minutes within the artificial saliva at 37ºC was measured as 253.33 ±30.91, 263.33 ±24.94, 270 ±.21.60 for lozenges compressed under 9.1, 7.7 and 6.3 tonf/$m^2$, respectively. Similarly, the lozenge shell was fabricated using peptide as an active ingredient. In addition to sorbitol and magnesium stearate, talc was used as the main filler material to keep the overall sugar content of the lozenge low. The dissolution amount in 5 minutes in the artificial saliva at 37ºC was measured as 106.67 ±8.16, 110.00 ±16.33 and 113.33 ±9.43 for lozenges compressed under 9.1, 7.7 and 6.3 tonf/$m^2$, respectively (Figure 37c).

*Structural Characterization of Remineralized Layer:*

The calcium and phosphate ions that are delivered into the artificial saliva by the lozenge core (170 mg) manufactured at under 9.1 tonf/$m^2$ is calculated to be 9.6 mM and 5.76 mM, respectively, which is the optimum ratio for remineralization reaction. Therefore, following the disintegration analysis, the core-shell lozenge compressed at 9.1 tonf/$m^2$ was selected as an optimal tablet formulation to be used in the remineralization process. With this aim, the tablet in core-shell design was manufactured with the listed amounts of ingredient in Table 8 under at 9.1 tonf/$m^2$. An extracted human tooth sample was placed into the USP-2 Dissolution Apparatus and mineralization treatment was performed for 15 mins. The sample was drip rinsed with distilled water, fractured in the parasagittal direction and

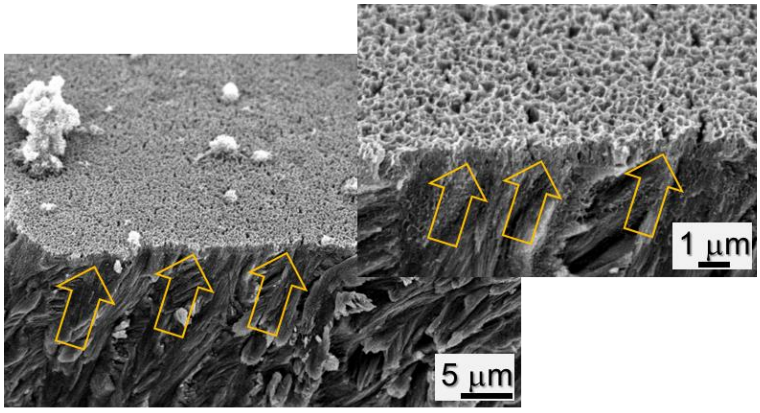


**Figure 38:** Representative SEM images taken after one round of lozenge treatment of human enamel.

visualized under SEM. As shown in **Figure 38**, a continuous mineral layer with plate-like crystals was formed on enamel with an average thickness of ~1.2 ±.0.4 µm.

*Optical Characterization of Whitening Effect:*

The whitening performance of the remineralizing lozenge was measured by macro-photography and color analysis and expressed in L, a, b units. The CIE L*a*b* system is a color space defined by the International Commission on Illumination (CIE) which has been widely used in dentistry to express the color of the tooth numerically.[217-219] In this system, color is expressed as three numerical values, L* for the lightness and a* and b* for the green–red and blue–yellow color components. Unlike the other color theories, e.g., RGB, CMYK and CIE XYZ, CIE L*a*b* system is designed to approximate human vision, meaning that the difference in L*a*b* (numeric) values corresponds to similar amount of visually perceived change. Another important attribute of the CIE L*a*b* system is that it defines color of the object as independent of the device that are acquired and/or visualized.[200, 219]

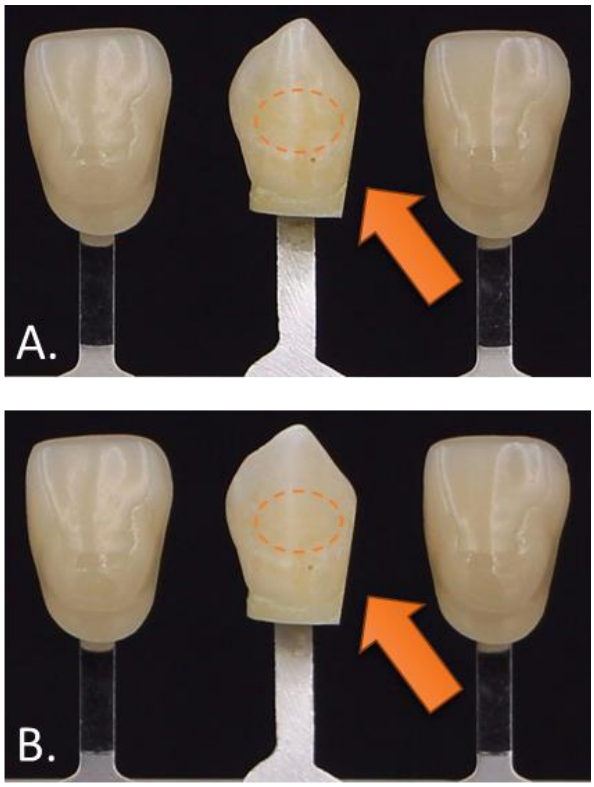


**Figure 39:** Optical images of inherently stained extracted human teeth (a) before and (b) after remineralizing whitening treatment. Circled area shows the region where the color quantification analysis is done. Shade tabs were placed on both sides of the extracted human teeth for internal reference.

The core-shell lozenge was fabricated by compressing at 9.1 tonf/m$^2$. An extracted human tooth sample with inherently dark shade was mounted on a stainless-steel holder and placed into shade guide rack. Images under pre-set light settings were recorded. The specimen was placed into the USP 2 dissolution apparatus and mineralization was performed for 15 mins. The sample was removed, drip washed with distilled water and placed back into same position on the shade rack and optical images were taken (**Figure 39**). Next, the color of the teeth was quantified by analyzing

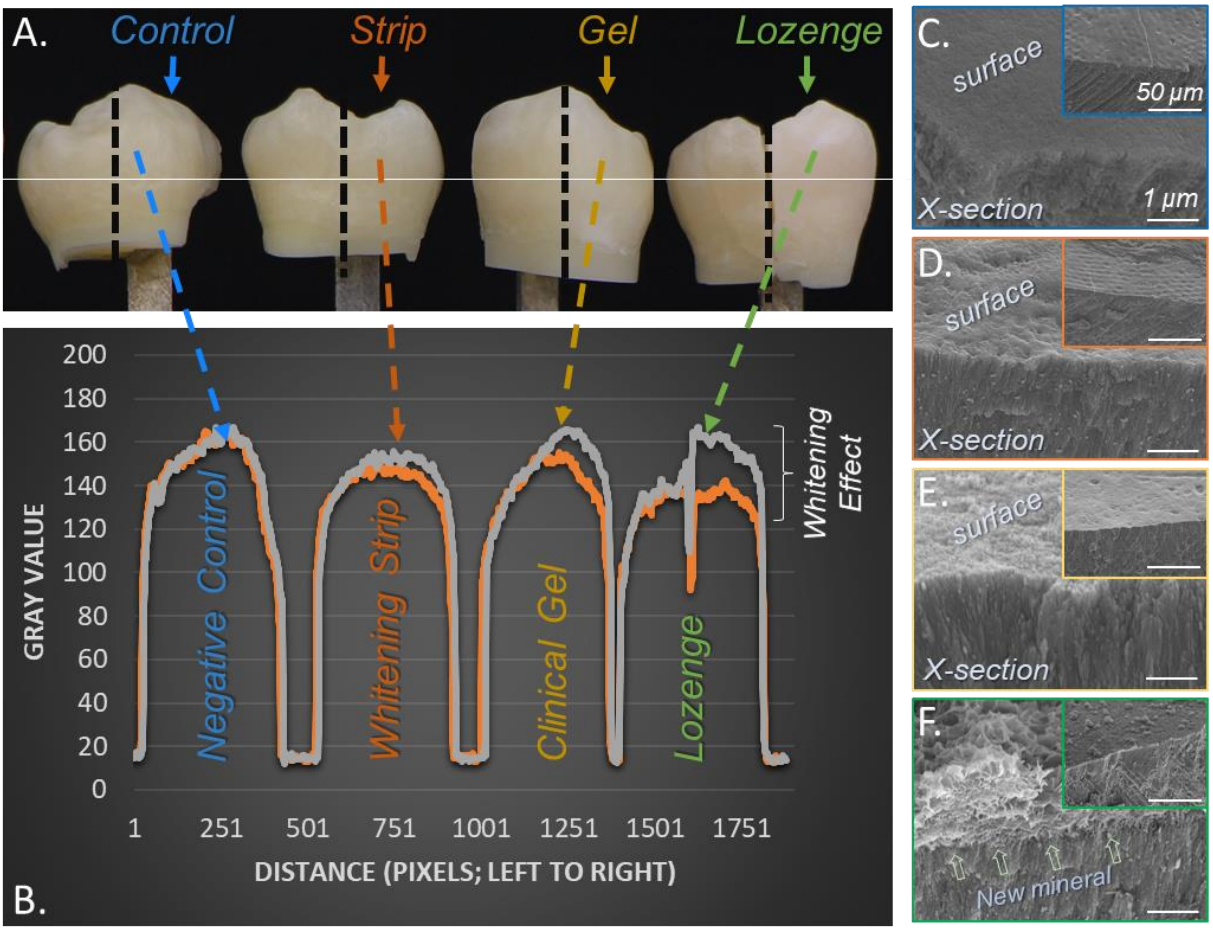


**Figure 40:** A) Optical images of extracted human teeth treated for 7 days (1 treatment per day) by OTC-whitening strips, clinical whitening gel and lozenges. B) Quantitative micro-densitometer trace analysis performed through the region represented via white line on the side-by-side image before (gray line) and after (orange line) the treatment. The difference in gray and orange lines represent the change in the whiteness of the specimen in response to treatment. Edge-on SEM images of tooth specimen after C) No treatment; D) Whitening strip; E) Clinical Gel and F) Whitening lozenge treatments.

the raw images using Adobe Lightroom image processing software. As shown in Figure 39, the

average color of untreated sample (within the orange circle) was measured as L=68.93, a=2.93, b=27.92 while after the remineralization treatment it is measured as L=69.37, a=3.93, b=22.47. The ΔE value that indicates the total change in whiteness was calculated as 5.56 using the equation 1; given below:

$$\Delta \boldsymbol{E_{Lab}} = \sqrt{(\Delta \boldsymbol{L}^*)^2 + (\Delta \boldsymbol{a}^*)^2 + (\Delta \boldsymbol{b}^*)^2} \quad (1)$$

Next, head-to-head comparison for the whitening lozenge with HP-based commercial tooth whitening products was performed on extracted human teeth mounted on metal strips. While the left half of the specimen received no treatment (internal control), the right half of the sample was treated for 7 consecutive days (1 treatment per day). 4 test groups were used: 1) No treatment, 2) Treatment with 14% HP containing whitening strips, 3) Treatment with 40% HP containing clinical whitening gel and 4) Whitening Lozenge treatment. After each treatment, teeth were placed on a shade rock and images were taken using Canon Rebel T5i camera w/ Macro Lens 18-135mm within a custom-made photo-station equipped with white LED and diffuser. Samples were kept in artificial saliva in between each treatment. As shown in Figure 40, while no significant change was observed between the left and right side of the negative control sample (received no treatment), the other 3 groups which received different types of whitening treatment demonstrate whiter color. The change in whiteness (ΔE) of each test sample was found as 4.0 ±2.8, 11.1 ±2.8, 10.2 ±1.1 for specimens treated with 7 rounds of whitening strips (14% HP), clinical gel (40% HP) and whitening lozenge, respectively.

To demonstrate the effect of these treatment modalities on the natural tooth surface, following whitening quantification, samples were subjected to SEM analysis. As shown in Figure 40, the natural tooth surface which received no whitening treatment is fairly smooth as indicated by the uniform contrast across the surface. On the other hand, after whitening strip treatment, the surface

became rougher, which is a possible indication of demineralization in response to hydrogen peroxide treatment. More importantly, the roughness of the tooth surface after clinical gel treatment was increased which could be explained by extensive demineralization due to the higher hydrogen peroxide content of clinical whitening gel. On the other, in contrast to the chemical etching effect of commercial whitening products, lozenge treatment created a new mineral layer with an average thickness of ~2.1 ±.0.5 µm.

5.1.4. Discussion

A biomimetic, cell-free remineralization model was developed to reverse the tooth discoloration of extracted human teeth through a peptide-guided remineralization approach. With this aim, first a fast-disintegrating dental lozenge was developed to deliver the remineralization agents effectively into the oral environment. To ensure the sequential delivery of peptide and calcium/phosphate ions into the oral environment, lozenges were designed to be composed of 2 layers (a peptide containing shell on the outer region and calcium and phosphate containing core at the center). The inactive ingredients were identified by examining the most commonly used FDA approved oral lozenges in the market. Magnesium stearate, sorbitol and talc were used as lubricating, flavoring and main filler materials. The lozenge was fabricated by using a hydraulic tablet press and complete dissolution time was tailored to be 15 minutes in total. The lozenges were fabricated under different compression forces and 9.1 tonf/$m^2$ was selected as an optimal tablet formulation to be used in the procedures. The SEM analysis demonstrated that after single round of lozenge treatment, ~1.2 µm thick continuous mineral layer with plate-like crystals forms on the surface of stained enamel. The successful formation of a mineral layer indicates that the lozenge is an effective product in enabling the peptide-guided remineralization in artificial saliva.

As a whitening product, in the next step, the whitening performance of the lozenge was tested by remineralizing the inherently stained human teeth. As shown in Figure 39, lozenge treatment improved the whiteness of teeth by ΔE=5.56. As a comparison, it is reported that after administration of a single round of 40 minutes-in office whitening gel containing 36% HP (NUPRO White Gold In-office Kit) the whiteness of extracted human tooth is improved by ΔE=6.26 ±0.54 while 3 rounds of 15 minute clinical treatments with the same whitening gel is reported to change the color of the teeth by ΔE=5.10 ±0.44.[220] On the other hand, according to another study, the whiteness of the teeth was improved by ΔE=19.06 ±2.92 as a result of 7 consecutive rounds of whitening treatment using 10 % HP gel.[205] Although these results indicate the potential success of the developed lozenge both as a therapeutic (remineralizing) and cosmetic (whitening) product, these findings have to be supported by other characterization procedures.

With this aim whitening performance of the lozenge is demonstrated by side-by-side comparisons with existing dental whitening products (shown in Figure 40). Both lozenge and clinical whitening gel (professional use only, containing 40% HP) yielded similar enhancement of whiteness with total change (ΔE) of 11.1 ±2.8 and 10.2 ±1.1 for professional-use clinical gel (40% HP) and whitening-lozenge, respectively. On the other hand, the whitening performance of the OTC strips was ~3x less than the whitening-lozenge with a total change (ΔE) of 4.0 ±2.8. The microdensitometer trace analysis performed through the white line before and after the treatment clearly shows that lozenge treatment significantly improved the whiteness of the specimen (expressed in terms of gray value, 0=Black & 255=White) that is similar to 40% HP containing clinical gels which can only be used by dental professionals in chairside. After the whitening analysis, each specimen was subjected to SEM analysis to characterize the structural effects of each treatment modality to the natural tooth surface. Both OTC and clinical HP-based whitening

treatments increased the roughness of the enamel surface in comparison to sound enamel, which received no treatment, indicating that the severity of demineralization (mineral etching/loss) activity of HP-based treatment modalities. In contrast, the enamel thickness of the lozenge-treated sample increased more than of ~2.1 ±.0.5 µm showing that whitening action is achieved by surface remineralization which strengthens the tooth enamel through continuously grown, uniform natural mineral. These results demonstrate that under similar treatment conditions, the whitening lozenges are three times more effective than their OTC counterparts, whitening strips.

5.1.5. Conclusions

Building upon findings in Task I-II, herein (**Task-III**), a tooth whitening lozenge that enables the efficient transfer of components of the peptide-guided remineralization treatment is developed (**Figure 41**). The oral lozenge, and the peripheral formulations described herein have a high potential as consumer products not only for a cosmetic whitening purposes but also as an adjunct therapeutic agent to restore and correct enamel, dentin, and cementum demineralization related dental diseases. When developed fully, the proposed oral lozenge will have a high potential to be used not only a cosmetic whitening product but also an adjunct therapeutic agent to restore enamel and dentin demineralization related dental diseases.

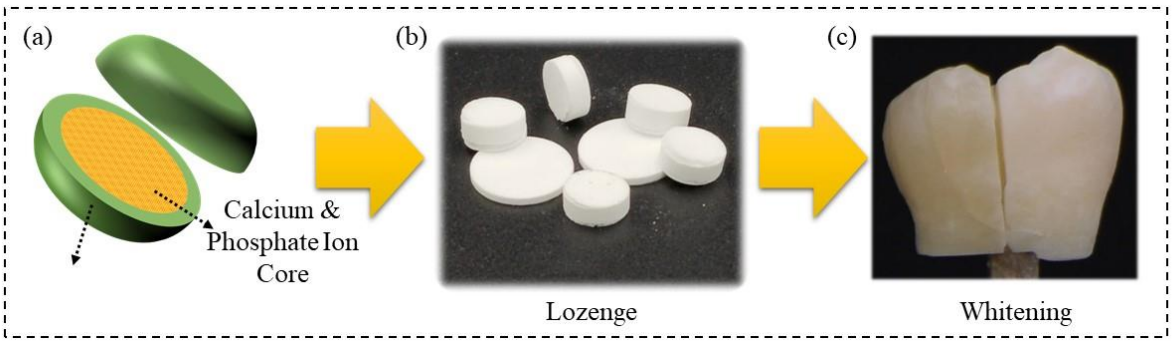


**Figure 41:** Schematic representation of the tasks accomplished during the translational study; (a) lozenge design, (b) manufacturing and (c) characterization.

Chapter 6: Enhancing the Functionality of Dental Implants

*Preamble: Further Implementation of Solid-Binding Peptides Towards Addressing Whole Dental Care – Biofunctionalization of Implant Surfaces*

The final task of this dissertation (**Task-IV)** thesis focuses on improving the functionality (resistance to infection) of dental implants through solid-binding peptide based chimeric antimicrobial coatings. Dental implants have been a commonly used treatment modality in dentistry to replace the missing dentition. However, infection-related failure of these materials limits their long-term success while posing serious risks to patients. Recent clinical reports demonstrate that nearly 4-10% of patients receiving dental implants develop infections mainly due to ineffective antibiotic treatment.[221] Keeping in mind the overarching goal of developing a universal biomimetic dental care, in the final task area (Task IV), the aim is set to develop an implant coating strategy to improve the life-time of dental implants. In an earlier study, the efficacy of hetero-functional chimeric peptides in preventing bacterial colonization on titanium implants was demonstrated.[180] Herein, zirconia has been selected as the material-of-choice due to holding a unique place amongst ceramic implants (and implant coatings) due to its excellent mechanical

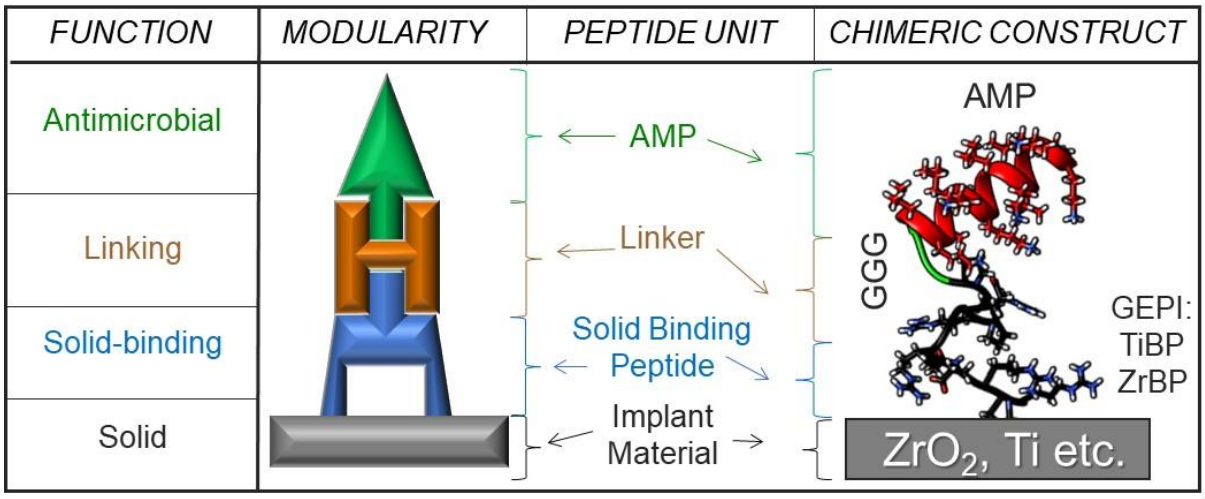


**Figure 42:** Chimeric peptide design to incorporate solid binding and antimicrobial peptide for bifunctionality.

properties. **Figure 42** outlines the experimental design for developing heterofunctional solid binding peptides chimerized with antimicrobial moieties.

## 6.1. Engineered Chimeric Peptides as Antimicrobial Coatings for Zirconia Implants

### 6.1.1. Introduction

*Implants in Medicine and Dentistry:* The use of implants is a well-accepted treatment modality in dentistry and medicine to repair and reconstruct damaged parts of the musculoskeletal system.[222] Titanium alloys has been the gold standard for implants in dentistry for decades. One particular limitation of titanium implants, however, is the metal ions that are released from implant surface in response to corrosion may form complexes with native proteins and act as allergens, causing hypersensitivity reactions.[223-225] As a potential alternative, among many different ceramics, e.g., alumina, bioactive glasses, and spinel, biomedical grade zirconia is regarded as the suitable implant material. In particular, with its high flexural strength, excellent corrosion and wear resistance, and high fracture toughness, zirconia has been a well-established implant material in orthopedics, especially in femoral head and hip replacements.[226-228] The aesthetic benefits of zirconia have also contributed to its popularity in dentistry where the gray color of conventional titanium based implants can often be perceived through the peri-implant mucosa and therefore gives rise to aesthetic concerns due to the unnatural bluish/grey appearance of the gingiva. The opacity and bright white color of zirconia makes it a very suitable alternative to titanium based implants especially in the anterior sites of the mouth.[226, 229] Moreover, the biocompatibility and the non-allergenic nature of zirconia are other advantages that render it a very suitable implant material for prosthodontics and restorative dentistry.[230-232]

*Issues with Implants:* However, despite their excellent mechanical properties and biocompatibility, the risk of failure of these implants due to microbial invasion and colonization still poses a threat

to patients.[233-235] In medicine, especially in hip, knee and arthroplasty implants where implant replacement is very tedious processes, implant associated bacterial infections cause significant post-surgical challenges to the surgeons.[236] Following initial adhesion of early colonizers on the implant surface and the surrounding soft tissues, these pathogens evolve into a complex biofilm and thereby create a protective microenvironment for themselves where the penetration of antimicrobial agents is very limited.[237] Such infections are difficult to treat due to their resistance to local and systemic antibiotics as well as to the natural components of the defense system of the body.[238, 239] The limited therapeutic utility of current antibiotic treatments and the host immune response against these implant associated bacterial infections has fueled substantial interest in developing infection resistant biomaterials to prevent initial adhesion and early colonization on the implant surface.[240-242] To achieve this goal, numerous strategies including local release of metallic nanoparticles from implants,[243] polymer-based surface functionalization,[244] non-antibiotic bactericide-loaded coatings[245] and formation of nanotube oxide structures via anodization[246] have been developed. While these methods have been shown to reduce bacterial adhesion, they often require cumbersome and multi-step surface treatment which makes the manufacturing process correspondingly complex, time-consuming and expensive.[247] Additionally, exposure of surrounding tissues to high doses of released antimicrobial agents poses serious concerns about increased bacterial resistance and tissue toxicity.[248] Therefore, there is an urge to develop more effective strategies that prevent bacterial infection on implant surfaces without evoking either toxicity or antibiotic resistance.

*Current Approaches:* A new class of antibacterial agent, known as antimicrobial peptides (AMPs), is emerging as a novel therapeutic modality to treat septic infection, partly due to their broader inhibition activity against microorganisms as well as difficulty of microorganisms to develop

resistance towards them.[249, 250] These short, cationic and amphipathic peptides are often considered as Nature's antibiotics due to being evolutionary conserved constituents of the immune system which exist in virtually every life form, including insects, plants, animals and humans.[251] By their cationic properties, AMPs are preferentially attracted to negatively-charged microbial cell membranes where they penetrate into membrane bilayers, form pores and eventually lead to lysis of the microbial cell.[252] However, the risk of eukaryotic cell lysis due to the lack of a specific cell targeting mechanism is the major barrier that hampers their utilization in the form of injectable therapeutics.[253] A practical way to circumvent these issues is to immobilize AMP's onto implant surfaces where they can act as a local therapeutic agents and thereby prevent bacterial invasion.[254] AMP's can be tethered to implant coating materials by different immobilization strategies including covalent attachment via surface functional groups or coupling to polymer-based resins[255, 256] and physical entrapment using phospholipid.[257] However, besides bringing additional costs to the manufacturing process due to the requirement of multi-step surface activation procedures, these approaches often compromise the antimicrobial efficacy of AMP's due to limited control of AMP orientation on the implant surface.[258, 259]

*Proposed Biomimetic Approach:* Over the past decade, the potential utility of solid binding peptides as surface functionalizing agents has increasingly been demonstrated. Their exquisite molecular recognition and long range self-assembly properties make them ideal candidates to be utilized as molecular linkers in biomolecule immobilization and surface bio-activation of variety of materials.[63, 66, 67, 260] The structural and functional modularity of these peptides allows them to be utilized in association with various fusion partners i.e., peptides, proteins and organic molecules, to build multifunctional chimeric units where newly integrated active domains can be displayed within the desired orientation while the solid binding peptide provides surface binding

and interface control as a result of preferential molecular interactions with the support surface.[261-264] Moreover, the self-driven surface binding and organization capabilities of such multi-functional chimeric assemblies on materials with varying compositions and topographical complexities under physiological conditions make them highly desirable by eliminating the need for complex and expensive surface activation processes.[73, 265, 266]

Building upon this, in this study the utilization of engineered chimeric peptides as an effective antimicrobial coating agent on zirconia ceramic implants is reported. The designed bifunctional chimeric peptide construct features an experimentally selected zirconia-binding peptide (ZrBP) on one end while freely exposing the AMP motif on the other site, hence, forming a highly versatile biomolecular tool to cover the implant surface while retaining antimicrobial activity (**Figure 43**). Two chimeric peptides were produced, ZrBP1-GGG-AMP and ZrBP2-GGG-AMP, by incorporating an AMP sequence with well-known antimicrobial properties into two experimentally selected zirconia binding peptides (ZrBP1 and ZrBP2) having different surface binding and organization characteristics. The designed chimeric peptides were tested both in solution and on implant-grade zirconia disc surfaces to determine their concomitant zirconia-binding properties and antimicrobial efficacy against common oral and orthopedic pathogens i.e., *Escherichia coli*, *Staphylococcus epidermidis*, and *Streptococcus mutans*.[180] The outlined approach here could be a potential solution for developing bacteria-resistant implant surfaces. The principles laid out in this work could be applied to design of new chimeric constructs with a variety of functional domains and solid binding peptides and thereby expanded to develop different functional coating agents for other biomaterials.

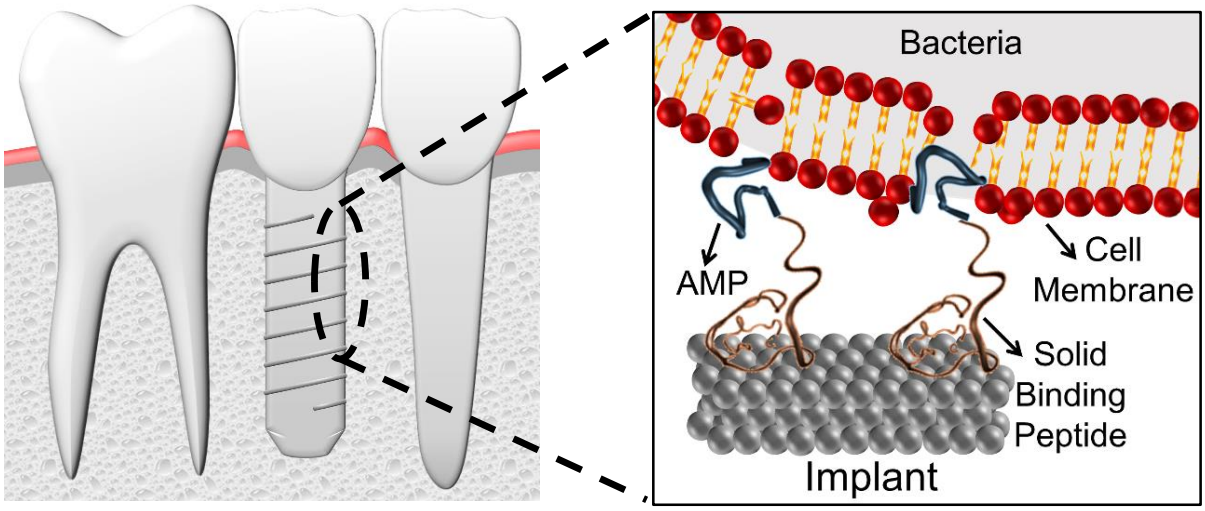


**Figure 43:** Schematics of chimeric antimicrobial peptide coating on zirconia implant surface

6.1.2 Materials and Methods

*Zirconia Substrate Surface Characterization:*

Surface characterization and elemental composition analysis of implant grade zirconia discs (3M ESPE, St. Paul, MN) were performed using scanning electron microscopy (SEM, JEOL 6100) operating at 20kV and onboard energy-dispersive X-ray spectroscopy (EDS), respectively. Before SEM imaging, samples were coated with 5 nm of Au for conductivity.

The surface morphology and the roughness of implant grade zirconia discs were examined by recording AFM images with a Digital Instruments Multimode Nanoscope IIIa scanning probe microscope (Veeco, Santa Barbara, CA) with MikroMasch HQ:NSC14;No-Al tips (MikroMasch, Watsonville, CA). These soft contact mode AFM tips were operated in tapping mode with a drive amplitude of 480mV and a setpoint voltage of 0.5V. Images were recorded from randomly selected areas (10x10 μm) on the specimen and values of mean square roughness ($R_a$) and root mean square roughness (rms) were calculated from the height values in the AFM images using the Gwyddion software (Czech Metrology Institute, Czech Republic).

Before experimental use, implant grade zirconia discs were cleaned by ultrasonication in acetone/methanol (1:1), isopropanol and deionized water for 2 minutes, respectively and vacuum dried. For bacterial adhesion experiments, substrates were sterilized for 15 minutes under UV light.

*Zirconia Binding Peptide (ZrBP) Library Screening and Binding Analysis:*

Zirconia binding peptides were experimentally selected from a peptide library using a similar approach as reported previously.[267] Briefly, biotinylated ZrBP candidates were incubated on implant grade zirconia discs at 37ºC for 3 h, after which substrates were washed three times with Dulbecco's phosphate buffered saline (DPBS; Gibco, Grand Island, NY) to remove loosely bound peptides. Next, the surface-bound peptides were labelled with Streptavidin-Alexa Fluor 488 conjugate (Molecular Probes, Eugene, OR) by incubating the zirconia discs for 15 min in the dark. Excess stain was removed by rinsing with DPBS. Specimens were visualized by fluorescence microscopy (Nikon Eclipse TE-2000U, Nikon, Melville, NY) using a FITC filter (exciter 460−500 nm, dichroic 505 nm, emitter 510−560 nm; Chroma Technology Co., Brattleboro, VT). The fluorescence intensities on the surfaces were recorded from five random areas via METAMORPH (Universal Imaging, West Chester, PA) imaging software and further analysis and quantification was done using ImageJ (National Institute of Health) image processing and analysis software.

*Peptide Synthesis and Purification:*

Peptides were synthesized with an automated peptide synthesizer (CS336X, CS-Bio Inc., Menlo Park, CA) through Fmoc-chemistry. Briefly, in the reaction vessel, the Wang resin (Novabiochem, West Chester, PA), was treated with 20% (v/v) piperidine in DMF to remove the preloaded Fmoc group. Next, the incoming side chain protected amino acid was activated separately with N,N,N′,N′-Tetramethyl-O-(1H-benzotriazol-1-yl)uronium hexafluorophosphate (HBTU; Sigma-Aldrich, St Louis, MO) in dimethylformamide (DMF, Sigma-Aldrich, St Louis, MO) and then

transferred into the vessel where it was incubated with the resin for 45 min. After washing the resin with DMF, this protocol was applied for the addition of each of the next amino acids and synthesis reaction was monitored by UV-absorbance at 301 nm.

Following synthesis, the resulting resin-bound peptides were cleaved from the resin and the side-chain de-protected using reagent-K (TFA/thioanisole/$H_2O$/phenol/ethanedithiol (87.5:5:5:2.5) and then precipitated by cold ether. Crude peptides were purified by reversed-phase high-performance liquid chromatography (RP-HPLC) with up to 98% purity (Gemini 10u C18 110A column). The molecular masses of the peptides were confirmed by MALDI-TOF mass spectrometry with reflectron (RETOF-MS) on an Autoflex II (Bruker Daltonics, Billerica, MA) mass spectrometer in positive-ion mode.

For the fluorescein coupling, 5-carboxyfluorescein (5-FAM, AnaSpec, San Jose, CA) was weighed into an amino acid tube to have 2X the amount in excess of the peptide resin. The 5-FAM was then placed on the automated peptide synthesizer and a similar protocol was used as for a regular amino acid, with a longer mixing time. The fluorescent peptide was then cleaved from the resin using reagent-K.

Stock solutions of each peptide at 4 mM were prepared in sterile DPBS. The molecular weight (MW), isoelectronic point (pI), net charge and grand average of hydropathy value (G.R.A.V.Y.) parameters for each peptide were calculated using ExPASy Proteomics Server.

*Bacteria Culture Preparation and Maintenance:*

*Escherichia coli* American Type Culture Collection (ATCC) 2592, *Staphylococcus epidermidis* ATCC 29886 and, *Streptococcus mutans* ATCC 25175 were used in the present study and stock solutions were prepared according to ATCC instructions as described previously.[180] *E. coli* and *S. epidermidis* were cultured in Trypticase Soy Broth (TSB) and Nutrient Broth (NB), respectively

under aerobic conditions at 37°C with constant agitation (200 rpm) whereas *S. mutans* was grown in Brain Heart Infusion (BHI) Broth anaerobically at 37ºC in the presence of 5% $CO_2$ under static conditions.

*Antimicrobial Activity of Chimeric Peptides in Solution:*

The antimicrobial activity of the designed chimeric peptides was analyzed in *S. mutans, S. epidermidis,* and *E. coli* cultures spectrophotometrically. Briefly, selected chimeric peptides were dissolved in respective media in different concentrations ranging from 1 μM to 400 μM with two-fold increments. Next, bacteria were seeded into each chimeric peptide containing media to a final concentration of approximately $10^7$ cells $mL^{-1}$, and their growth was monitored over the course of 24 hours by periodic optical density measurements at 600 nm in a spectrophotometer. Each experiment was performed with a positive control sample in which $10^7$ cells $mL^{-1}$ bacteria were suspended in the specified media in the absence of chimeric peptide.

*Binding Characterization of Chimeric Peptides:*

5-carboxyfluorescein (Anaspec, Fremont, CA) conjugated peptides (F-ZrBP1-AMP, F-ZrBP2-AMP and F-AMP) were utilized to characterize the binding strengths of designed antimicrobial chimeric peptides on implant grade zirconia discs. Substrates were incubated with 100 μM chimeric peptide solution at 37ºC under constant agitation (200 rpm) for 3 hours and then excess peptide was rinsed off with deionized water. Next, substrates were visualized by fluorescence microscopy using a FITC filter (exciter 460−500 nm, dichroic 505 nm, emitter 510−560 nm) and the total fluorescence intensities were recorded and quantified from five random areas using ImageJ™ image analysis software.

*Bacterial Adhesion and Quantification of Chimeric Peptides on Zirconia Implant Surface:*

Chimeric peptide coating was performed by incubating implant grade zirconia discs with 100 μM chimeric peptide solution at 37ºC under constant agitation (200 rpm) for 3 hours. Excess peptide was washed off by rinsing with DPBS from disc surfaces.

For bacterial adhesion experiments, overnight cultures of bacteria strains were inoculated into fresh media grown until mid-log phase. Next, cells were harvested by centrifugation at 2000 x g for 5 min. The supernatant was removed and the bacterial pellet was re-suspended in sterile DPBS to a final concentration of $10^8$ cells $mL^{-1}$. Chimeric peptide coated substrates were placed into wells (in 24-well plate) and 1 mL of bacteria suspension was added onto each and incubated for 2 h. It is noted that for *S. mutans* experiments, incubation was carried out anaerobically at 37ºC in the presence of 5% $CO_2$ under static conditions whereas for *S. epidermidis* and *E. coli* incubations were carried out aerobically at 37ºC under constant agitation (200 rpm). Following the incubation, the bacterial suspension was removed by aspiration and the surfaces were gently rinsed with DPBS. Adhering cells were fixed with 2% glutaraldehyde for 30 min and dehydrated in a series of ethanol:water mixtures (40%, 50%, 60%, 70%, 80%, 90%, and 100% (v/v)).

Next, bacterial cells were stained by 5 μM SYTO9 green fluorescent dye for 20 min and the excess stain was rinsed off by deionized water. Each substrate was examined in detail under the fluorescent microscope. The fluorescence intensities on the surfaces were recorded on five random areas via METAMORPH (Universal Imaging, West Chester, PA) imaging software and further analyzed using the ImageJ software.

*Structural Decoy Generation and Rule Induction:*

Structural decoys were generated with the PyRosetta Windows 64-bit Release 57935 for AMP, ZrBP1-AMP and ZrBP2-AMP. Fragment insertion from the Robetta server was used to initialize the backbone angles of the residues, and the Fast Relax method was used for determining the

rotamers of the side chains. 1000 structural decoys were made for each sequence. The structural decoys were evaluated with the DSSP program to count secondary structures. The lowest energy decoys from the 1000 generated decoys were selected.

*Statistical Analysis:*

Results are expressed as the mean ± standard error. Statistical analysis was done using Microsoft Excel Worksheet and statistical significance of mean values was determined by Student's t-test, and a P value of <0.01 was considered significant.

6.1.3. Results

*Surface Characterization and Elemental Composition Analysis of Zirconia Substrate:*

Before experimental use, surface characterization and elemental composition analysis of implant grade zirconia discs were done using SEM, EDXS and AFM. As shown in **Figure 44a**, SEM images indicated that the implant material has a fairly uniform and rough surface. The average grain size obtained from the higher SEM magnification was less than 1 μm (Figure 44a, inset). Elemental analysis of the specimen surface by EDXS indicated the presence of yttria ($Y_2O_3$) to be approximately 5.25 mol% (Figure 44b). It is noted that due to the overlap between the L-alpha energies of Zirconium (Zr, 2.042 keV) and Yttrium (Y, 1.922 keV) on EDXS spectra, the reported mol percentage values were calculated using onboard EDXS analysis software. Further quantification regarding the surface topography of zirconia specimen was done using atomic force microscopy (Figure 44c and 44d). With this aim, height images (10x10 μm) were obtained by scanning five randomly selected areas and then using the Gwyddion image analysis software, mean square roughness ($R_a$) and root mean square roughness (rms) were calculated. The average $R_a$ and rms values were calculated to be 113.72 ±6.21 nm and 149.15 ±8.47 nm respectively. The highest peak-to-valley distance within the scanned region was also found to be 1.15 μm.

*Selection and Characterization of Zirconia Binding Peptides*

Zirconia binding peptides were screened from a rationally selected set of 16 candidates using a method that was reported previously.[267] In the screening assay, a set of biotinylated ZrBP candidates were incubated with implant grade zirconia discs and after a stringent washing process, and the amount of peptide bound to the substrate was quantified using fluorescent streptavidin-Alexa probes (**Figure 45a**). The relative binding affinity of each peptide was estimated as the percentage ratio of the fluorescence area to total visualized area (Figure 45b and 45c). As shown in Figure 45c, each peptide candidate demonstrated different relative surface binding coverages on the substrate surface ranging from 96.41% (±3.32) to 0.08% (±0.01).

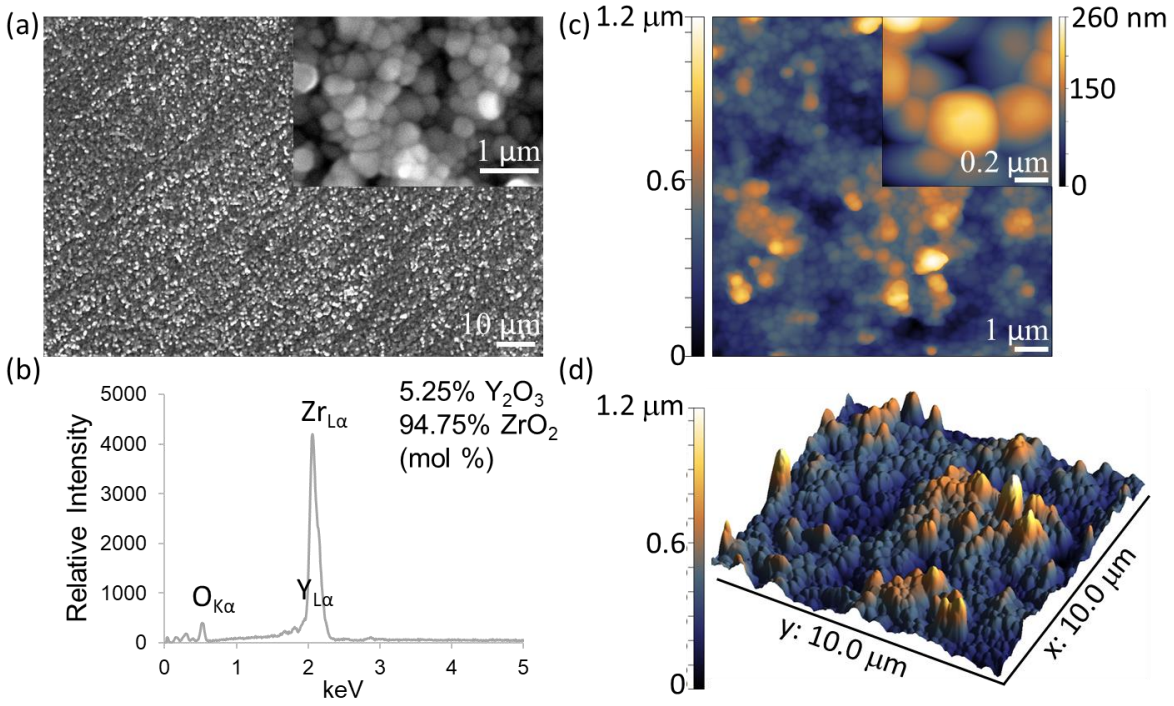


**Figure 44:** Surface characterization and elemental composition analysis of implant grade zirconia discs. (a) Representative face-on SEM image of zirconia substrate. Inset shows individual grains. (b) EDXS spectra of zirconia substrate and mol percentages of yttria and zirconia phases. (c) Representative height image of zirconia substrate. Inset shows individual grains. (d) Surface topography image of zirconia substrate constructed using height image taken by AFM.

*Design and Characterization of Chimeric Antimicrobial Zirconia Binding Peptides:*

Chimeric antimicrobial peptides with zirconia binding affinity and antimicrobial activity were constructed by coupling the selected ZrBP peptides, ZrBP1 and ZrBP2, to the well-characterized antimicrobial peptide[268] (AMP) domain using a structurally flexible triple glycine (GGG) spacer region in between ZrBP and AMP motifs. The resulting chimeric conjugates were abbreviated as ZrBP1-AMP and ZrBP2-AMP. The amino acid sequences and theoretical parameters, i.e., molecular weight, isoelectronic point, net charge and hydropathy, are listed in **Table 9.**

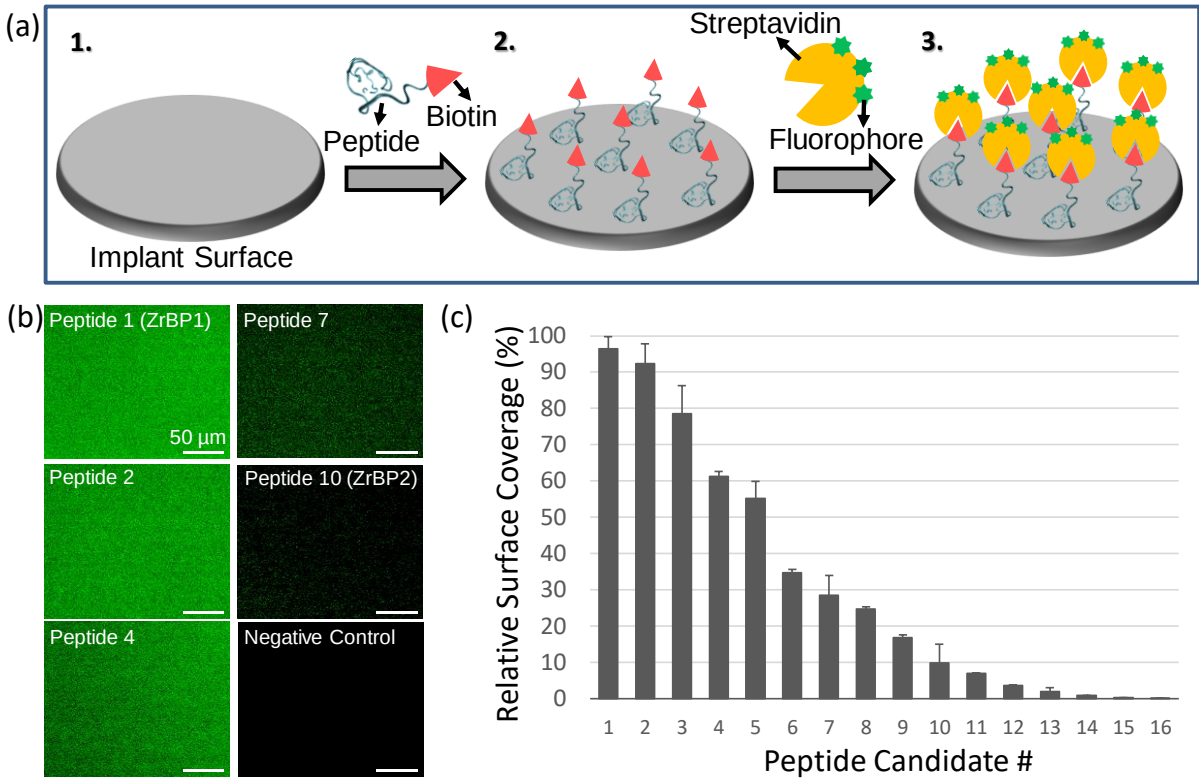


**Figure 45:** Selection and characterization of zirconia binding peptides on zirconia discs. (a) Schematics of peptide selection, (b) representative FM images of peptides with different binding affinities, (c) categorization of the zirconia binding peptides based on relative binding affinity analysis via FM.

**Table 9.** Molecular characteristics of the engineered peptides.

| Peptide | Sequence | MW | pI | GRAVY | Charge |
|---|---|---|---|---|---|
| **AMP[268]** | **LKLLKKLLKLLKKL** | 1692.34 | 10.70 | 0.5 | +6 |
| **ZrBP1-Spacer-AMP** | **RPREQRGERPRPGGG LKLLKKLLKLLKKL** | 3379.1 | 11.85 | -1.117 | +9 |
| **ZrBP2-Spacer-AMP** | **LSLPHFRSRRIQGGG LKLLKKLLKLLKKL** | 3355.2 | 12.32 | -0.093 | +9 |

*Antimicrobial Efficacy of Chimeric Peptides in the Solution: Minimum Inhibitory Concentration Assays:*

For the minimum inhibitory concentration assays, previously reported MIC values 10 μM, 5 μM and 40 μM against *E. coli*, *S. epidermidis*, and *S. mutans*, respectively[180] were chosen as the lowest test concentrations for each assay and the concentration of peptide in the solution was increased gradually until the MIC was reached. As shown in **Figure 46a-b**, MIC was found to be 20 μM and 10 μM against *E. coli* and *S. epidermidis* for both chimeric designs. On the other hand, both chimeric peptides demonstrated 5-fold attenuation in the antimicrobial activities against *S. mutans* (200 μM) in comparison to AMP only (40 μM).

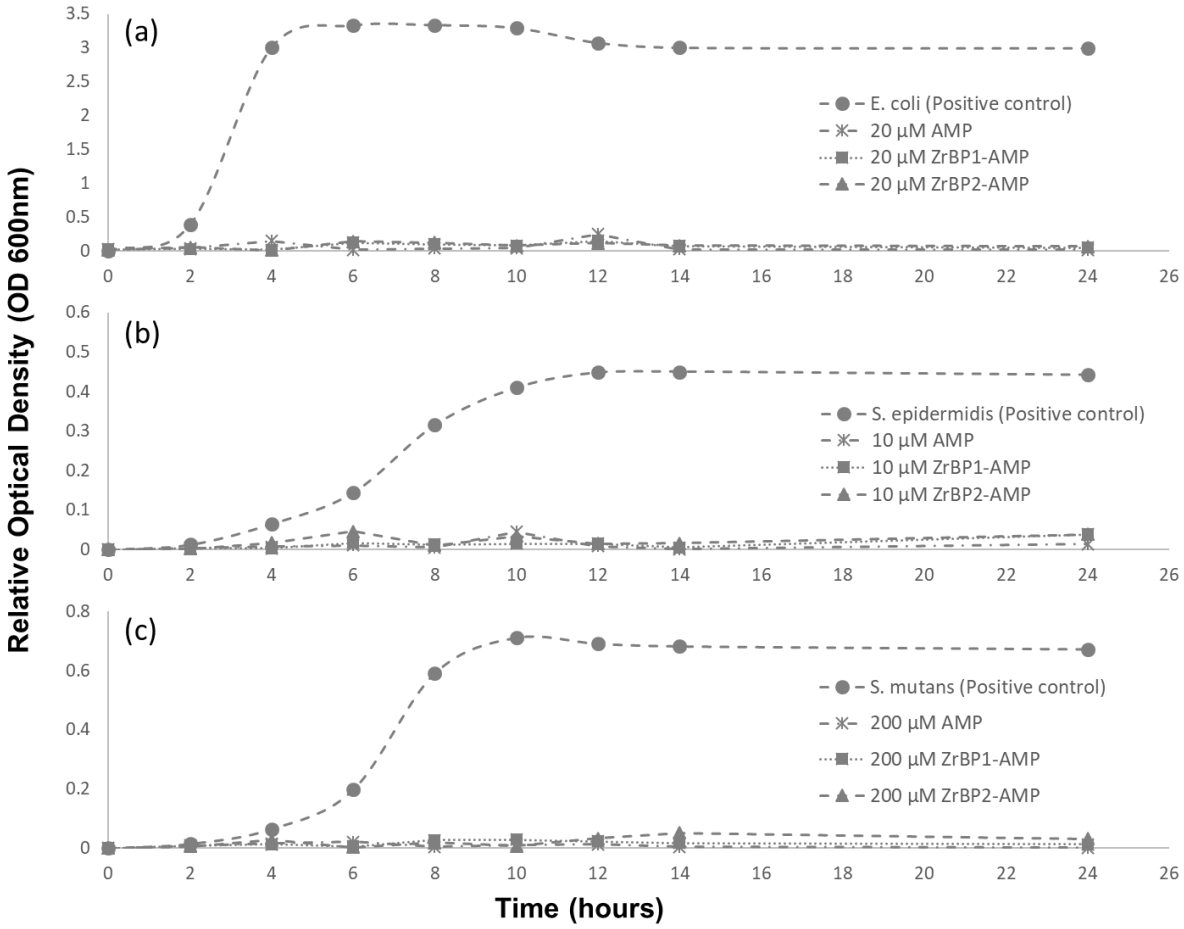


**Figure 46:** Minimum growth inhibition concentration (MIC's) of engineered peptides against (a) *E. coli*, (b) *S. epidermidis*, (c) *S. mutans*.

*Efficacy of Chimeric Peptide Coatings in Preventing Bacterial Adhesion on Zirconia Surfaces:*

Following analysis of antimicrobial properties of these peptides in the solution, the efficacy of each peptide was tested again on the zirconia surface against *E. coli*, *S. epidermidis*, and *S. mutans*. With this aim, implant grade zirconia discs were soaked in a 100 µM chimeric peptide solution in DPBS and incubated for 3 hours by allowing self-adsorption. Upon incubation, excess of nonspecifically adsorbed peptides was removed by rinsing with DPBS. Next, $10^8$ cells $mL^{-1}$ were

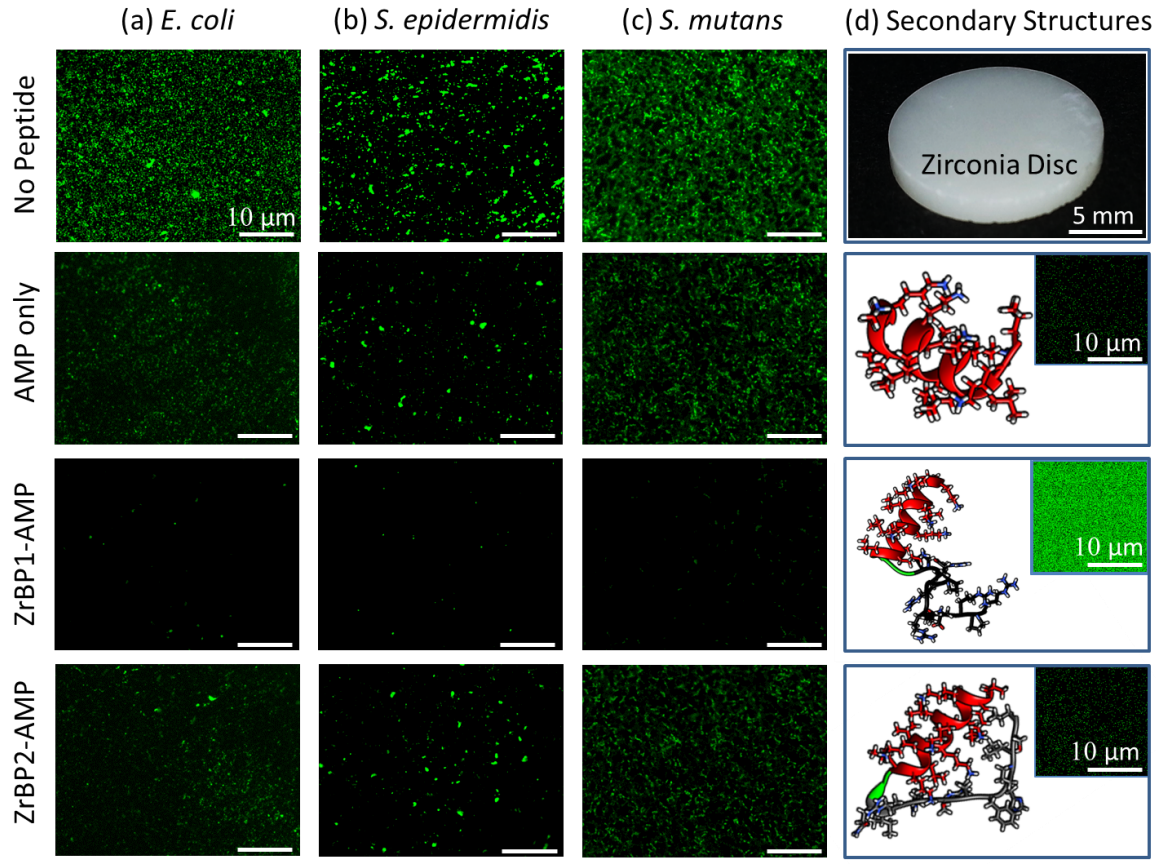


**Figure 47:** Bacterial adhesion on peptide coated zirconia disc surfaces against (a) *E. coli*, (b) *S. epidermidis*, (c) *S. mutans*. (d) Bare zirconia disc and energy minimized computer-generated structures of peptides. Inset images show total surface coverages of each peptide. Size bars indicate 10µm.

seeded onto each substrate and incubated for 2 h. After fixing and labelling the adhering cells with fluorescent probes, surfaces were examined in detail via FM to form a correlation between bacterial binding and antimicrobial efficacy of the chimeric peptides on substrate surfaces.

The FM results demonstrated a significant reduction in the colonization level of each species on the surfaces incubated with peptides compared to bare zirconia (**Figure 47**). While a dramatic decrease in the level of bacterial colonization was observed for the substrates coated with ZrBP1-AMP which consists a strong zirconia binding domain (ZrBP1), the reduction was only about 40-60% for the specimens that were incubated with non-specific (AMP-only) or weak (ZrBP2-AMP)

binders (**Figure 48**). Specifically, in the case of *E. coli* (Figure 47, first row), ~ 98% reduction in the number of adhered bacteria was observed on ZrBP1-AMP coated surface which is ~80- and 55-fold more efficient than the AMP-only and ZrBP2-AMP treatments, respectively. Similarly, in the case of *S. epidermidis* (Figure 47, second row), ~17- and 12-fold more efficient antimicrobial effects are observed on the ZrBP1-AMP coated surface compared to AMP-only and ZrBP2-AMP treatments, respectively. The difference in the ratio of bacterial surface coverage between the ZrBP1-AMP modified surface and the bare zirconia (negative control) was ~30-fold. In the case of *S. mutans* (Figure 47, third row), another gram-positive species, ~95% reduction in the number of adhered bacteria was observed on the ZrBP1-AMP coated surface which was also 12- and 7-fold more efficient than the AMP-only and ZrBP2-AMP treatments, respectively.

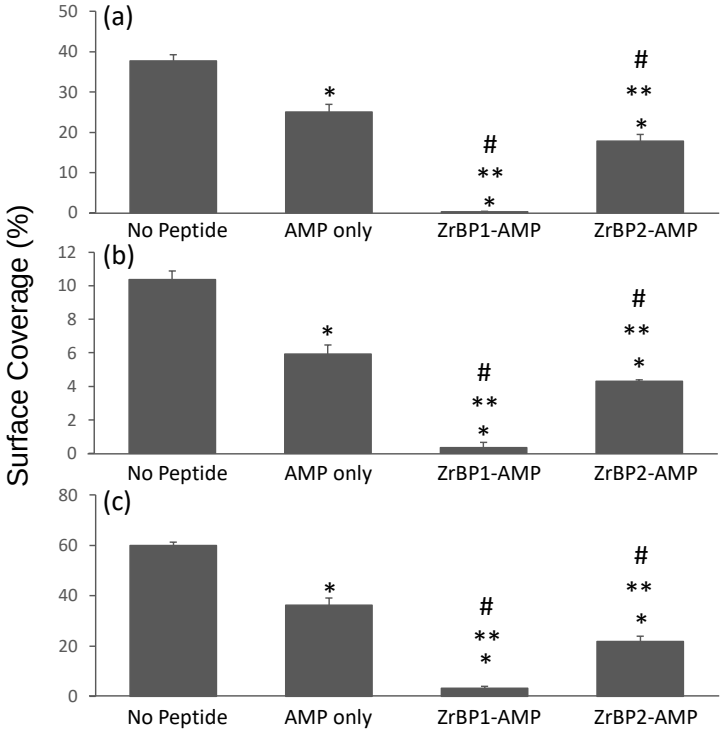


**Figure 48:** Surface coverage analysis of zirconia discs functionalized by the peptides against (a) *E. coli*, (b) *S. epidermidis*, (c) *S. mutans*, *p < 0.01 compared to no peptide (bare), **p < 0.01 compared to AMP, #p < 0.01 comparison in between ZrBP1-AMP and ZrBP2-AMP.

Bacterial protection was also expressed as the relative decrease in bacterial coverage compared to bare surface. As shown in **Table 10**, AMP-only reduced bacteria from ~34% to 43% compared to the bare surface. ZrBP2-AMP improved this reduction by ~53%-64%. The improvement likely did

not come from enhanced individual activity because the in-solution effectiveness of ZrBP2-AMP was less than AMP-only. The collective activity of the peptides on the surface was greater possibly due to the higher peptide affinity to implant surface (Figure 46d). ZrBP1-AMP further showed this trend with significantly increased reductions of ~95%-99% by increasing the surface coverage of chimeric peptide beyond that of ZrBP2-AMP (Figure 46d).

**Table 10**. Relative decrease in bacterial coverage on peptide coated surfaces compared to bare implant.

| **Peptide** | ***E. coli*** | ***S. epidermidis*** | ***S. mutans*** |
|---|---|---|---|
| **AMP** | 33.7% | 42.9% | 39.5% |
| **ZrBP1-Spacer-AMP** | 99.2% | 96.7% | 94.5% |
| **ZrBP2-Spacer-AMP** | 52.7% | 58.5% | 63.7% |

6.1.4. Discussion

In this study, the utilization of chimeric zirconia binding peptides to develop an antimicrobial coating material for zirconia implants was demonstrated. Chimeric peptides, featuring experimentally selected zirconia binding and computationally-designed antimicrobial domains, were constructed.[268] Surface binding characteristics of peptides as well as their efficacies in preventing bacterial colonization on zirconia surfaces were investigated in detail using fluorescent peptide binding measurements, minimum inhibitory concentration and bacterial cell adhesion assays. Prior to experimental utilization, the surface properties and composition of zirconia discs were characterized via SEM, EDXS and AFM. The SEM and AFM images revealed a rough

surface topography with an average $R_a$ and rms values of 113.72 ±6.21 nm and 149.15 ±8.47 nm, respectively. Elemental composition analysis demonstrated the presence of yttria ($Y_2O_3$) in 5.25 (mol %). Yttria is a common element utilized in stabilization of implant grade zirconia. Following substrate characterization, peptide selection was performed. Due to its uniform and high surface coverage binding characteristics, peptide #1 was selected as a suitable candidate for chimeric peptide construction and designated as ZrBP1. As an internal control, peptide #10 was selected as being a weak binder and named ZrBP2.

Chimeric antimicrobial peptides having both zirconia binding affinity and antimicrobial activity were constructed by coupling the selected ZrBP peptides, ZrBP1 and ZrBP2, to the well-characterized antimicrobial peptide (AMP) domain. A structurally flexible triple glycine (GGG) spacer region was included in between ZrBP and AMP motifs in order to preserve the lateral mobility of the AMP domain on the solid surface when the ZrBP was bound to the zirconia surface. Although ZrBP1 and ZrBP2 have same net charge values (+3), the charged amino acids, i.e., Aspartic acid (D), Glutamic acid (E), Arginine (R), Lysine (K), were more evenly distributed in ZrBP1 compared to ZrBP2 where positively charged Arginine was localized near the C-terminal. Furthermore, ZrBP2 was more hydrophobic than ZrBP1 due to the hydrophobic amino acids Leucine (L), Phenylalanine (F) and Isoleucine (I) within the structure. Successful design of any chimeric peptide requires retaining the functionality of each domain that is embedded in the final construct. Therefore, the efficacy of the designed chimeric peptides was investigated with respect to their zirconia binding affinity as well as antimicrobial activity. To assess antimicrobial functionalities, chimeric peptides were tested against common oral and orthopedic pathogens i.e., *E. coli*, *S. epidermidis*, and *S. mutans*, by minimum inhibitory concentration (MIC) assay which involves monitoring of bacterial growth spectrophotometrically in the presence of chimeric

peptides in varying concentrations. While MIC was found to be 20 μM and 10 μM against *E. coli* and *S. epidermidis* for both chimeric designs, about a 5-fold attenuation was observed in the antimicrobial activities against *S. mutans* (200 μM) in comparison to AMP only (40 μM). It has been widely assumed that cationic amino acids have a significant contribution to the overall antimicrobial property of AMPs by facilitating the targeting of the negatively charged bacterial cell membrane and penetration into it. Therefore, the reduction in antimicrobial activity of AMP when it is linked to ZrBP's could be explained by the altered charge distribution on the chimeric peptides due to presence of the 12-aa long zirconia binding domain. Furthermore, the higher reduction in the antibacterial activity of chimeric peptides against *S. mutans* could be attributed to the increased peptide length which may lead to higher resistance to transport across the bacterial membrane. Moreover, if the antimicrobial activity mechanism of AMP's includes intracellular targets, the additional peptide length may also make those interactions less specific. Furthermore, hydrophobicity is another important parameter in the antimicrobial reaction mechanism of AMP's (Table 8) that could also explain the reduction in antimicrobial activity.

Unlike natural proteins, these short peptides can often adopt different conformations when adsorbed on a solid surface due to the series of molecular recognition events including electrostatic interaction between surface atoms of the substrate and the peptide and/or supramolecular interactions between peptides. In chimeric form, these interactions are usually dominated by electrostatic interactions between surface atoms of the substrate and the solid binding peptide domain. This preferential interaction may reduce the ionic shielding of the AMP domain by the zirconia binding domain. This effect may lead to increased antimicrobial activity on the surface of the chimeric peptides even though a reduction of antimicrobial activity was observed in solution. FM analysis with fluorophore attached to AMP (F-AMP) demonstrated that even AMP-alone has

some affinity to zirconia surfaces. The non-specific binding of AMP to the zirconia discs could be explained by the high surface roughness of the substrate (Figure 43c and 28d) as well as the ionic interaction between the charged residues of peptide and the native-zirconium dioxide ($ZrO_2$) surface. However due to the weak and non-specific nature of this interaction, complete coverage of the surface was not achieved (Figure 36d, insets). Therefore, only about 2-fold reduction in the number of adhered bacteria was observed against each species. On the other hand, F-ZrBP1-AMP showed almost complete surface coverage due to the presence of the strong surface binding domain (ZrBP1) on its amino end. In addition to its high surface coverage, the presence of a triple glycine linker in between ZrBP1 and AMP, as well as electrostatic repulsions between positively charged residues of these domains, might possibly have contributed to its superior antimicrobial efficacy on the surface by displaying the AMP domain better. Moreover, although F-ZrBP2-AMP demonstrated slightly better yet incomplete surface coverage than F-AMP, its antimicrobial efficacy on the surface was still limited due to lack of a strong surface binding domain.

### 6.1.5. Conclusions

In conclusion, a single step, peptide-based implant surface biofunctionalization approach toward tailoring zirconia implant surfaces capable of preventing bacterial infection was demonstrated. Two chimeric peptides were designed, each consisting of zirconia binding and antimicrobial peptide (AMP) domains, which allowed the molecular coating agent to bind to the implant surface while freely exposing the AMP motif to combat invading bacteria. The antimicrobial efficacy of chimeric peptides, ZrBP1-AMP and ZrBP2-AMP, was first evaluated by MIC assays in the solution and then on the substrate surface by a detailed FM analysis against *E. coli*, *S. epidermidis*, and *S. mutans*. Surfaces treated with a chimeric peptide (ZrBP1-AMP) that included a strong zirconia binding domain were found to provide a significant amount of resistance against each

bacterial species compared to the bare implant. On the other hand, AMP and ZrBP2-AMP as a coating material were ineffective due to the non-specific and weak nature of their peptide-surface interaction.

Collectively, the engineered chimeric peptide based antimicrobial implant coating approach offers a number of advantages for developing infection-free implants. First, unlike the conventional cumbersome and multi-step surface treatment processes, chimeric peptide-based implant coating does not require any chemical modification on the implant surface. Therefore, it provides a biofriendly way of implant coating by eliminating the use of harsh chemicals. Secondly, by eliminating the multi-step surface treatment process, it enables rapid fabrication of such implants. Thirdly, utilization of AMP has a high potential to combat bacterial antibiotic resistance. Finally, the modular nature of solid-binding peptides, which can be experimentally isolated on virtually any material, holds a promise to develop new chimeric units using other AMP fusion partners. Principles laid out in this study can be applied to other implant materials and can lead to development of infection-free implant materials (**Figure 49**).

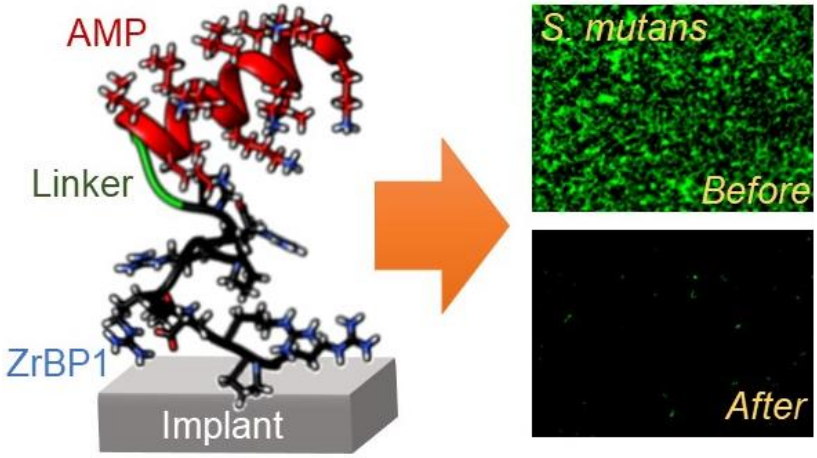


**Figure 49:** Schematics representation of chimeric antimicrobial peptides that provides microbial resistance to implant surfaces.

Chapter 7: Conclusions and Future Prospects of Dental Remineralization and Functionalization

This dissertation research focuses on developing a universal biomimetic dental hard tissue remineralization therapy against prevalent dental diseases and conditions including white-spot lesions, enamel caries, dental hypersensitivity, tooth staining and infection-related implant failure. Current dental therapies mostly rely on replacement of the defective hard tissues with synthetic dental materials which has limited success. From an engineering point of view, the primary reasons for the failure of current dental restoration therapies are four-fold: (i) Limited ability to reinstate the structure-function of the lost tissue, (ii) Lack of structural and functional integration (interface problem), (iii) Low thermal, mechanical, and chemical durability, and (iv) Tissue toxicity and low biocompatibility.

The common denominator to overcome current limitations is to enable natural biomineralization *in situ* either on the defective hard tissues or at the tissue-material interface. The ideal approach would, therefore, be biomimetically developed repair and replacement materials, and regeneration therapies that follow the lessons from biology in dental tissue formation. Herein, it is postulated that "*Using solid binding peptides, it can be possible to remineralize/repair the dental hard tissues; e.g., dentin, enamel and cementum, and restore the structure and function of the tooth with a well-integrated and durable mineral layer which could be administered via variety of formulations such as aqueous, gel and lozenge in treating dental problem*." The validity of this hypothesis is aimed to be tested through four different tasks that include;

***Task-I:*** *In vitro Peptide-guided Biomimetic Repair of Dental Hard Tissues (Enamel and Dentin);*

***Task-II:*** *In vivo Peptide-guided Remineralization to Restore Dental Caries (Rat Model);*

***Task-III:*** *Development of Mineralizing Peptide-based Restorative/Therapeutic Dental Care Products (Dental Lozenges);*

***Task-IV:*** *Improving the functionality (preventing risks associated with failure) of implants*.

In the first task area, it was aimed to develop an *in vitro* remineralization strategy using small peptide domains derived from amelogenin (ADP's) to restore lost mineral on human enamel and dentin. The findings in this task area was used to establish the basis of *in vivo* dental hard tissue remineralization therapy for both enamel and dentin that was executed in the following tasks.

In Task-I, remineralization of human enamel and dentin through the formation of a crystalline mineral layer on artificially created lesions in the presence of $Ca^{2+}$ and $PO_4^{3-}$ ions under physiologically viable conditions by using amelogenin-derived peptides has been demonstrated. The mechanical and chemical durability of the mineral layer as well as its adherence to the underlying tooth structure is demonstrated by series of characterization procedures and assays. It is noted that one of the major finding of this task area is that the biomineralizing peptide, shADP5, enables the delivery and incorporation of fluoride ions into the remineralized layer even at low fluoride concentrations.

In order to implement this advanced remineralization technology under *in vivo* conditions, in the next task area (Task-II) we focused on creating stimulated carious lesions in rats and treating them using a clinically applicable peptide delivery system. With this aim, a novel dental gel formulation containing remineralization ingredients was developed. Next, an *in vivo* rat model that promotes slow progression of mild caries was developed. In contrast to earlier studies, in this model the cariogenic bacteria implementation was facilitated via vertical transmission and thereby requirement of antibiotics has been eliminated. By using qPCR, the colonization of *S. mutans* was closely monitored during the caries formation period. A detailed morphology, mineral content and

local nanomechanical properties analysis of induced carious lesions was provided. In the next step, the resulting carious lesions were treated using the peptide containing remineralizing gel formulation. As a result, it is demonstrated that a functionally integrated new mineral layer is formed onto the carious enamel with a thickness of ~7 micrometer.

After demonstrating the *in vivo* efficacy of peptide-guided remineralization treatment strategy in restoration of demineralized hard tissues, in Task-III, we proposed to develop a therapeutic product that can be utilized to combat demineralization-related dental diseases (WSL, Hypersensitivity) and aesthetic conditions (Tooth Staining). Remineralizing tooth whitening lozenges was selected to be the first target prototype (also known as minimum viable product) to translate peptide-guided remineralization into clinical settings.

The tooth whitening lozenges were developed in a core-shell design through a uniaxial tablet pressing system. The findings demonstrated that the whitening lozenges enable *in situ* remineralization of human enamel within 15 minutes of treatment time. In addition, repeated rounds of lozenge treatment also provide a whitening effect by masking the underlying tooth stains with a newly formed mineral atop. As evidenced from head-to-head comparison analysis, under similar treatment conditions, whitening-lozenges provided faster, whiter, healthier & cheaper whitening treatment than the existent HP-based OTC and clinical whitening products. Towards developing a market-ready product, the main objective of the future studies will be to fully develop a remineralizing tooth whitening-lozenge prototype for eventual clinical trials.

Keeping in mind the overarching goal of developing a universal biomimetic dental care, in the final task area (Task IV), it was aimed to develop an implant coating strategy to improve life-time of dental implants. Herein, zirconia has been selected as material-of-choice due to being the most commonly used implants in clinical dentistry. In order to prevent infection related early failure of

dental implants, a peptide-based implant surface biofunctionalization approach using a hetero-functional chimeric peptide that is designed to combine zirconia binding and antimicrobial peptide (AMP) was developed. This molecular construct preferentially binds to the implant surface while freely exposing the AMP motif to combat invading bacteria. The antimicrobial efficacy of chimeric peptide was evaluated through series of optical and spectrophotometric assays. When successfully translated into over-the-counter and/or clinical products, biomimetic dental products could be the game changer in cosmetic dentistry as well as be used in oral care.

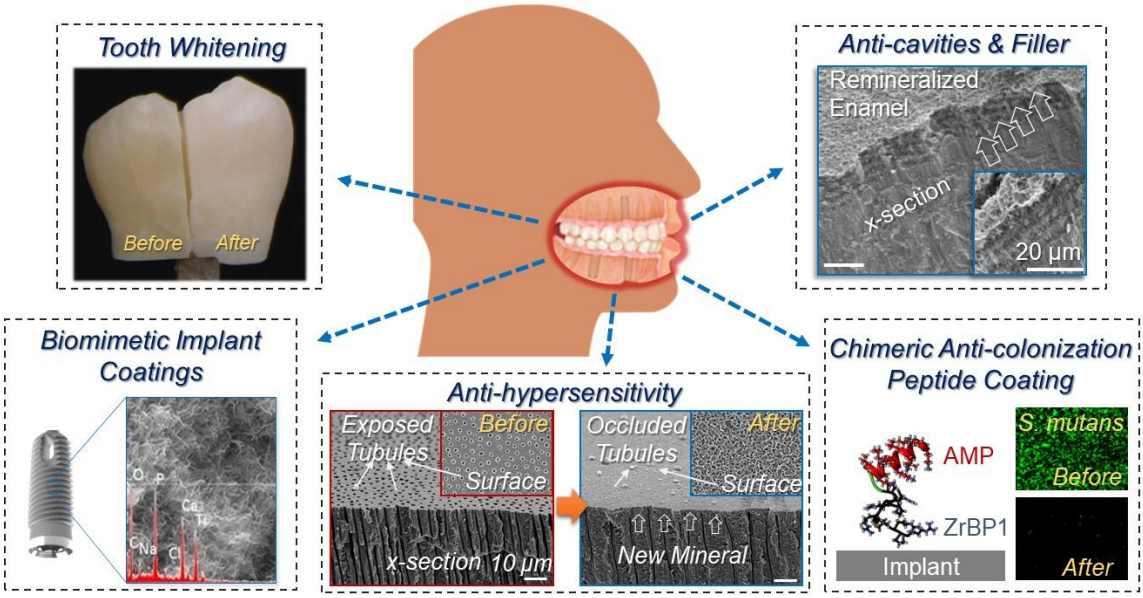


**Figure 50:** Schematics of peptide-guided biomimetic therapies for whole dental care.

Bibliography


1. RH Selwitz, AI Ismail, and NB Pitts, "Dental caries" *Lancet*, **369**(9555) 51-59 (2007).
2. A Sheiham, "Oral health, general health and quality of life" *Bulletin of the World Health Organization*, **83**(9) 644-644 (2005).
3. PE Petersen, "World Health Organization global policy for improvement of oral health-World Health Assembly 2007" *International dental journal*, **58**(3) 115-121 (2008).
4. PE Petersen, D Bourgeois, H Ogawa, S Estupinan-Day, and C Ndiaye, "The global burden of oral diseases and risks to oral health" *Bulletin of the World Health Organization*, **83**(9) 661-669 (2005).
5. R Adhani, B Sukmana, and E Suhartono, "Effect pH on demineralization dental erosion" *International Journal of Chemical Engineering and Applications*, **6**(2) 138 (2015).
6. DT Zero, "Dental caries process" *Dental Clinics of North America*, **43**(4) 635-664 (1999).
7. A Watts and M Addy, "Tooth discolouration and staining: Tooth discolouration and staining: a review of the literature" *British dental journal*, **190**(6) 309-316 (2001).
8. RC Oliver, LJ Brown, and H Löe, "Periodontal diseases in the United States population" *Journal of periodontology*, **69**(2) 269-278 (1998).
9. PK Moy, D Medina, V Shetty, and TL Aghaloo, "Dental implant failure rates and associated risk factors" *International Journal of Oral & Maxillofacial Implants*, **20**(4)(2005).
10. I Kleinberg and G Jenkins, "The pH of dental plaques in the different areas of the mouth before and after meals and their relationship to the pH and rate of flow of resting saliva" *Archives of oral biology*, **9**(5) 493-516 (1964).

11. W Edgar, "The role of saliva in the control of pH changes in human dental plaque" *Caries Res*, **10**(4) 241-254 (1976).
12. D Abelson and I Mandel, "The effect of saliva on plaque pH in vivo" *Journal of dental research*, **60**(9) 1634-1638 (1981).
13. OB Dirks, "Posteruptive changes in dental enamel" *Journal of Dental Research*, **45**(3) 503-511 (1966).
14. ME Jensen, "Responses of interproximal plaque pH to snack foods and effect of chewing sorbitol-containing gum" *The Journal of the American Dental Association*, **113**(2) 262-266 (1986).
15. N Markovic, DC Abelson, and ID Mandel, "Sorbitol Gum in Xerostomics: The Effects on Dental Plaque pH and Salivary Flow Rates 1" *Gerodontology*, **7**(2) 71-75 (1988).
16. M Dodds, S Hsieh, and D Johnson, "The effect of increased mastication by daily gum-chewing on salivary gland output and dental plaque acidogenicity" *Journal of dental research*, **70**(12) 1474-1478 (1991).
17. RM Stephan, "Changes in hydrogen-ion concentration on tooth surfaces and in carious lesions" *The Journal of the American Dental Association*, **27**(5) 718-723 (1940).
18. HR Englander, IL Shklair, and LS Fosdick, "The Effects of Saliva on the pH and Lactate Concentration in Dental Plaques: I. Caries-Rampant Individuals" *Journal of dental research*, **38**(5) 848-853 (1959).
19. AJ Delgado and VG Olafsson, "Acidic oral moisturizers with pH below 6.7 may be harmful to teeth depending on formulation: a short report" *Clinical, cosmetic and investigational dentistry*, **9** 81 (2017).

20. AJ Delgado, VG Olafsson, and TE Donovan, "pH and erosive potential of commonly used oral moisturizers" *Journal of Prosthodontics,* **25**(1) 39-43 (2016).

21. DP DePaola, "Saliva: The precious body fluid" *The Journal of the American Dental Association*, **139** 5S-6S (2008).

22. P Surmont and L Martens, "Root surface caries: an update" *Clinical preventive dentistry*, **11**(3) 14-20 (1989).

23. P Hoppenbrouwers, F Driessens, and J Borggreven, "The mineral solubility of human tooth roots" *Archives of Oral Biology*, **32**(5) 319-322 (1987).

24. Y-H Sung, H-H Son, K Yi, and J Chang, "Elemental analysis of caries-affected root dentin and artificially demineralized dentin" *Restorative dentistry & endodontics*, **41**(4) 255-261 (2016).

25. EAA Neel, A Aljabo, A Strange, S Ibrahim, M Coathup, AM Young, L Bozec, and V Mudera, "Demineralization–remineralization dynamics in teeth and bone" *International journal of nanomedicine*, **11** 4743 (2016).

26. BM Culbertson, "Glass-ionomer dental restoratives" *Progress in Polymer Science*, **26**(4) 577-604 (2001).

27. JW McLean, "Evolution of dental ceramics in the twentieth century" *Journal of Prosthetic Dentistry*, **85**(1) 61-66 (2001).

28. JR Kelly, "Dental ceramics: current thinking and trends" *Dental Clinics of North America*, **48**(2) 513-530 (2004).

29. JC Wataha, "Alloys for prosthodontic restorations" *The Journal of prosthetic dentistry*, **87**(4) 351-363 (2002).

30. A Kishore, KK Mehrotra, and CS Saimbi, "Effectiveness of desensitizing agents" *Journal of endodontics*, **28**(1) 34-35 (2002).

31. M Bernardo, H Luis, MD Martin, BG Leroux, T Rue, J Leitão, and TA DeRouen, "Survival and reasons for failure of amalgam versus composite posterior restorations placed in a randomized clinical trial" *The Journal of the American Dental Association*, **138**(6) 775-783 (2007).

32. JL Drummond, "Degradation, fatigue, and failure of resin dental composite materials" *Journal of Dental Research*, **87**(8) 710-719 (2008).

33. I Mjor and V Gordan, "Failure, repair, refurbishing and longevity of restorations" *Operative Dentistry*, **27**(5) 528-534 (2002).

34. IA Mjör, JE Moorhead, and JE Dahl, "Reasons for replacement of restorations in permanent teeth in general dental practice" *International dental journal*, **50**(6) 361-366 (2000).

35. NU Zitzmann and T Berglundh, "Definition and prevalence of peri-implant diseases" *Journal of clinical periodontology*, **35**(s8) 286-291 (2008).

36. I Denry and J Holloway, "Microstructural and crystallographic surface changes after grinding zirconia-based dental ceramics" *Journal of Biomedical Materials Research Part B: Applied Biomaterials*, **76**(2) 440-448 (2006).

37. T Leventouri, "Synthetic and biological hydroxyapatites: crystal structure questions" *Biomaterials*, **27**(18) 3339-3342 (2006).

38. K Yamagishi, K Onuma, T Suzuki, F Okada, J Tagami, M Otsuki, and P Senawangse, "Materials chemistry: a synthetic enamel for rapid tooth repair" *Nature*, **433**(7028) 819 (2005).

39. A Peutzfeldt, S Mühlebach, A Lussi, and S Flury, "Marginal gap formation in approximal “bulk fill” resin composite restorations after artificial ageing" *Operative dentistry*, **43**(2) 180-189 (2018).

40. GM Holt and TC Dumsha, "Leakage of amalgam, composite, and Super-EBA, compared with a new retrofill material: bone cement" *Journal of endodontics*, **26**(1) 29-31 (2000).

41. G Smee, OR Bolanos, DR Morse, ML Furst, and C Yesilsoy, "A comparative leakage study of P-30 resin bonded ceramic, Teflon, amalgam, and IRM as retrofilling seals" *Journal of endodontics*, **13**(3) 117-121 (1987).

42. I Islam, HK Chng, and AUJ Yap, "Comparison of the physical and mechanical properties of MTA and Portland cement" *Journal of Endodontics*, **32**(3) 193-197 (2006).

43. M Atai, M Nekoomanesh, S Hashemi, and S Amani, "Physical and mechanical properties of an experimental dental composite based on a new monomer" *Dental Materials*, **20**(7) 663-668 (2004).

44. V Imbeni, J Kruzic, G Marshall, S Marshall, and R Ritchie, "The dentin–enamel junction and the fracture of human teeth" *Nat. Mater.*, **4**(3) 229-232 (2005).

45. H Fong, M Sarikaya, SN White, and ML Snead, "Nano-mechanical properties profiles across dentin–enamel junction of human incisor teeth" *Materials Science and Engineering: C*, **7**(2) 119-128 (1999).

46. SN White, ML Paine, W Luo, M Sarikaya, H Fong, Z Yu, ZC Li, and ML Snead, "The dentino-enamel junction is a broad transitional zone uniting dissimilar bioceramic composites" *Journal of the American Ceramic Society*, **83**(1) 238-40 (2000).

47. H Fong, SN White, ML Paine, W Luo, ML Snead, and M Sarikaya, "Enamel structure properties controlled by engineered proteins in transgenic mice" *J Bone Miner Res*, **18**(11) 2052-2059 (2003).

48. BD Ratner, "Replacing and renewing: synthetic materials, biomimetics, and tissue engineering in implant dentistry" *Journal of dental education*, **65**(12) 1340-1347 (2001).

49. JDB Featherstone, "The science and practice of caries prevention" *J Am Dent Assoc*, **131**(7) 887-899 (2000).

50. Q Ruan and J Moradian-Oldak, "Amelogenin and enamel biomimetics" *Journal of Materials Chemistry B*, **3**(16) 3112-3129 (2015).

51. QC Ruan, YZ Zhang, XD Yang, S Nutt, and J Moradian-Oldak, "An amelogenin-chitosan matrix promotes assembly of an enamel-like layer with a dense interface" *Acta Biomaterialia*, **9**(7) 7289-7297 (2013).

52. V Uskoković. *Prospects and pits on the path of biomimetics: the case of tooth enamel*. in *Journal of Biomimetics, Biomaterials and Tissue Engineering*. 2010. Trans Tech Publ.

53. V Uskoković, W Li, and S Habelitz, "Amelogenin as a promoter of nucleation and crystal growth of apatite" *Journal of crystal growth*, **316**(1) 106-117 (2011).

54. M Gungormus, H Fong, IW Kim, JS Evans, C Tamerler, and M Sarikaya, "Regulation of in vitro calcium phosphate mineralization by combinatorially selected hydroxyapatite-binding peptides" *Biomacromolecules*, **9**(3) 966-973 (2008).

55. M Gungormus, EE Oren, JA Horst, H Fong, M Hnilova, MJ Somerman, ML Snead, R Samudrala, C Tamerler, and M Sarikaya, "Cementomimetics-constructing a cementum-like biomineralized microlayer via amelogenin-derived peptides" *International Journal of Oral Science*, **4**(2) 69-77 (2012).

56. P-A Fang, JF Conway, HC Margolis, JP Simmer, and E Beniash, "Hierarchical self-assembly of amelogenin and the regulation of biomineralization at the nanoscale" *Proceedings of the National Academy of Sciences*, **108**(34) 14097-14102 (2011).

57. S Lyngstadaas, J Wohlfahrt, S Brookes, M Paine, M Snead, and J Reseland, "Enamel matrix proteins; old molecules for new applications" *Orthodontics & craniofacial research*, **12**(3) 243-253 (2009).

58. Y Fan, Z Sun, and J Moradian-Oldak, "Controlled remineralization of enamel in the presence of amelogenin and fluoride" *Biomaterials*, **30**(4) 478-83 (2009).

59. E Le Norcy, S-Y Kwak, F Wiedemann-Bidlack, E Beniash, Y Yamakoshi, J Simmer, and H Margolis, "Leucine-rich amelogenin peptides regulate mineralization in vitro" *Journal of dental research*, **90**(9) 1091-1097 (2011).

60. T Yokoi, M Kawashita, K Kikuta, and C Ohtsuki, "Biomimetic mineralization of calcium phosphate crystals in polyacrylamide hydrogel: effect of concentrations of calcium and phosphate ions on crystalline phases and morphology" *Materials Science and Engineering: C*, **30**(1) 154-159 (2010).

61. M Esposito, M Grusovin, N Papanikolaou, P Coulthard, and H Worthington, "Enamel matrix derivative (Emdogain®) for periodontal tissue regeneration in intrabony defects" *Australian Dental Journal*, **55**(1) 101-104 (2010).

62. S Listl, YK Tu, and CM Faggion Jr, "A cost-effectiveness evaluation of enamel matrix derivatives alone or in conjunction with regenerative devices in the treatment of periodontal intra-osseous defects" *Journal of clinical periodontology*, **37**(10) 920-927 (2010).

63. JM Slocik and RR Naik, "Probing peptide-nanomaterial interactions" *Chemical Society Reviews*, **39**(9) 3454-3463 (2010).

64. SR Whaley, D English, EL Hu, PF Barbara, and AM Belcher, "Selection of peptides with semiconductor binding specificity for directed nanocrystal assembly" *Nature*, **405**(6787) 665-668 (2000).

65. M Sarikaya, C Tamerler, AK-Y Jen, K Schulten, and F Baneyx, "Molecular biomimetics: nanotechnology through biology" *Nat. Mater.*, **2**(9) 577-585 (2003).

66. C Tamerler, D Khatayevich, M Gungormus, T Kacar, EE Oren, M Hnilova, and M Sarikaya, "Molecular biomimetics: GEPI-based biological routes to technology" *Peptide Science*, **94**(1) 78-94 (2010).

67. C Tamerler and M Sarikaya, "Molecular biomimetics: utilizing nature's molecular ways in practical engineering" *Acta biomaterialia*, **3**(3) 289-299 (2007).

68. H Yazici, H Fong, B Wilson, EE Oren, FA Amos, H Zhang, JS Evans, ML Snead, M Sarikaya, and C Tamerler, "Biological response on a titanium implant-grade surface functionalized with modular peptides" *Acta Biomaterialia*, **9**(2) 5341-5352 (2013).

69. V Puddu and CC Perry, "Peptide adsorption on silica nanoparticles: evidence of hydrophobic interactions" *ACS nano*, **6**(7) 6356-6363 (2012).

70. C-Y Chiu, Y Li, L Ruan, X Ye, CB Murray, and Y Huang, "Platinum nanocrystals selectively shaped using facet-specific peptide sequences" *Nature chemistry*, **3**(5) 393-399 (2011).

71. RH Sedlak, M Hnilova, C Grosh, H Fong, F Baneyx, D Schwartz, M Sarikaya, C Tamerler, and B Traxler, "Engineered Escherichia coli silver-binding periplasmic protein

that promotes silver tolerance" *Applied and environmental microbiology*, **78**(7) 2289-2296 (2012).

72. SS Shankar, A Rai, B Ankamwar, A Singh, A Ahmad, and M Sastry, "Biological synthesis of triangular gold nanoprisms" *Nat. Mater.*, **3**(7) 482-488 (2004).

73. M Hnilova, D Khatayevich, A Carlson, EE Oren, C Gresswell, S Zheng, F Ohuchi, M Sarikaya, and C Tamerler, "Single-step fabrication of patterned gold film array by an engineered multi-functional peptide" *Journal of Colloid and Interface Science*, **365**(1) 97-102 (2012).

74. M Gungormus, M Branco, H Fong, JP Schneider, C Tamerler, and M Sarikaya, "Self assembled bi-functional peptide hydrogels with biomineralization-directing peptides" *Biomaterials*, **31**(28) 7266-7274 (2010).

75. Q Ye, P Spencer, E Yuca, and C Tamerler, "Engineered Peptide Repairs Defective Adhesive–Dentin Interface" *Macromolecular Materials and Engineering*, **302**(5)(2017).

76. E Yuca, AY Karatas, UOS Seker, M Gungormus, G Dinler-Doganay, M Sarikaya, and C Tamerler, "In vitro labeling of hydroxyapatite minerals by an engineered protein" *Biotechnology and bioengineering*, **108**(5) 1021-1030 (2011).

77. EE Oren, C Tamerler, D Sahin, M Hnilova, UOS Seker, M Sarikaya, and R Samudrala, "A novel knowledge-based approach to design inorganic-binding peptides" *Bioinformatics*, **23**(21) 2816-2822 (2007).

78. S Dogan, H Fong, DT Yucesoy, T Cousin, C Gresswell, S Dag, G Huang, and M Sarikaya, "Biomimetic Tooth Repair: Amelogenin-derived peptide enables in vitro remineralization of human enamel" *ACS Biomaterials Science & Engineering*, **5**(4) 1788-1796 (2018).

79. L Gorelick, AM Geiger, and AJ Gwinnett, "Incidence of White Spot Formation after Bonding and Banding" *Am J Orthod Dentofac*, **81**(2) 93-98 (1982).

80. Z Huang, CJ Newcomb, P Bringas, SI Stupp, and ML Snead, "Biological synthesis of tooth enamel instructed by an artificial matrix" *Biomaterials*, **31**(35) 9202-9211 (2010).

81. ADACS Affair, "Professionally applied topical fluoride: Evidence-based clinical recommendations" *J Am Dent Assoc*, **137**(8) 1151-1159 (2006).

82. AB Ammari, A Bloch-Zupan, and PF Ashley, "Systematic review of studies comparing the anti-caries efficacy of children's toothpaste containing 600 ppm of fluoride or less with high fluoride toothpastes of 1,000 ppm or above" *Caries Res*, **37**(2) 85-92 (2003).

83. LG Petersson, S Twetman, H Dahlgren, A Norlund, AK Holm, G Nordenram, F Lagerlof, B Soder, C Kallestal, I Mejare, S Axelsson, and P Lingstrom, "Professional fluoride varnish treatment for caries control: a systematic review of clinical trials" *Acta Odontol Scand*, **62**(3) 170-176 (2004).

84. JM tenCate, "Review on fluoride, with special emphasis on calcium fluoride mechanisms in caries prevention" *Eur J Oral Sci*, **105**(5) 461-465 (1997).

85. AM Al-Mullahi and KJ Toumba, "Effect of Slow-Release Fluoride Devices and Casein Phosphopeptide/Amorphous Calcium Phosphate Nanocomplexes on Enamel Remineralization in vitro" *Caries Res*, **44**(4) 364-371 (2010).

86. J Krithikadatta, C Fredrick, M Abarajithan, and D Kandaswamy, "Remineralisation of Occlusal White Spot Lesions with a Combination of 10% CPP-ACP and 0.2% Sodium Fluoride Evaluated Using Diagnodent: A Pilot Study" *Oral Hlth Prev Dent*, **11**(2) 191-196 (2013).

87. H Meyer-Lueckel, RJ Wierichs, T Schellwien, and S Paris, "Remineralizing Efficacy of a CPP-ACP Cream on Enamel Caries Lesions in situ" *Caries Res*, **49**(1) 56-62 (2015).

88. G Rolla and E Saxegaard, "Critical evaluation of the composition and use of topical fluorides, with emphasis on the role of calcium fluoride in caries inhibition" *J Dent Res*, **69 Spec No** 780-5; discussion 820-3 (1990).

89. T Sitthisettapong, P Phantumvanit, C Huebner, and T Derouen, "Effect of CPP-ACP paste on dental caries in primary teeth: a randomized trial" *J Dent Res*, **91**(9) 847-52 (2012).

90. S Vanichvatana and P Auychai, "Efficacy of two calcium phosphate pastes on the remineralization of artificial caries: a randomized controlled double-blind in situ study" *Int J Oral Sci*, **5**(4) 224-8 (2013).

91. MC Wong, J Clarkson, AM Glenny, EC Lo, VC Marinho, BW Tsang, T Walsh, and HV Worthington, "Cochrane reviews on the benefits/risks of fluoride toothpastes" *J Dent Res*, **90**(5) 573-9 (2011).

92. M Balakrishnan, RS Simmonds, and JR Tagg, "Dental caries is a preventable infectious disease" *Aust Dent J*, **45**(4) 235-45 (2000).

93. JD Featherstone, "The caries balance: the basis for caries management by risk assessment" *Oral Health Prev Dent*, **2 Suppl 1** 259-64 (2004).

94. S Huang, S Gao, L Cheng, and H Yu, "Remineralization potential of nano-hydroxyapatite on initial enamel lesions: an in vitro study" *Caries Res*, **45**(5) 460-8 (2011).

95. GS Ingram and LM Silverstone, "A chemical and histological study of artificial caries in human dental enamel in vitro" *Caries Res*, **15**(5) 393-8 (1981).

96. T Koulourides, H Cueto, and W Pigman, "Rehardening of softened enamel surfaces of human teeth by solutions of calcium phosphates" *Nature*, **189** 226-7 (1961).

97. JM ten Cate, WL Jongebloed, and J Arends, "Remineralization of artificial enamel lesions in vitro. IV. Influence of fluorides and diphosphonates on short- and long-term reimineralization" *Caries Res*, **15**(1) 60-9 (1981).

98. K Bleek and A Taubert, "New developments in polymer-controlled, bioinspired calcium phosphate mineralization from aqueous solution" *Acta Biomater*, **9**(5) 6283-321 (2013).

99. CE Fowler, M Li, S Mann, and HC Margolis, "Influence of surfactant assembly on the formation of calcium phosphate materials - A model for dental enamel formation" *J Mater Chem*, **15**(32) 3317-3325 (2005).

100. J Kirkham, A Firth, D Vernals, N Boden, C Robinson, RC Shore, SJ Brookes, and A Aggeli, "Self-assembling peptide scaffolds promote enamel remineralization" *Journal of Dental Research*, **86**(5) 426-430 (2007).

101. QL Li, TY Ning, Y Cao, WB Zhang, ML Mei, and CH Chu, "A novel self-assembled oligopeptide amphiphile for biomimetic mineralization of enamel" *Bmc Biotechnol*, **14**(2014).

102. F Shafiei, BG Hossein, MM Farajollahi, M Fathollah, B Marjan, and JK Tahereh, "Leucine-rich amelogenin peptide (LRAP) as a surface primer for biomimetic remineralization of superficial enamel defects: An in vitro study" *Scanning*, **37**(3) 179-185 (2015).

103. D Wu, JJ Yang, JY Li, L Chen, B Tang, XY Chen, W Wu, and JS Li, "Hydroxyapatite-anchored dendrimer for in situ remineralization of human tooth enamel" *Biomaterials*, **34**(21) 5036-5047 (2013).

104. J Moradian-Oldak, ML Paine, YP Lei, AG Fincham, and ML Snead, "Self-assembly properties of recombinant engineered amelogenin proteins analyzed by dynamic light scattering and atomic force microscopy" *J Struct Biol*, **131**(1) 27-37 (2000).

105. ML Paine, SN White, W Luo, H Fong, M Sarikaya, and ML Snead, "Regulated gene expression dictates enamel structure and tooth function" *Matrix Biol*, **20**(5-6) 273-292 (2001).

106. ML Snead, EC Lau, M Zeichnerdavid, AG Fincham, SLC Woo, and HC Slavkin, "DNA-Sequence for Cloned Cdna for Murine Amelogenin Reveal the Amino-Acid Sequence for Enamel-Specific Protein" *Biochem Bioph Res Co*, **129**(3) 812-818 (1985).

107. PMM Hoppenbrouwers and FCM Driessens, "The Effect of Lactic and Acetic-Acid on the Formation of Artificial Caries Lesions" *Journal of Dental Research*, **67**(12) 1466-1467 (1988).

108. RJM Lynch and JM ten Cate, "The effect of lesion characteristics at baseline on subsequent de- and remineralisation behaviour" *Caries Res*, **40**(6) 530-535 (2006).

109. EA Naumova, N Niemann, L Aretz, and WH Arnold, "Effects of different amine fluoride concentrations on enamel remineralization" *J Dent*, **40**(9) 750-755 (2012).

110. H Fong, M Sarikaya, SN White, and ML Snead, "Nano-mechanical properties profiles across dentin-enamel junction of human incisor teeth" *Mat Sci Eng C-Bio S*, **7**(2) 119-128 (2000).

111. RR Gallagher, M Balooch, G Balooch, RS Wilson, SJ Marshall, and GW Marshall, "Coupled Nanomechanical and Raman Microspectroscopic Investigation of Human Third Molar DEJ" *J Dent Biomech*, **2010**(2010).

112. WC Oliver and GM Pharr, "An improved technique for determining hardness and elastic modulus using load and displacement sensing indentation experiments" *J Mater Res*, **7**(6) 1564-1583 (1992).

113. J Featherstone and S Doméjean, "The role of remineralizing and anticaries agents in caries management" *Advances in dental research*, **24**(2) 28-31 (2012).

114. J Ten Cate, "Novel anticaries and remineralizing agents: prospects for the future" *Journal of Dental Research*, **91**(9) 813-815 (2012).

115. N Pitts and J Wefel, "Remineralization/desensitization: what is known? What is the future?" *Advances in dental research*, **21**(1) 83-86 (2009).

116. HJ Shiau, "Dentin hypersensitivity" *Journal of Evidence-Based Dental Practice*, **12**(3) 220-228 (2012).

117. J Rees, "The prevalence of dentine hypersensitivity in general dental practice in the UK" *Journal of clinical periodontology*, **27**(11) 860-865 (2000).

118. DQ Taani and F Awartani, "Prevalence and distribution of dentin hypersensitivity and plaque in a dental hospital population" *Quintessence International*, **32**(5)(2001).

119. M Chabanski, D Gillam, J Bulman, and H Newman, "Prevalence of cervical dentine sensitivity in a population of patients referred to a specialist Periodontology Department" *Journal of Clinical Periodontology*, **23**(11) 989-992 (1996).

120. CT Bamise and TA Esan, "Mechanisms and treatment approaches of dentine hypersensitivity: a literature review" *Oral Hlth Prev Dent*, **9**(4)(2011).

121. DH Pashley, "Dentine permeability and its role in the pathobiology of dentine sensitivity" *Archives of Oral Biology*, **39** S73-S80 (1994).

122. BL Foster, TE Popowics, HK Fong, and MJ Somerman, "Advances in defining regulators of cementum development and periodontal regeneration" *Current Topics in Developmental Biology*, **78** 47-126 (2007).

123. T Popowics, B Foster, E Swanson, H Fong, and M Somerman, "Defining the roots of cementum formation" *Cells Tissues Organs*, **181**(3-4) 248-257 (2005).

124. M Brännström, "The hydrodynamic theory of dentinal pain: sensation in preparations, caries, and the dentinal crack syndrome" *Journal of endodontics*, **12**(10) 453-457 (1986).

125. M Brännström, "Etiology of dentin hypersensitivity" *Proceedings of the Finnish Dental Society. Suomen Hammaslaakariseuran toimituksia*, **88** 7-13 (1992).

126. M Brännström and A Åström, "A study on the mechanism of pain elicited from the dentin" *Journal of dental research*, **43**(4) 619-625 (1964).

127. PL Jacobsen and G Bruce, "Clinical dentin hypersensitivity: understanding the causes and prescribing a treatment" *The Journal of contemporary dental practice*, **2**(1) 1-12 (2001).

128. C Dorter, B Efes, F Koray, and G Kulekci. *Dental caries prevalance and caries-related factors*. in *JOURNAL OF DENTAL RESEARCH*. 2003. INT AMER ASSOC DENTAL RESEARCHI ADR/AADR 1619 DUKE ST, ALEXANDRIA, VA 22314-3406 USA.

129. K Markowitz and DH Pashley, "Discovering new treatments for sensitive teeth: the long path from biology to therapy" *Journal of oral rehabilitation*, **35**(4) 300-315 (2008).

130. PA Walters, "Dentinal hypersensitivity: a review" *J Contemp Dent Pract*, **6**(2) 107-17 (2005).

131. R Dababneh, A Khouri, and M Addy, "dentine hypersensitivity: Dentine hypersensitivity—an enigma? a review of terminology, mechanisms, aetiology and management" *British dental journal*, **187**(11) 606-611 (1999).

132. M Wolff, "Dentin hypersensitivity, the biofilm and remineralization: what is the connection?" *Advances in dental research*, **21**(1) 21-24 (2009).

133. M Addy, "Etiology and clinical implications of dentine hypersensitivity" *Dental Clinics of North America*, **34**(3) 503-514 (1990).

134. R Orchardson and DG Gillam, "Managing dentin hypersensitivity" *The Journal of the American Dental Association*, **137**(7) 990-998 (2006).

135. S Sharma, NJ Shetty, and A Uppoor, "Evaluation of the clinical efficacy of potassium nitrate desensitizing mouthwash and a toothpaste in the treatment of dentinal hypersensitivity" *Journal of clinical and experimental dentistry*, **4**(1) e28 (2012).

136. T Nagata, H Ishida, H Shinohara, S Nishikawa, S Kasahara, Y Wakano, S Daigen, and ES Troullos, "Clinical evaluation of a potassium nitrate dentifrice for the treatment of dentinal hypersensitivity" *Journal of clinical periodontology*, **21**(3) 217-221 (1994).

137. IC Porto, AK Andrade, and MA Montes, "Diagnosis and treatment of dentinal hypersensitivity" *Journal of oral science*, **51**(3) 323-332 (2009).

138. EM Varoni, T Zuccheri, A Carletta, B Palazzo, A Cochis, M Colonna, and L Rimondini, "In vitro efficacy of a novel potassium oxalate hydrogel for dentin hypersensitivity" *Eur J Oral Sci*, **125**(2) 151-159 (2017).

139. ST Taha, H Han, S-R Chang, I Sovadinova, K Kuroda, RM Langford, and BH Clarkson, "Nano/micro fluorhydroxyapatite crystal pastes in the treatment of dentin hypersensitivity: an in vitro study" *Clinical oral investigations*, **19**(8) 1921-1930 (2015).

140. T Wang, S Yang, L Wang, and H Feng, "Use of multifunctional phosphorylated PAMAM dendrimers for dentin biomimetic remineralization and dentinal tubule occlusion" *RSC Advances*, **5**(15) 11136-11144 (2015).

141. J Yu, H Yang, K Li, J Lei, L Zhou, and C Huang, "A novel application of nanohydroxyapatite/mesoporous silica biocomposite on treating dentin hypersensitivity: An in vitro study" *J Dent*, **50** 21-29 (2016).

142. G Craig, G Knight, and J McIntyre, "Clinical evaluation of diamine silver fluoride/potassium iodide as a dentine desensitizing agent. A pilot study" *Australian dental journal*, **57**(3) 308-311 (2012).

143. J Castillo, S Rivera, T Aparicio, R Lazo, T-C Aw, L Mancl, and P Milgrom, "The short-term effects of diammine silver fluoride on tooth sensitivity: a randomized controlled trial" *Journal of dental research*, **90**(2) 203-208 (2011).

144. I Duran and A Sengun, "The long-term effectiveness of five current desensitizing products on cervical dentine sensitivity" *Journal of oral rehabilitation*, **31**(4) 351-356 (2004).

145. AV Ritter, WL de Dias, P Miguez, DJ Caplan, and EJ Swift, "Treating cervical dentin hypersensitivity with fluoride varnish" *The Journal of the American Dental Association*, **137**(7) 1013-1020 (2006).

146. DG Gillam, RK Chesters, DC Attrill, P Brunton, M Slater, P Strand, H Whelton, and D Bartlett, "Dentine hypersensitivity–guidelines for the management of a common oral health problem" *Dental update*, **40**(7) 514-524 (2013).

147. T Schiff, E Delgado, Y Zhang, D Cummins, W DeVizio, and L Mateo, "Clinical evaluation of the efficacy of an in-office desensitizing paste containing 8% arginine and

calcium carbonate in providing instant and lasting relief of dentin hypersensitivity" *American journal of dentistry*, **22**(Spec No. A) 8A-15A (2009).

148. CW Gibson, Y Li, B Daly, C Suggs, ZA Yuan, H Fong, D Simmons, M Aragon, AB Kulkarni, and JT Wright, "The Leucine-Rich Amelogenin Peptide Alters the Amelogenin Null Enamel Phenotype" *Cells Tissues Organs*, **189**(1-4) 169-174 (2009).

149. WJ Loesche, "Role of Streptococcus mutans in human dental decay" *Microbiol Rev*, **50**(4) 353-80 (1986).

150. TT Zhang, HJ Guo, XJ Liu, JP Chu, and XD Zhou, "Galla chinensis Compounds Remineralize Enamel Caries Lesions in a Rat Model" *Caries Res*, **50**(2) 159-65 (2016).

151. WH Bowen, "Rodent model in caries research" *Odontology*, **101**(1) 9-14 (2013).

152. AR Firestone, R Schmid, and HR Muhlemann, "Cariogenic Effects of Cooked Wheat-Starch Alone or with Sucrose and Frequency-Controlled Feedings in Rats" *Archives of Oral Biology*, **27**(9) 759-763 (1982).

153. B Guggenheim, KG Konig, E Herzog, and HR Muhlemann, "The cariogenicity of different dietary carbohydrates tested on rats in relative gnotobiosis with a Streptococcus producing extracellular polysaccharide" *Helv Odontol Acta*, **10**(2) 101-13 (1966).

154. JM Navia, H Lopez, and RS Harris, "Purified diet for dental caries research with rats" *J Nutr*, **97**(1) 133-40 (1969).

155. T Klinke, B Guggenheim, W Klimm, and T Thurnheer, "Dental caries in rats associated with Candida albicans" *Caries Res*, **45**(2) 100-6 (2011).

156. MD Willcox, DB Drucker, and RM Green, "Comparative cariogenicity and dental plaque-forming ability in gnotobiotic rats of four species of mutans streptococci" *Arch Oral Biol*, **34**(10) 825-8 (1989).

157. EL Hietala, J Autio, and M Larmas, "The effect of early weaning on dentin formation and dentinal caries in rats" *Acta Odontol Scand*, **55**(4) 201-5 (1997).

158. R Bao, J Yang, Y Sun, D Zhou, Y Yang, Y Li, Y Cao, Y Xiao, W Li, and J Yu, "Flagellin-PAc fusion protein inhibits progression of established caries" *Journal of dental research*, **94**(7) 955-960 (2015).

159. GS Schuster, JM Navia, S Amsbaugh, and RH Larson, "Sources of variability in rat caries studies: microbial infection and caging procedure" *J Dent Res*, **57**(2) 355-60 (1978).

160. S Han, Y Fan, Z Zhou, H Tu, D Li, X Lv, L Ding, and L Zhang, "Promotion of enamel caries remineralization by an amelogenin-derived peptide in a rat model" *Archives of oral biology*, **73** 66-71 (2017).

161. S Liu, T Wu, X Zhou, B Zhang, S Huo, Y Yang, K Zhang, L Cheng, X Xu, and M Li, "Nicotine is a risk factor for dental caries: An in vivo study" *Journal of Dental Sciences*, **13**(1) 30-36 (2018).

162. R Free, K DeRocher, S Stock, D Keane, K Scott-Anne, W Bowen, and D Joester, "Characterization of enamel caries lesions in rat molars using synchrotron X-ray microtomography" *Journal of synchrotron radiation*, **24**(5) 1056-1064 (2017).

163. PS Kumar and MR Mason, "Mouthguards: does the indigenous microbiome play a role in maintaining oral health?" *Frontiers in cellular and infection microbiology*, **5** 35 (2015).

164. JM Tanzer, J Livingston, and AM Thompson, "The microbiology of primary dental caries in humans" *J Dent Educ*, **65**(10) 1028-37 (2001).

165. J van Houte, "Role of micro-organisms in caries etiology" *J Dent Res*, **73**(3) 672-81 (1994).

166. A Yoshida, N Suzuki, Y Nakano, M Kawada, T Oho, and T Koga, "Development of a 5' nuclease-based real-time PCR assay for quantitative detection of cariogenic dental pathogens Streptococcus mutans and Streptococcus sobrinus" *J Clin Microbiol*, **41**(9) 4438-41 (2003).

167. A Yoshida, N Suzuki, Y Nakano, T Oho, M Kawada, and T Koga, "Development of a 5' fluorogenic nuclease-based real-time PCR assay for quantitative detection of Actinobacillus actinomycetemcomitans and Porphyromonas gingivalis" *J Clin Microbiol*, **41**(2) 863-6 (2003).

168. W Bowen, G Coccodrilli, R Fitzgerald, R Havenaar, D Johnson, and A Kingman, "Animal caries–Working group consensus report" *J Dent Res*, **65** 1528-1529 (1986).

169. RH Larson. *Merits and modifications of scoring rat dental caries by Keyes' method*. in *Proceedings of" Symposium on animal models in cariology", Spl. Supp. Microbiology Abstracts, 1981*. 1981.

170. PH Keyes, "Dental caries in the molar teeth of rats: II. A method for diagnosing and scoring several types of lesions simultaneously" *Journal of dental research*, **37**(6) 1088-1099 (1958).

171. U Hafstrom-Bjorkman, F Sundstrom, and B Angmar-Mansson, "Initial caries diagnosis in rat molars, using laser fluorescence" *Acta Odontol Scand*, **49**(1) 27-33 (1991).

172. EL Hietala, L Tjaderhane, and M Larmas, "Dentin caries recording with Schiff's reagent, fluorescence, and back-scattered electron image" *J Dent Res*, **72**(12) 1588-92 (1993).

173. D Cummins, "The development and validation of a new technology, based upon 1.5% arginine, an insoluble calcium compound and fluoride, for everyday use in the prevention and treatment of dental caries" *J Dent*, **41** S1-S11 (2013).

174. IA Pretty, "Caries detection and diagnosis: novel technologies" *J Dent*, **34**(10) 727-39 (2006).

175. A-H Yen and P Yelick, "Dental tissue regeneration–a mini-review" *Gerontology*, **57**(1) 85-94 (2011).

176. IA Pretty and RP Ellwood, "The caries continuum: opportunities to detect, treat and monitor the re-mineralization of early caries lesions" *J Dent*, **41 Suppl 2** S12-21 (2013).

177. L Angker, C Nockolds, MV Swain, and N Kilpatrick, "Quantitative analysis of the mineral content of sound and carious primary dentine using BSE imaging" *Arch Oral Biol*, **49**(2) 99-107 (2004).

178. EC Reynolds, F Cai, NJ Cochrane, P Shen, GD Walker, MV Morgan, and C Reynolds, "Fluoride and casein phosphopeptide-amorphous calcium phosphate" *J Dent Res*, **87**(4) 344-8 (2008).

179. C Kilkenny, WJ Browne, IC Cuthill, M Emerson, and DG Altman, "Improving bioscience research reporting: the ARRIVE guidelines for reporting animal research" *PLoS biology*, **8**(6) e1000412 (2010).

180. DT Yucesoy, M Hnilova, K Boone, PM Arnold, ML Snead, and C Tamerler, "Chimeric Peptides as Implant Functionalization Agents for Titanium Alloy Implants with Antimicrobial Properties" *JOM*, **67**(4) 754-766 (2015).

181. SM Michalek, JR McGhee, and JM Navia, "Virulence of Streptococcus mutans: a sensitive method for evaluating cariogenicity in young gnotobiotic rats" *Infect Immun*, **12**(1) 69-75 (1975).

182. ME Saravia, P Nelson-Filho, RA Silva, A De Rossi, G Faria, LA Silva, and CG Emilson, "Recovery of mutans streptococci on MSB, SB-20 and SB-20M agar media" *Arch Oral Biol*, **58**(3) 311-6 (2013).

183. JR Lukacs and LL Largaespada, "Explaining sex differences in dental caries prevalence: saliva, hormones, and “life-history” etiologies" *American Journal of Human Biology: The Official Journal of the Human Biology Association*, **18**(4) 540-555 (2006).

184. JM Navia and RS Harris, "Longitudinal study of cariostatic effects of sodium trimetaphosphate and sodium fluoride when fed separately and together in diets of rats" *J Dent Res*, **48**(2) 183-91 (1969).

185. DT Yucesoy, H Fong, C Gresswell, S Saadat, WO Chung, S Dogan, and M Sarikaya, "Early Caries in an In Vivo Model: Structural and Nanomechanical Characterization" *Journal of Dental Research*, **97**(13) 1452-1459 (2018).

186. F García-Godoy and MJ Hicks, "Maintaining the integrity of the enamel surface: the role of dental biofilm, saliva and preventive agents in enamel demineralization and remineralization" *The Journal of the American Dental Association*, **139** 25S-34S (2008).

187. J Arends and J Ten Bosch, "Demineralization and remineralization evaluation techniques" *Journal of Dental Research*, **71**(1992).

188. S Ranjitkar, JA Kaidonis, and RJ Smales, "Gastroesophageal reflux disease and tooth erosion" *International Journal of Dentistry*, **2012**(2012).

189. J Featherstone, "Dental caries: a dynamic disease process" *Australian dental journal*, **53**(3) 286-291 (2008).

190. K Chun, H Choi, and J Lee, "Comparison of mechanical property and role between enamel and dentin in the human teeth" *Journal of dental biomechanics*, **5**(2014).

191. JA Cury and LMA Tenuta, "Enamel remineralization: controlling the caries disease or treating early caries lesions?" *Brazilian oral research*, **23** 23-30 (2009).

192. JL Ferracane, "Current trends in dental composites" *Critical Reviews in Oral Biology & Medicine*, **6**(4) 302-318 (1995).

193. M Cenci, T Pereira-Cenci, J Cury, and J Ten Cate, "Relationship between gap size and dentine secondary caries formation assessed in a microcosm biofilm model" *Caries Res*, **43**(2) 97-102 (2009).

194. M Fontana, A Dunipace, R Gregory, T Noblitt, Y Li, K Park, and G Stookey, "An in vitro microbial model for studying secondary caries formation" *Caries Res*, **30**(2) 112-118 (1996).

195. A Kielbassa, J Schulte-Monting, F Garcia-Godoy, and H Meyer-Lueckel, "Initial in situ secondary caries formation: effect of various fluoride-containing restorative materials" *OPERATIVE DENTISTRY-UNIVERSITY OF WASHINGTON-*, **28**(6) 765-772 (2003).

196. M Alkhatib, R Holt, and R Bedi, "Prevalence of self-assessed tooth discolouration in the United Kingdom" *J Dent*, **32**(7) 561-566 (2004).

197. L Odioso, R Gibb, and R Gerlach, "Impact of demographic, behavioral, and dental care utilization parameters on tooth color and personal satisfaction" *Compendium of continuing education in dentistry.(Jamesburg, NJ: 1995). Supplement*, (29) S35-41; quiz S43 (2000).

198. A Qualtrough and F Burke, "A look at dental esthetics" *Quintessence international*, **25**(1)(1994).

199. SA NATHOO, "The chemistry and mechanisms of extrinsic and intrinsic discoloration" *The Journal of the American Dental Association*, **128** 6S-10S (1997).

200. M Sulieman, "An overview of tooth discoloration: extrinsic, intrinsic and internalized stains" *Dental update*, **32**(8) 463-4, 466-8, 471 (2005).

201. AR Sánchez, RS Rogers, and PJ Sheridan, "Tetracycline and other tetracycline-derivative staining of the teeth and oral cavity" *International journal of dermatology*, **43**(10) 709-715 (2004).

202. S Sundell and G Koch, "Hereditary amelogenesis imperfecta. I. Epidemiology and clinical classification in a Swedish child population" *Swedish Dental Journal*, **9**(4) 157-169 (1985).

203. K Watanabe, T Shibata, T Kurosawa, I Morisaki, M Kinehara, S Igarashi, and M Arisue, "Bilirubin pigmentation of human teeth caused by hyperbilirubinemia" *Journal of oral pathology & medicine*, **28**(3) 128-130 (1999).

204. J Link, "Discolouration of the teeth in alkaptonuria and Parkinsonism" *Chron Omaha Dist Dent Soc*, **36** 136 (1973).

205. M Sulieman, M Addy, E MacDonald, and J Rees, "The effect of hydrogen peroxide concentration on the outcome of tooth whitening: an in vitro study" *J Dent*, **32**(4) 295-299 (2004).

206. JJ Pindborg, "Pathology of the dental hard tissues" (1970).

207. J Dahl and U Pallesen, "Tooth bleaching—a critical review of the biological aspects" *Critical Reviews in Oral Biology & Medicine*, **14**(4) 292-304 (2003).

208. D Hein, B Ploeger, J Hartup, R Wagstaff, T Palmer, and L Hansen, "In-office vital tooth bleaching--what do lights add?" *Compendium of continuing education in dentistry (Jamesburg, NJ: 1995)*, **24**(4A) 340-352 (2003).

209. K Luk, L Tam, and M Hubert, "Effect of light energy on peroxide tooth bleaching" *The Journal of the American Dental Association*, **135**(2) 194-201 (2004).

210. J-h Chen, C-x Shi, M Wang, S-j Zhao, and H Wang, "Clinical evaluation of 546 tetracycline-stained teeth treated with porcelain laminate veneers" *J Dent*, **33**(1) 3-8 (2005).

211. R Nixon, "Masking severely tetracycline-stained teeth with ceramic laminate veneers" *Practical periodontics and aesthetic dentistry: PPAD*, **8**(3) 227-35; quiz 237 (1996).

212. DE Arens, JJ Rich, and HJ Healey, "A practical method of bleaching tetracycline-stained teeth" *Oral Surgery, Oral Medicine, Oral Pathology*, **34**(5) 812-817 (1972).

213. H Rodrigues, A Brochado, M Troilo, and A Mohsin, "Mirror, mirror on the wall, who's the fairest of them all? A critical content analysis on medical tourism" *Tourism Management Perspectives*, **24** 16-25 (2017).

214. C Tredwin, S Naik, N Lewis, and C Scully, "Hydrogen peroxide tooth-whitening (bleaching) products: review of adverse effects and safety issues" *British dental journal*, **200**(7) 371-376 (2006).

215. C Hanks, J Fat, J Wataha, and J Corcoran, "Cytotoxicity and dentin permeability of carbamide peroxide and hydrogen peroxide vital bleaching materials, in vitro" *Journal of Dental Research*, **72**(5) 931-938 (1993).

216. E Gjorgievska and JW Nicholson, "Prevention of enamel demineralization after tooth bleaching by bioactive glass incorporated into toothpaste" *Australian dental journal*, **56**(2) 193-200 (2011).

217. MD Fairchild and RS Berns, "Image color-appearance specification through extension of CIELAB" *Color Research & Application*, **18**(3) 178-190 (1993).

218. AR Robertson, "The CIE 1976 color-difference formulae" *Color Research & Application*, **2**(1) 7-11 (1977).

219. AG Wee, DT Lindsey, S Kuo, and WM Johnston, "Color accuracy of commercial digital cameras for use in dentistry" *Dental Materials*, **22**(6) 553-559 (2006).

220. B Matis, M Cochran, G Wang, and G Eckert, "A clinical evaluation of two in-office bleaching regimens with and without tray bleaching" *Operative dentistry*, **34**(2) 142-149 (2009).

221. O Camps-Font, R Figueiredo, E Valmaseda-Castellón, and C Gay-Escoda, "Postoperative infections after dental implant placement: prevalence, clinical features, and treatment" *Implant dentistry*, **24**(6) 713-719 (2015).

222. J Chevalier and L Gremillard, "Ceramics for medical applications: A picture for the next 20 years" *Journal of the European Ceramic Society*, **29**(7) 1245-1255 (2009).

223. A Siddiqi, AG Payne, RK De Silva, and WJ Duncan, "Titanium allergy: could it affect dental implant integration?" *Clinical Oral Implants Research*, **22**(7) 673-680 (2011).

224. A Sicilia, S Cuesta, G Coma, I Arregui, C Guisasola, E Ruiz, and A Maestro, "Titanium allergy in dental implant patients: a clinical study on 1500 consecutive patients" *Clinical oral implants research*, **19**(8) 823-835 (2008).

225. T Chaturvedi, "An overview of the corrosion aspect of dental implants (titanium and its alloys)" *Indian Journal of Dental Research*, **20**(1) 91 (2009).

226. B Stadlinger, M Hennig, U Eckelt, E Kuhlisch, and R Mai, "Comparison of zirconia and titanium implants after a short healing period. A pilot study in minipigs" *International Journal of Oral and Maxillofacial Surgery*, **39**(6) 585-592 (2010).

227. H Lüthy, F Filser, O Loeffel, M Schumacher, LJ Gauckler, and CHF Hammerle, "Strength and reliability of four-unit all-ceramic posterior bridges" *Dental Materials*, **21**(10) 930-937 (2005).

228. Y Akagawa, Y Ichikawa, H Nikai, and H Tsuru, "Interface histology of unloaded and early loaded partially stabilized zirconia endosseous implant in initial bone healing" *The Journal of prosthetic dentistry*, **69**(6) 599-604 (1993).

229. M Andreiotelli and R-J Kohal, "Fracture Strength of Zirconia Implants after Artificial Aging" *Clinical Implant Dentistry and Related Research*, **11**(2) 158-166 (2009).

230. M Hisbergues, S Vendeville, and P Vendeville, "Zirconia: Established facts and perspectives for a biomaterial in dental implantology" *Journal of biomedical materials research. Part B, Applied biomaterials*, **88**(2) 519-29 (2009).

231. C Piconi and G Maccauro, "Zirconia as a ceramic biomaterial" *Biomaterials*, **20**(1) 1-25 (1999).

232. Y Ichikawa, Y Akagawa, H Nikai, and H Tsuru, "Tissue compatibility and stability of a new zirconia ceramic in vivo" *The Journal of Prosthetic Dentistry*, **68**(2) 322-326 (1992).

233. ASD Al-Radha, D Dymock, C Younes, and D O'Sullivan, "Surface properties of titanium and zirconia dental implant materials and their effect on bacterial adhesion" *J Dent*, **40**(2) 146-153 (2012).

234. P Christel, A Meunier, M Heller, JP Torre, and CN Peille, "Mechanical properties and short-term in vivo evaluation of yttrium-oxide-partially-stabilized zirconia" *Journal of Biomedical Materials Research*, **23**(1) 45-61 (1989).

235. Z Ozkurt and E Kazazoglu, "Zirconia dental implants: a literature review" *The Journal of oral implantology*, **37**(3) 367-76 (2011).

236. SM Kurtz, E Lau, J Schmier, KL Ong, K Zhao, and J Parvizi, "Infection Burden for Hip and Knee Arthroplasty in the United States" *The Journal of Arthroplasty*, **23**(7) 984-991 (2008).

237. PS Stewart and J William Costerton, "Antibiotic resistance of bacteria in biofilms" *The Lancet*, **358**(9276) 135-138 (2001).

238. A Scarano, M Piattelli, S Caputi, GA Favero, and A Piattelli, "Bacterial adhesion on commercially pure titanium and zirconium oxide disks: an in vivo human study" *Journal of periodontology*, **75**(2) 292-6 (2004).

239. R van Brakel, MS Cune, AJ van Winkelhoff, C de Putter, JW Verhoeven, and W van der Reijden, "Early bacterial colonization and soft tissue health around zirconia and titanium abutments: an in vivo study in man" *Clinical Oral Implants Research*, **22**(6) 571-577 (2011).

240. H Yazici, MB O'Neill, T Kacar, BR Wilson, EE Oren, M Sarikaya, and C Tamerler, "Engineered Chimeric Peptides as Antimicrobial Surface Coating Agents toward Infection-Free Implants" *ACS Applied Materials & Interfaces*, **8**(8) 5070-5081 (2016).

241. X Shen, F Zhang, K Li, C Qin, P Ma, L Dai, and K Cai, "Cecropin B loaded TiO2 nanotubes coated with hyaluronidase sensitive multilayers for reducing bacterial adhesion" *Materials & Design*, **92** 1007-1017 (2016).

242. F Ordikhani, SP Zustiak, and A Simchi, "Surface Modifications of Titanium Implants by Multilayer Bioactive Coatings with Drug Delivery Potential: Antimicrobial, Biological, and Drug Release Studies" *JOM*, **68**(4) 1100-1108 (2016).

243. S-F Ou, M-S Huang, S-Y Chiou, and K-L Ou, "Research of antibacterial activity on silver containing yttria-stabilized–zirconia bioceramic" *Ceramics International*, **39**(4) 3591-3596 (2013).

244. I Azócar, E Vargas, N Duran, A Arrieta, E González, J Pavez, MJ Kogan, JH Zagal, and MA Paez, "Preparation and antibacterial properties of hybrid-zirconia films with silver nanoparticles" *Materials Chemistry and Physics*, **137**(1) 396-403 (2012).

245. L Esteban-Tejeda, A Smirnov, C Prado, JS Moya, R Torrecillas, and JF Bartolomé, "Multifunctional ceramic-metal biocomposites with Zinc containing antimicrobial glass coatings" *Ceramics International*, **42**(6) 7023-7029 (2016).

246. S Grigorescu, C Ungureanu, R Kirchgeorg, P Schmuki, and I Demetrescu, "Various sized nanotubes on TiZr for antibacterial surfaces" *Applied Surface Science*, **270** 190-196 (2013).

247. JC Love, LA Estroff, JK Kriebel, RG Nuzzo, and GM Whitesides, "Self-assembled monolayers of thiolates on metals as a form of nanotechnology" *Chemical reviews*, **105**(4) 1103-1170 (2005).

248. L Zhao, PK Chu, Y Zhang, and Z Wu, "Antibacterial coatings on titanium implants" *Journal of Biomedical Materials Research Part B: Applied Biomaterials*, **91B**(1) 470-480 (2009).

249. REW Hancock and H-G Sahl, "Antimicrobial and host-defense peptides as new anti-infective therapeutic strategies" *Nat Biotech*, **24**(12) 1551-1557 (2006).

250. K Reddy, R Yedery, and C Aranha, "Antimicrobial peptides: premises and promises" *International journal of antimicrobial agents*, **24**(6) 536-547 (2004).

251. M Zasloff, "Antimicrobial peptides of multicellular organisms" *Nature*, **415**(6870) 389-395 (2002).

252. KA Brogden, "Antimicrobial peptides: pore formers or metabolic inhibitors in bacteria?" *Nat Rev Microbiol*, **3**(3) 238-250 (2005).

253. Y Shai and Z Oren, "From "carpet" mechanism to de-novo designed diastereomeric cell-selective antimicrobial peptides" *Peptides*, **22**(10) 1629-1641 (2001).

254. SA Onaizi and SS Leong, "Tethering antimicrobial peptides: current status and potential challenges" *Biotechnology advances*, **29**(1) 67-74 (2011).

255. L Zhang, C Ning, T Zhou, X Liu, KWK Yeung, T Zhang, Z Xu, X Wang, S Wu, and PK Chu, "Polymeric Nanoarchitectures on Ti-Based Implants for Antibacterial Applications" *ACS Applied Materials & Interfaces*, **6**(20) 17323-17345 (2014).

256. AK Muszanska, ETJ Rochford, A Gruszka, AA Bastian, HJ Busscher, W Norde, HC van der Mei, and A Herrmann, "Antiadhesive Polymer Brush Coating Functionalized with Antimicrobial and RGD Peptides to Reduce Biofilm Formation and Enhance Tissue Integration" *Biomacromolecules*, **15**(6) 2019-2026 (2014).

257. M Kazemzadeh-Narbat, BFL Lai, C Ding, JN Kizhakkedathu, REW Hancock, and R Wang, "Multilayered coating on titanium for controlled release of antimicrobial peptides for the prevention of implant-associated infections" *Biomaterials*, **34**(24) 5969-5977 (2013).

258. F Costa, IF Carvalho, RC Montelaro, P Gomes, and MCL Martins, "Covalent immobilization of antimicrobial peptides (AMPs) onto biomaterial surfaces" *Acta Biomaterialia*, **7**(4) 1431-1440 (2011).

259. M Hnilova, EE Oren, UOS Seker, BR Wilson, S Collino, JS Evans, C Tamerler, and M Sarikaya, "Effect of Molecular Conformations on the Adsorption Behavior of Gold-Binding Peptides" *Langmuir*, **24**(21) 12440-12445 (2008).

260. A Sengupta, CK Thai, MSR Sastry, JF Matthaei, DT Schwartz, EJ Davis, and F Baneyx, "A Genetic Approach for Controlling the Binding and Orientation of Proteins on Nanoparticles" *Langmuir*, **24**(5) 2000-2008 (2008).

261. M Hnilova, X Liu, E Yuca, C Jia, B Wilson, A Karatas, C Gresswell, F Ohuchi, K Kitamura, and C Tamerler, "Multifunctional protein-enabled patterning on arrayed ferroelectric materials" *ACS applied materials & interfaces*, **4**(4) 1865-1871 (2012).

262. M Hnilova, BT Karaca, J Park, C Jia, BR Wilson, M Sarikaya, and C Tamerler, "Fabrication of hierarchical hybrid structures using bio-enabled layer-by-layer self-assembly" *Biotechnology and Bioengineering*, **109**(5) 1120-1130 (2012).

263. S Cetinel, HB Caliskan, DT Yucesoy, AS Donatan, E Yuca, M Urgen, NG Karaguler, and C Tamerler, "Addressable self-immobilization of lactate dehydrogenase across multiple length scales" *Biotechnology Journal*, **8**(2) 262-272 (2013).

264. DT Yucesoy, BT Karaca, S Cetinel, HB Caliskan, E Adali, N Gul-Karaguler, and C Tamerler, "Direct bioelectrocatalysis at the interfaces by genetically engineered dehydrogenase" *Bioinspired, Biomimetic and Nanobiomaterials*, **4**(1) 79-89 (2015).

265. BF Bell, M Schuler, S Tosatti, M Textor, Z Schwartz, and BD Boyan, "Osteoblast response to titanium surfaces functionalized with extracellular matrix peptide biomimetics" *Clinical oral implants research*, **22**(8) 865-72 (2011).

266. E Fernandez-Garcia, X Chen, CF Gutierrez-Gonzalez, A Fernandez, S Lopez-Esteban, and C Aparicio, "Peptide-functionalized zirconia and new zirconia/titanium biocermets for dental applications" *J Dent*, **43**(9) 1162-74 (2015).

267. D Carson, M Hnilova, X Yang, CL Nemeth, JH Tsui, AST Smith, A Jiao, M Regnier, CE Murry, C Tamerler, and D-H Kim, "Nanotopography-Induced Structural Anisotropy and Sarcomere Development in Human Cardiomyocytes Derived from Induced Pluripotent Stem Cells" *ACS Applied Materials & Interfaces*, (2016).

268. SL Haynie, GA Crum, and BA Doele, "Antimicrobial activities of amphiphilic peptides covalently bonded to a water-insoluble resin" *Antimicrobial agents and chemotherapy*, **39**(2) 301-7 (1995).

# VITA

By Deniz Tanil Yucesoy

| INSTITUTION AND LOCATION | DEGREE | DURATION | FIELD OF STUDY |
|---|---|---|---|
| Izmir Institute of Technology, Izmir, TR | B.S. | 2005-2009 | Molecular Biology & Genetics |
| Istanbul Technical University, Istanbul, TR | M.S. | 2009-2011 | Mol. Biology & Biotechnology |
| University of Washington, Seattle, USA | M.S. | 2012-2014 | Materials Science & Engineering |
| University of Washington, Seattle, USA | Ph.D. | 2014-2018 | Materials Science & Engineering |

## PUBLICATIONS

1. Yucesoy D.T., Akkineni S., Hinds B., Sarikaya M. (2018). *Peptide Enabled Addressable Immobilization of Kinetically Matched Fusion Enzymes in Membrane Flow Bioreactors*, (*in preparation, to be submitted in Oct. 2018**).
2. Yucesoy D.T., Fong H., Gresswell C., Saadat S., Chung W.O., Dogan S., Sarikaya M. (2018). *Dentomimetics – Amelogenin Derived Peptide-Enabled Biomimetic Tooth Repair in vivo.* (*in preparation, to be submitted in Dec. 2018**).
3. Yucesoy D.T., Hall E., Fong H., Ericksen K., Gresswell C., Dogan S., Sarikaya M., *Biomimetic hypersensitivity treatment: Amelogenin-derived peptide enables in vitro restoration of human cementum* (*in preparation, to be submitted in Dec.* 2018*).
4. Yucesoy D.T., Fong H., Dao A., Dogan S., Sarikaya M., *Remineralizing lozenges for additive tooth whitening* (*in preparation, to be submitted in Jan.* 2019*).
5. Yucesoy D.T., Boone K., Chin N., Tamerler C., *Engineered Chimeric Peptides as Antimicrobial Surface Coating Agents for Zirconia Implants* (*in preparation, to be submitted in Dec.* 2018*).
6. Yucesoy D.T., Fong H., Gresswell C., Chung W.O., Dogan S., Sarikaya M. (2018). *Early Caries in an In Vivo Model: Structural and Nanomechanical Characterization*. *JDR, 97 (13), 1452-1459.*
7. Dogan S., Fong H., Yucesoy D.T., Cousin T., Gresswell C., Dag S., Huang G., Sarikaya M. (2018) *Biomimetic Tooth Repair: Amelogenin-derived peptide enables in vitro remineralization of human enamel*. *ACS Biomater. Sci. Eng., **4**(5), 1788-1796.*
8. Yucesoy D.T., Hnilova M., Boone K., Arnold P. M., Snead M. L., Tamerler C. (2015). *Chimeric peptides as implant functionalization agents for titanium alloy implants with antimicrobial properties*. *JOM, **67***(4), 754-766.
9. Yucesoy D.T., Karaca B.T., Cetinel S., Caliskan H. B., Adali E., Gul-Karaguler N., Tamerler C. (2015). *Direct bioelectrocatalysis at the interfaces by genetically engineered dehydrogenase*. *Bioinspired, Biomimetic and Nanobiomaterials, **4***(1), 79-89.
10. Yucesoy D.T., Gungormus M., Fong H., Sarikaya M., Tamerler C. (2013). *Biomimetic Interface Design for Peptide Based Antimicrobial Implant Coatings, International Association for Dental Research Conference Proceedings,* doi: 10.13140/rg.2.1.4299.7529:

11. Hnilova M., Yucesoy D.T., Sarikaya M., Tamerler C. (2013). *Controlling biological functionalization of surfaces by engineered peptides*. *Biomaterials Science: Processing, Properties and Applications III: Ceramic Transactions*, ***242***, 137-150.
12. Cetinel S., Caliskan H.B., Yucesoy, D.T., Tamerler C. (2013). *Addressable self-immobilization of lactate dehydrogenase across multiple length scales*. *Biotechnology Journal*, 8(2), 262-272.

**SELECTED PRESENTATIONS (Last two years)**

1. Yucesoy D.T., Fong H., Gresswell C., Saadat S., Dogan S., Sarikaya M., *Biomimetic Tooth Repair: Amelogenin-Derived Peptide Guides in vitro Remineralization of Human Enamel and Dentin.* MRS Fall Meeting, Boston, oral presentation (November, 2017)
2. Yucesoy D.T., Fong H., Gresswell C., Saadat S., Dogan S., Sarikaya M., *Biomimetic Tooth Repair: Amelogenin-Derived Peptides enables Dental Hard Tissue Regeneration.* MSE Industry Day-2017, Seattle, poster presentation (October, 2017)
3. Yucesoy D.T., Fong H., Gresswell C., Saadat S., Dogan S., Sarikaya M., *Biomimetic Tooth Repair: Amelogenin-derived Peptides enable in vitro and in vivo Enamel Remineralization.* TMS Spring Meeting, San Francisco, oral presentation (February, 2017)
4. Yucesoy D.T., Akkineni S., Hinds B., Sarikaya M., *Peptide Enabled Immobilization of Kinetically Matched Enzymes in Membrane Flow Bioreactors.* TMS Spring Meeting, San Francisco, oral presentation (February, 2017)
5. Yucesoy D.T., Akkineni S., Hinds B., Sarikaya M., *Peptide Enabled Addressable Immobilization of Kinetically Matched Fusion Enzymes in Membrane Flow Bioreactors*. Energy Innovations Workshop, San Juan Island-Seattle, poster presentation (August, 2016)
6. Yucesoy D.T., Fong H., Gresswell C., Saadat S., Huang G., Dogan S., Sarikaya M., *Peptide-guided Dental Tissue Regeneration for Oral Healthcare.* MSE Departmental Seminar -2016, oral presentation (November, 2016)
7. Yucesoy D.T., Fong H., Gresswell C., Saadat S., Dogan S., Sarikaya M., *Peptide-enabled Remineralization Strategies Towards Novel Dental Health Care.* MSE Industry Day-2016, oral presentation (October, 2016)

**PATENTS**

1. M. Sarikaya, H. Fong, D.T. Yucesoy, *"Reagents and methods for whitening teeth"* PCT, WIPO - Int Publ no: WO2016115283A3, 09/09/2016.
2. M. Sarikaya, S. Dogan, H. Fong, D.T. Yucesoy, *"Reagents and methods for mineralization of tooth enamel"* PCT, WIPO - Int Publ no: WO2017123986A1, 20/07/2017.
3. M. Sarikaya, H. Fong, D.T. Yucesoy, S. Dogan, *"Materials and Method for Peptide-Enabled Incorporation of Fluoride into Dental Health Care Products"* Nationalized, 1/13/2017, PCT/US2017/013492.
4. M. Sarikaya, D.T. Yucesoy, S. Dogan, H. Fong *"Multipurpose Biomimetic Dental Care Products"* US Provisional Patent Application 62/725,160 filed 8/30/2018.
5. M. Sarikaya, D.T. Yucesoy, H. Fong, S. Dogan, "Materials and Methods for Treating Dental Hypersensitivity" US Provisional Patent Application 62/ 758,230 filed 11/9/2018.

**STUDENTS MENTORED BY DENIZ YUCESOY DURING GRADUATE STUDIES (2013-18)**

*Master's Students:*

- Keertana Krishnan | Materials Sci & Engineering; UG & Applied Master's Program (2016-current)
- Hailey Warren | Materials Sci & Engineering; Applied Master's Program (2016-2017)
- Aaron Garland | Materials Sci & Engineering; Applied Master's Program (2016-2017)
- Nicole Chin | Materials Sci & Engineering; UG & Applied Master's Program (2013-2016)

*Undergraduate Students:*

- Andrea Dao | Chemical Engineering; Undergraduate Program (2016-current)
- Yousef Baioumy | Chemical Engineering; Undergraduate Program (2016-current)
- Tatum Hennig | Applied Mathematics; Undergraduate Program (2016-current)
- Huan Nguyen | Molecular, Cellular & Developmental Biology; Undergraduate Program (2017-current)
- Eric Hall | Materials Science & Engineering; Undergraduate Program (2016-2018)
- Saleh Al-Hamad | Bioresource Science & Engineering; Undergraduate Program (2016-2017)
- Abbie Pickering | Materials Science & Engineering; Undergraduate Program (2016-2017)
- Nicole Bentzen | Materials Science & Engineering; Undergraduate Program (2016-2017)
- Aashna Abrol | Materials Science & Engineering; Undergraduate Program (2016-2017)
- Kathleen Ericksen | Materials Science & Engineering; Undergraduate Program (2015-2017)
- Allegra Branch | Mechanical Engineering; Undergraduate Program (2015-2017)
- Amanda Tran | Electrical Engineering; Undergraduate Program (2015-2016)